THE FLORIDA STATE UNIVERSITY

COLLEGE OF ARTS AND SCIENCES

# WIND DRIVEN EFFECTS ON THE YELLOW SEA WARM CURRENT

By

ANDREA C. MASK

A Thesis submitted to the
Department of Oceanography
in partial fulfillment of the
requirements for the degree of
Master of Science

Degree Awarded:
Fall Semester, 1996

Degree Awarded:
Fall Semester, 1996

The members of the Committee approve the thesis of Andrea C. Mask defended on October 4, 1996.

James J. O'Brien
Professor Directing Thesis

Ruth Preller
Outside Committee Member

Georges Weatherly
Committee Member

Richard Iverson
Committee Member

TABLE OF CONTENTS

LIST OF FIGURES

ABSTRACT

1. INTRODUCTION 1

2. MODEL 6

3. YELLOW SEA MODEL RESULTS 17

3.1 Full Wind Case at the Surface 17

3.2 No Wind Case at the Surface 29

3.3 Full Wind Case at 20 M 29

3.4 No Wind Case at 20 M 30

3.5 Full Wind Case at 50 M 39

3.6 No Wind Case at 50 M 39

4. YELLOW SEA WARM CURRENT INTRUSION 49

5. WIND AND THE YELLOW SEA WARM CURRENT RELATIONSHIP 55

5.1 Rotary Spectra 57

5.2 Coherency 61

6. CONCLUSIONS 74

APPENDIX A 78

REFERENCES 84

BIOGRAPHICAL SKETCH 86

BIOGRAPHICAL SKETCH 86

# ACKNOWLEDGMENTS

This research was conducted under Naval Research Laboratory grant N00014-94-1-G918. I would first like to recognize my major professor, Dr. James J. O'Brien, without who's guidance and support this thesis would not have been possible. Secondly, I would like to thank Dr. Ruth Preller from NRL at Stennis Space Center, MS. I cannot begin to list all the ways she has helped in this research, but particularly for the use of the NRL Yellow Sea Model and the guidance in choosing this topic. Also at Stennis, I would like to thank Shelley Riedlinger who, along with Lakshmi Kantha of the University of Colorado, developed the regional application of the POM model to the Yellow Sea and willingly answered al my questions about the model.

From COAPS (Center for Ocean-Atmosphere Prediction Studies) at Florida State University, I would like to thank Dr. Steve Meyers who offered editor skills and was a sounding board for ideas. Dr. Detlev Muller, who could offer solutions

LIST OF FIGURES


| Figure | | Page |
|---|---|---|
| 1. | Major currents of the Yellow Sea Region Yuan & Su (1994) (Top - Winter Circulation, Bottom - Summer Circulation) | 2 |
| 2. | Yellow Sea Model grid, (every other point plotted), with open boundaries at A, B, C, and D. | 7 |
| 3. | Bathymetry of the Yellow Sea Model and the river locations. | 9 |
| 4. | NAVOCEANO's January climatology for temperature at the surface. | 11 |
| 5. | NAVOCEANO's January climatology for temperature at 20 m. | 12 |
| 6. | NAVOCEANO's January climatology for temperature at 50 m. | 13 |
| 7. | NAVOCEANO's January climatology for salinity at the surface. | 14 |
| 8. | NAVOCEANO's January climatology for salinity at 20 m depth. | 15 |
| 9. | NAVOCEANO's January climatology for salinity at 50 m depth. | 16 |
| 10. | Magnitude of wind stress on February 3, 1993. Colors are in $N/m^2$ and the vectors are in m/s. | 18 |
| 10. | Magnitude of wind stress on February 3, 1993. Colors are in $N/m^2$ and the vectors are in m/s. | 18 |
| 11. | Magnitude of wind stress on August 15, 1993. Colors are in $N/m^2$ and the vectors are in m/s. | 19 |

12. Temperature and currents at the surface for the full wind case on February 3, 1993. The arrows have been truncated for currents greater than 0.5 m/s. 21

13. Temperature and currents at the surface for the full wind case on August 15, 1993. The arrows have been truncated for currents greater than 0.5 m/s. 22

14. Salinity and currents at the surface for the full wind case on February 3, 1993. The arrows have been truncated for currents greater than 0.5 m/s. 23

15. Salinity and currents at the surface for the full wind case on August 15, 1993. The arrows have been truncated for currents greater than 0.5 m/s. 24

21. Temperature and currents at 20 m depth for the full wind case on August 15, 1993. The arrows have been truncated for currents greater than 0.5 m/s. 32

22. Salinity and currents at 20 m depth for the full wind case on February 3, 1993. The arrows have been truncated for currents greater than 0.5 m/s. 33

23. Salinity and currents at 20 m depth for the full wind case on August 15, 1993. The arrows have been truncated for currents greater than 0.5 m/s. 34

24. Temperature and currents at 20 m depth for the no wind case on February 3, 1993. The arrows have been truncated for currents greater than 0.5 m/s. 35

25. Temperature and currents at 20 m depth for the no wind case on August 15, 1993. The arrows have been truncated for currents greater than 0.5 m/s. 36

26. Salinity and currents at 20 m depth for the no wind case on February 3, 1993. The arrows have been truncated for currents greater than 0.5 m/s. 37

27. Salinity and currents at 20 m depth for the no wind case on August 15, 1993. The arrows have been truncated for currents greater than 0.5 m/s. 38

28. Temperature and currents at 50 m depth for the full wind case on February 3, 1993. The arrows have been truncated for currents greater than 0.5 m/s. 40

29. Temperature and currents at 50 m depth for the full wind 41

29. Temperature and currents at 50 m depth for the full wind case on August 15, 1993. The arrows have been truncated 41

for currents greater than 0.5 m/s.

30. Salinity and currents at 50 m depth for the full wind case on February 3, 1993. The arrows have been truncated for currents greater than 0.5 m/s. 42

31. Salinity and currents at 50 m depth for the full wind case on August 15, 1993. The arrows have been truncated for currents greater than 0.5 m/s. 43

32. Temperature and currents at 50 m depth for the no wind case on February 3, 1993. The arrows have been truncated for currents greater than 0.5 m/s. 44

33. Temperature and currents at 50 m depth for the no wind case on August 15, 1993. The arrows have been truncated for currents greater than 0.5 m/s. 45

34. Salinity and currents at 50 m depth for the no wind case on February 3, 1993. The arrows have been truncated for currents greater than 0.5 m/s. 46

35. Salinity and currents at 50 m depth for the no wind case on August 15, 1993. The arrows have been truncated for currents greater than 0.5 m/s. 47

36. February's monthly averaged Yellow Sea Warm Current water mass properties. The gold shaded area is the area defined by the water mass properties for the full wind case. The black outline is the area defined by the water mass properties for the no wind case. 51

37. August's monthly averaged Yellow Sea Warm Current water 52

37. August's monthly averaged Yellow Sea Warm Current water mass properties. The gold shaded area is the area defined by the water mass properties for the full wind case. The black outline is the area defined by the water mass 52

properties for the no wind case.

38. February's monthly averaged northward velocities. The gold shaded area is the area of northward moving water for the full wind case. The black outline is the area of northward moving water for the no wind case. 53

39. August's monthly averaged northward velocities. The gold shaded area is the area of northward moving water for the full wind case. The black outline is the area of northward moving water for the no wind case. 54

40. Points chosen to study relationship between the wind and the Yellow Sea Warm Current. 56

41. Rotary Spectra of the wind at a.) point 2 (124.0E,34.0N) and b.) at point 6 (126.0E, 28.0N) with prewhitening and six hanning windows. 58

42. Rotary Spectra with prewhitening and 6 hanning windows of the full wind case and the no wind case at a.) point 1 (125.35E, 33.75N), b.) point 2 (124.0E, 34.0N), c.) point 3 (124.0E, 30.0N) d.) point 4 (128.0E, 32.0N), e.) point 5 (122.0E, 26.0N) and f.) point 6 (126.0E, 28.0N). 59

43. Coherence of the wind between a.) point 1(125.35E, 33.75N) and point 2 (124.0E, 34.0N) , b.) point 2 (124.0E, 34.0N) point 3 (124.0E, 30.0N) c.) point 2 (124.0E, 34.0N) and point 4 (128.0E, 32.0N) and d.) point 2 (124.0E, 34.0N) and point 6 (126.0E, 28.0N). 62

44. Coherence of the Yellow Sea Warm Current for the full and no wind cases between a.) point 1 (125.35E, 33.75N) and point 2 (124.0E, 34.0N), b.) point 1 (125.35E, 33.75N) and 65

44. Coherence of the Yellow Sea Warm Current for the full and no wind cases between a.) point 1 (125.35E, 33.75N) and point 2 (124.0E, 34.0N), b.) point 1 (125.35E, 33.75N) and point 3 (124.0E, 30.0N), c.) point 1 (125.35E, 33.75N) and 65

point 4 (128.0E, 32.0N), d.) point 1 (125.35E, 33.75N) and point 5 (122.0E, 26.0N), e.) point 2 (124.0E, 34.0N) and point 3 (124.0E, 30.0N) and f.) point 2 (124.0E, 34.0N) and point 4 (128.0E, 32.0N).

45. Coherence between the full wind current and the wind at a.) point 1 (125.35E, 33.75N) and b.) point 2 (124.0E, 34.0N) for a years worth of daily data. Coherence between the full wind current and the wind at c.) point 1 (125.35E, 33.75N) and d.) point 2 (124.0E, 34.0N) for winter. Coherence between the full wind current and the wind at e.) point 1 (125.35E, 33.75N) and f.) point 2 (124.0E, 34.0N) for the summer. 67

46. Coherences for the full wind case to the no wind case of the Yellow Sea Warm Current at a.) point 1 (125.35E, 33.75N) and b.) point 2 (124.0E, 34.0N) for a year of daily output. Coherences for the full wind case to the no wind case of the Yellow Sea Warm Current at c.) point 1 (125.35E, 33.75N) and d.) point 2 (124.0E, 34.0N) for winter. Coherences for the full wind case to the no wind case of the Yellow Sea Warm Current at e.) point 1 (125.35E, 33.75N) and f.) point 2 (124.0E, 34.0N) for summer. 71

47. a.) Hoffmuller diagram across 33.875E of the v-velocities for Julian days 1 to 181, b.) Hoffmuller diagram across 33.875E of the v-velocities for Julian days 182 to 365. 76

48. Two-dimensional external mode grid. 82

49. Three-dimensional internal mode grid. 83

## ABSTRACT

The Yellow Sea is a shallow basin with an average depth of 44 m located between China and the Korean Peninsula. One of the dominant ocean circulation features of the Yellow Sea is a warm water intrusion known as the Yellow Sea Warm Current. This feature is observed all year, but reaches its furthest extension in winter.

To better understand the dynamics of this feature, the circulation of the Yellow, East China and Bohai Seas were modelled using the Princeton Ocean Model with a modified mixed layer by Kantha and Clayton. The horizontal resolution of the model varies from 8 km in the Yellow Sea to 25 km in the East China Sea. Twenty-four sigma levels are used to define the vertical structure. The model was atmosperically forced with air temperature, wind stress, and vapor pressure from the Naval Operational Global Atmospheric Prediction System (NOGAPS) 1.25° x 1.25° model for 1993. Initial conditions were set using the Naval Oceanographic Offices' January climatology for temperature and salinity. The boundary conditions included open boundaries at the Taiwan Strait, the Tsushima (Korea) Strait, an area south of Taiwan, and the Tokara Strait, and a closed boundary south of the Ryukyu Islands.

Sensitivity tests were performed to study the influence of the wind on the Yellow Sea Warm Current. To simplify the study, tides were excluded from the calculation. The model results are examined to determine the effect of the wind on the northward extension of the warm water intrusion, using both water mass

characteristics and northward velocity components, and on the development of the Yellow Sea Warm Current.

# I. INTRODUCTION

The Yellow Sea is a marginal sea located between China and Korea. This sea, between the Bohai Sea and the East China Sea, has a maximum depth of 103 m and an average depth of 44 m. The Bohai Sea is a shallow bay area north of the Yellow Sea, and the East China Sea, a deeper sea with maximum depth of around 2000 m, is between the Yellow Sea and the Ryukyu Islands. The division between the East China Sea and the Yellow Sea is not definite, but is often taken to be from the mouth of the Yangtze River to Saishu Island off of Korea.

The Yellow Sea region is prevailed upon by a strong northerly (NNE-NW) monsoon from late November to March, that has an average velocity in January of approximately 10 m/s (Yuan & Su, 1984). This corresponds to the steep pressure gradient between the Siberian High, which covers most of the Asian continent, and the Aleutian Low, which covers the northern most section of the Pacific Ocean. April is the period of alternating monsoons, when the wind direction is variable. By the end of May the pressure systems have reversed and the southwest monsoon begins. During the summer the wind blows to the north with velocities that average around 1.5 m/sec. This is due to the seasonal low-pressure over China and the North Pacific High Pressure area southeast of Japan (Encyclopedia of Oceanography, 1966). These winds effect the local ocean currents and heat fluxes.

ocean currents and heat fluxes.

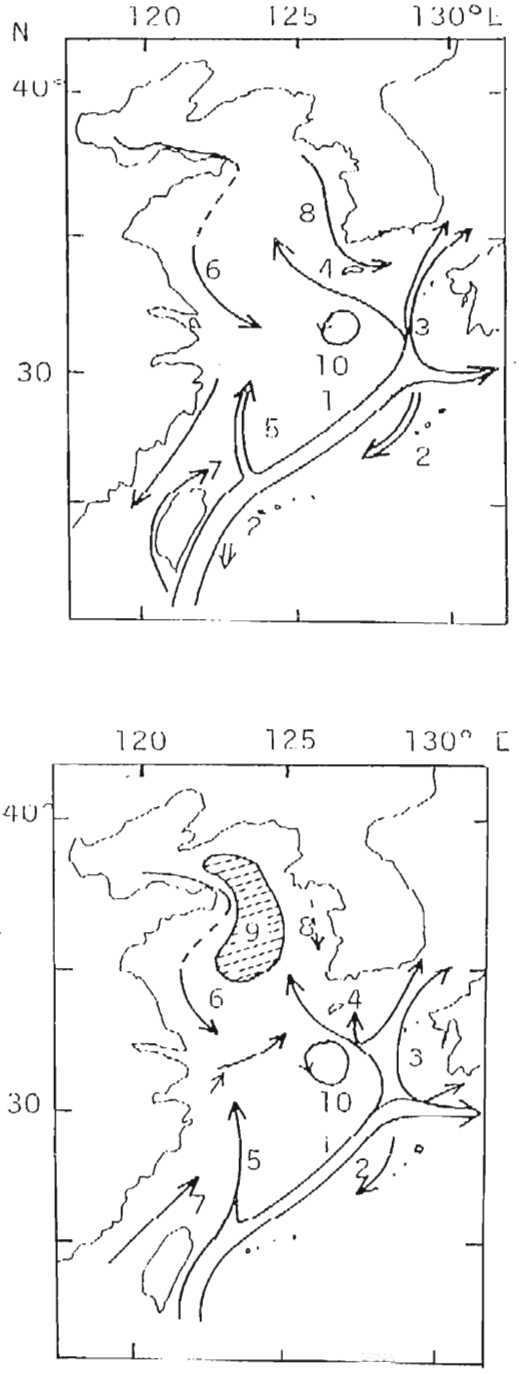


1. Kuroshio
2. Kuroshio Counter Current
3. Tsushima Current
4. Yellow Sea Warm Current
5. Taiwan Warm Current
6. Yellow Sea Coastal Current
7. Taiwan Coastal Current
8. Korean Coastal Current
9. Yellow Sea Cold Water
10. Chejudo Cyclonic Gyre

Figure 1: Major currents of the Yellow Sea Region Yuan & Su (1994) (Top - Winter Circulation, Bottom - Summer Circulation)

Winter Circulation, Bottom - Summer Circulation)

There are several important currents in the Yellow Sea and the East China Sea (Figure 1). The Kuroshio, the largest current with a maximum velocity $\geq$40 cm/sec (Song, 1994), enters the East China Sea around Taiwan, follows the continental slope to the northeast, and exits south of the Japanese island of Kyushu through the Tokara Strait. About 200 km west of Kyushu Island, the Kuroshio sheds a small northward branch, the Tsushima Warm Current, with a maximum velocity around 25 cm/sec (Song, 1994). The Tsushima Warm Current exits the East China Sea through the Korea (Tsushima) Strait. Another strong current in the Yellow Sea is the Yellow Sea Warm Current which flows northward along the central region of the basin. There is also a warm current that flows north from the Taiwan Strait into the East China Sea called the Taiwan Warm Current. During the winter, it is at its weakest, about 12.5 cm/s (Yuan & Su, 1984).

There are also several cold water currents. The Yellow Sea Cold Water is a water mass that is formed in the winter due to strong vertical mixing. In the summer, this mass flows southward under the thermocline (Park, 1986). The Yellow Sea Coastal Current flows southward along the China coast year round. The Zhejiang-Fujian Coastal Current hugs the coast of China from the Yangtze River southward, and exits out of the Taiwan Strait. The Korean Coastal Current flows southward along the western side of Korea and then flows along the southern edge of the Korean Peninsula, exiting through the Korea Strait. For details see Zheng & Klemas (1982) and Lie (1986).

Numerical ocean models are particularly important for investigating the coastal ocean of the Yellow Sea region. This is true because of the limited measurements completed in the Yellow Sea. Even though many oceanographic measurements have been done, most of these studies are

measurements completed in the Yellow Sea. Even though many oceanographic measurements have been done, most of these studies are done with time series less than a half a year in length. Long time series are

particularly difficult to obtain in the Yellow Sea region because of the intense fishing done in the area. Many moorings that have been placed in the Yellow and East China Seas have been damaged or pulled up by fishing nets (Gregg Jacobs, Personal Communication).

Yet, the data that have been collected have supplied the modellers with input to improve their coastal models to the point of producing, not just idealized, but realistic results. Among the most important of the improved measurements are the topography and winds. Winds and topography are important because of the role they play in the Yellow Sea, for example, the basin is so shallow in this area that in the winter the water is vertically mixed to the bottom.

Another important aspect of the dynamics of the region that a modeller must contend with is the impedance of the Kuroshio. This western boundary current dominates the oceanography of the East China Sea. The complicated shelf topography of the East China Sea promotes the shedding of smaller currents by the Kuroshio. These smaller currents are some of the most interesting and difficult aspects of the Yellow Sea for an oceanographer to model. The most perplexing of these currents is the Yellow Sea Warm Current.

The formation of the Yellow Sea Warm Current is poorly understood. In winter, the water mass intrudes into the Yellow Sea as far as 34°N (Hsueh , 1988 and Shuxun, et. al., 1992). However, in summer, the water mass does not penetrate into the Yellow Sea basin (Park, 1987). Yet, when the Yellow Sea Warm Current is discussed, it is discussed mostly as a flow, not a water mass, which can lead to conflicting results. Many studies have verified that the winter NE monsoon drives a mass balance flow northward in the Yellow

mass, which can lead to conflicting results. Many studies have verified that the winter NE monsoon drives a mass balance flow northward in the Yellow Sea basin (Hsueh, 1988). There is no agreement on the mechanism for the

summer Yellow Sea Warm Current. Both geostrophic balance (Lie, 1986) and a density current (Park, 1986) have been proposed as the driving force behind the summer northward flow. Neither of these have been verified. Questions pretaining to the effect of the wind on the water mass intrusion and the forcing of the flow of the Yellow Sea Warm Current will be investigated using a sensitivity test of a numerical ocean model.

In this paper, the model used in the investigation will be discussed first. Followed by the basic results of the model. The next section will include an investigation of the extent of the intrusion of the Yellow Sea Warm Current. This will be followed by a discussion of the relationship between the wind and the Yellow Sea Warm Current. And lastly, the conclusions will be discussed.

## 2. MODEL

The ocean model used in this study is a time dependent, three-dimensional, primitive equation model, originally developed by Alan Blumberg and George Mellor at Princeton University, and is commonly referred to as the Princeton Ocean Model (POM) with a modified mixed layer by Kantha and Clayton (1994). The governing equations and differencing schemes are discussed in Appendix A. This general coastal ocean model is employed at the Naval Research Laboratory (NRL) at Stennis Space Center to study the Yellow Sea region. This particular model is used because it is supported by the Naval Oceanographic Office (NAVOCEANO) as part of their Shallow Water Forecast System, and when model tests have been completed it will be run operationally at NAVOCEANO.

The Yellow Sea model uses a rectilinear grid (Figure 2) that has a horizontal resolution of 25 km at its southern most grid point (21.89°N, 122.44°E) and increases to 8 km at its northern most grid point (42.54°N, 122.801°E), and has twenty-four sigma levels in the vertical. There are four open boundaries, one each north and south of Taiwan and one each north and south of Kyushu, Japan. At each of these boundaries the temperature, salinity, and velocities are prescribed. At boundary A, the Taiwan Strait, the temperature and salinity are prescribed as seasonal profiles that are linearly interpolated to each model time step, and the transport velocities are assumed

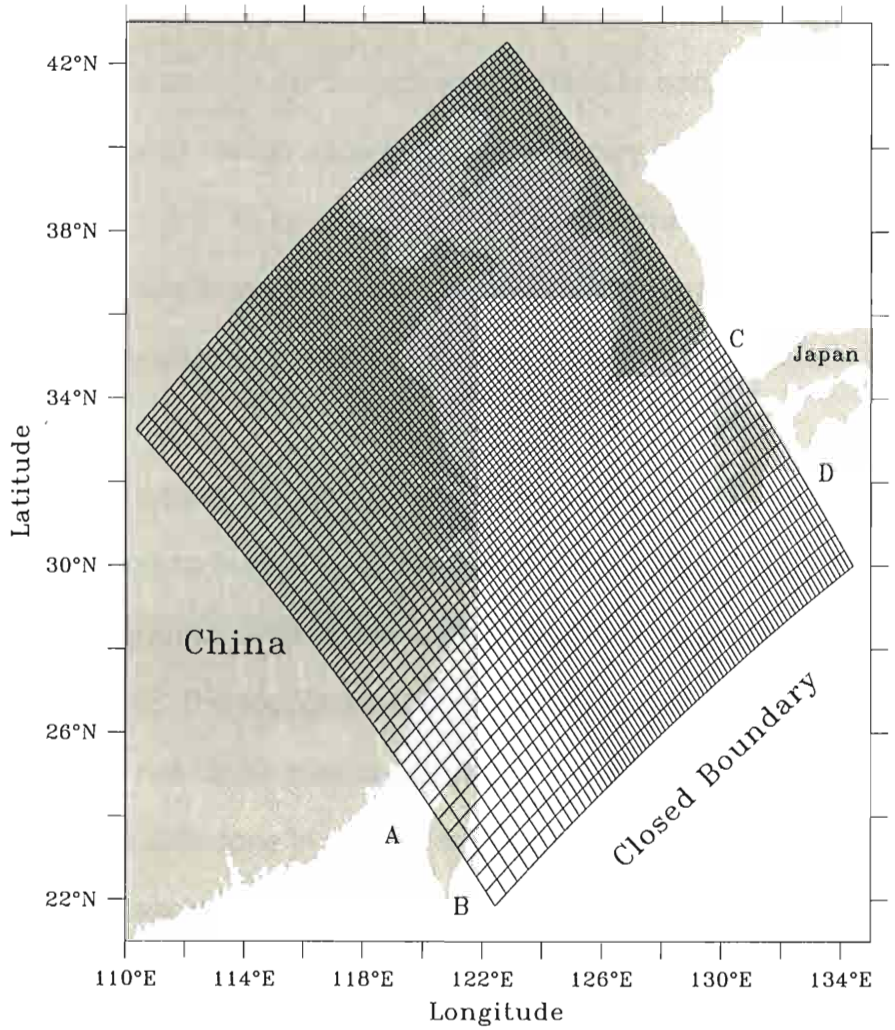


Figure 2: Yellow Sea Model grid, (every other point plotted), with open boundaries at A, B, C, and D.

to be 1 Sv (Sv = 1 X $10^6$ $m^3$/sec) less than through boundary C, the Tsushima (Korea) Strait. At boundary B, south of Taiwan, winter and summer temperature and salinity profiles are linearly interpolated to each model time step, and the transport velocities are geostrophically balanced inflows that are adjusted until the depth averaged velocities yield a transport of 23 Sv. At boundary C, if flow is into the Yellow Sea region, monthly profiles of temperature and salinity are linearly interpolated to each model time step, and the outflow velocity values applied at the boundary are seasonal with values between 2 and 4 Sv. At boundary D, the Tokara Strait, Japan, the conditions are the same as for boundary B, except that the transport velocity is 22 Sv. The Southern boundary is a closed boundary because of the lack of accurate information.

Figure 3 shows the model bathymetry for the Yellow Sea region. The topography's source is the Digital Bathymetric Data Base 5 (DBDB5) from the Naval Oceanographic Office. This realistic bottom topography has a maximum depth of 2000 m. The topography has been smoothed so that the sigma coordinates do not cause spurious currents in the region of steep topographic gradients. This was done in a three step method. First, the entire topography was filtered by assigning to each point (i,j) the average of the topography at its four closest points, and the values less than 100m are saved. Second, the values are adjusted until the ratio of the depth between two closest points is not greater than 1.7. Third, the values less than 100m from step one are reinserted and the data is then filtered twice using the method in step one.

There are four river inputs into the model; the Yangtze, Yellow, Liaohe, and Han. Each input is the monthly mean supplied by the World

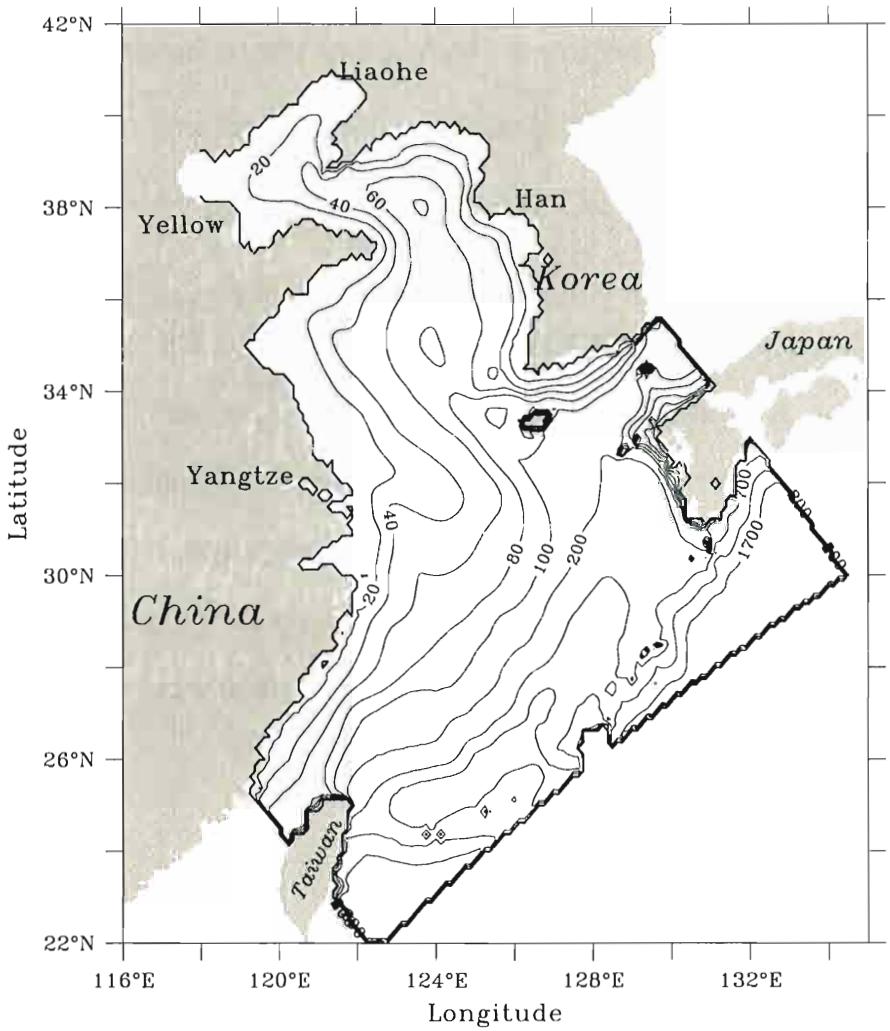


Figure 3: Bathymetry of the Yellow Sea Model and the river locations.

Meteorological Organization's (WMO) version of the United Nations Educational, Scientific and Cultural Organization's (UNESCO) river discharge data, except for the Liahoe which is approximated as 1/6 th the value of the Yellow River. The Yangtze is by far the largest with a yearly average flow rate of 2.9 X $10^4$ $m^3$/sec, and a maximum flow rate of 5.4 X $10^4$ $m^3$/sec in July. The Yellow is the second largest with a yearly averaged flow rate of 1588.3 $m^3$/sec, and a maximum flow rate of 4380.0 $m^3$/sec is September. The Liahoe and Han have averaged yearly flow rates around 250 $m^3$/sec and maximums less than 750 $m^3$/sec.

Except for the open boundaries, NAVOCEANO's January climatology for temperature (Figures 4, 5, and 6) and salinity (Figures 7, 8, and 9) is used for the initial condition over the entire region. Atmospheric forcing (air temperature, wind stress, and vapor pressure) is from the Navy Operational Global Atmospheric Prediction System (NOGAPS) 1.25° X 1.25° model for 1993. No tides have been included in this model.

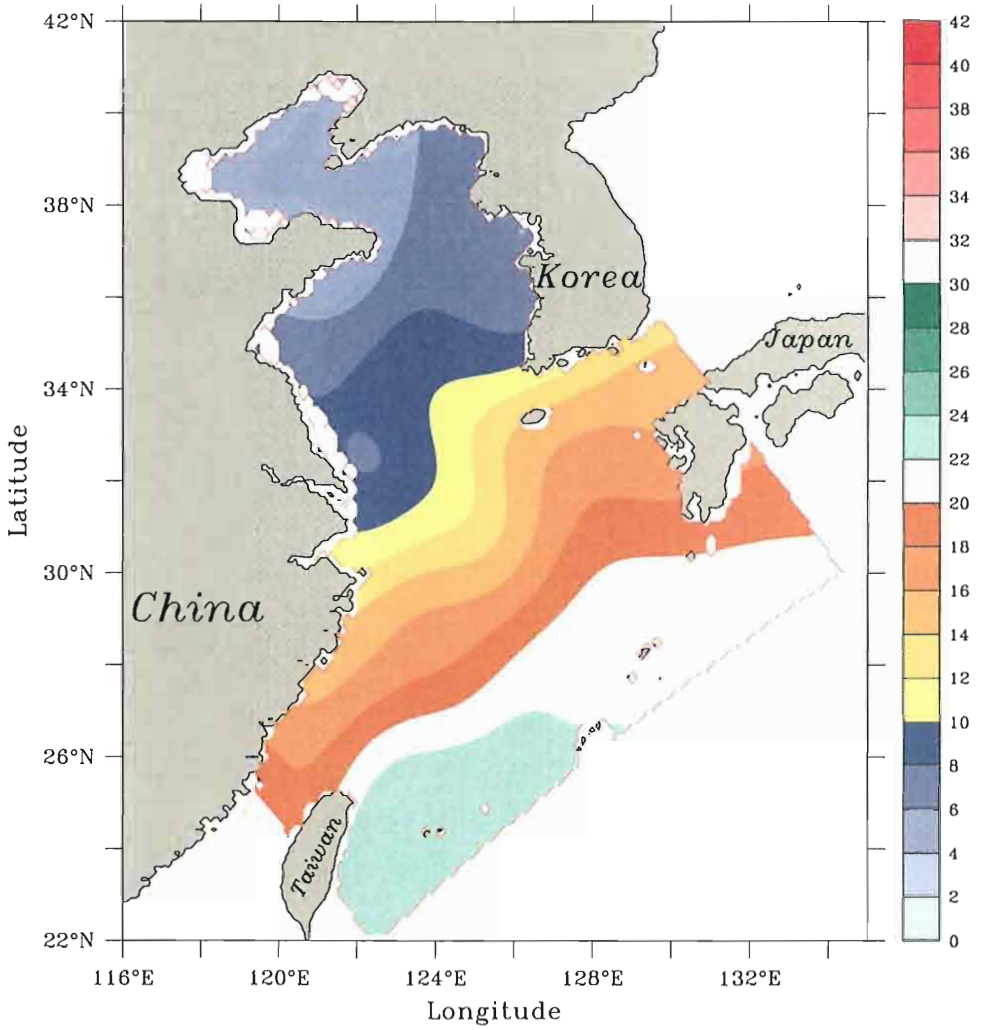


Figure 4: NAVOCEANO's January climatology for temperature at the surface.

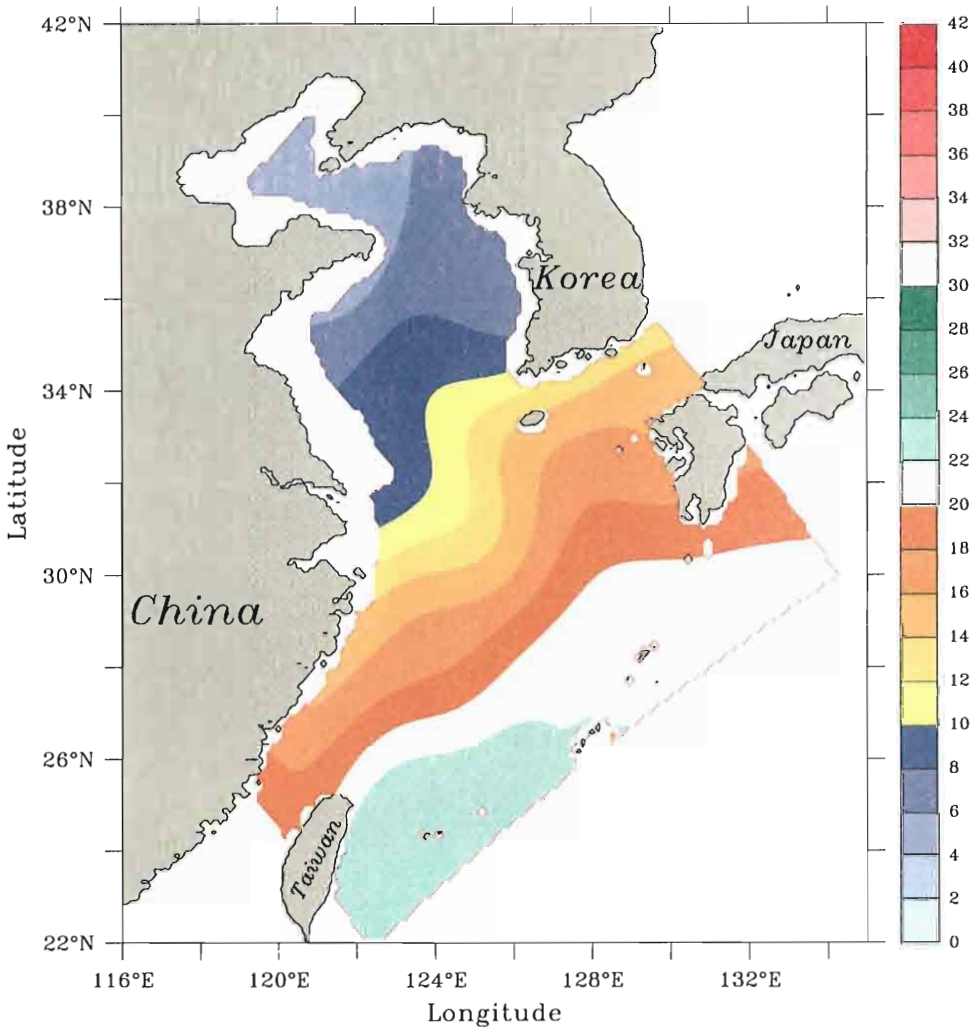


Figure 5: NAVOCEANO's January climatology for temperature at 20 m.

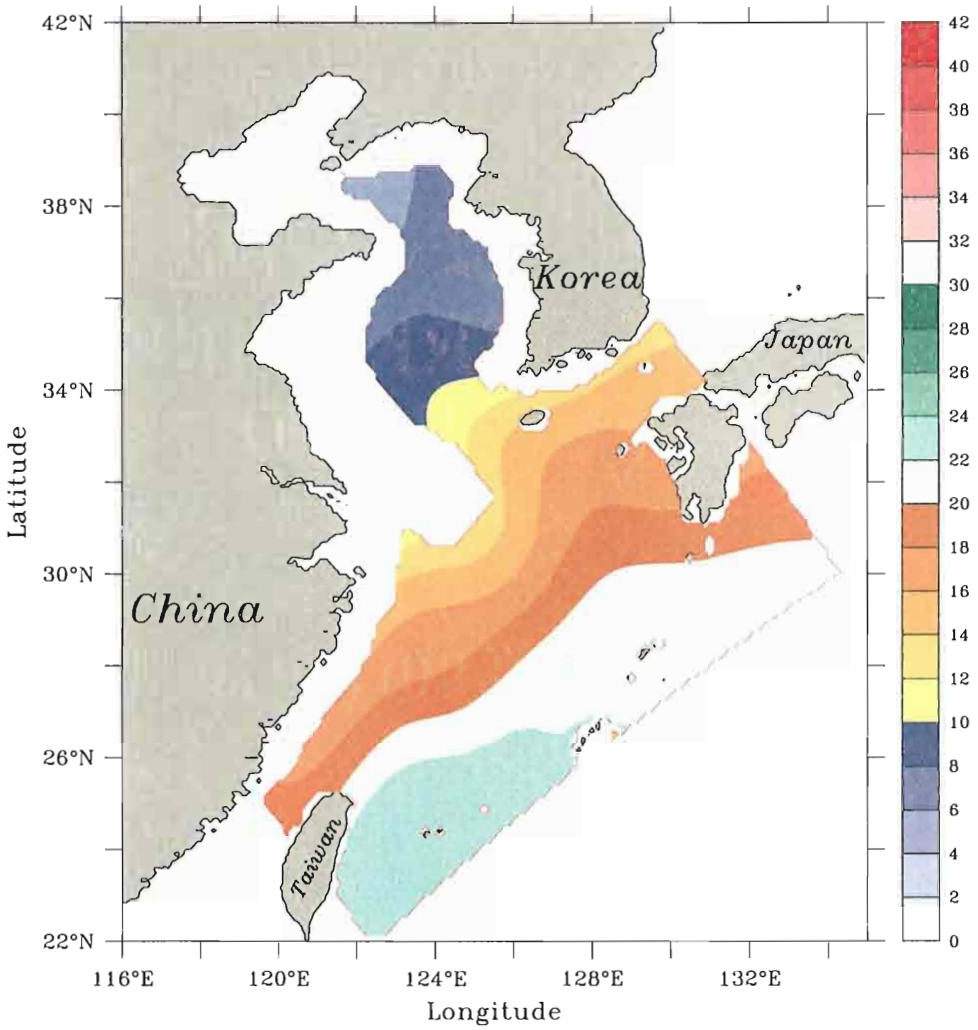


Figure 6: NAVOCEANO's January climatology for temperature at 50 m.

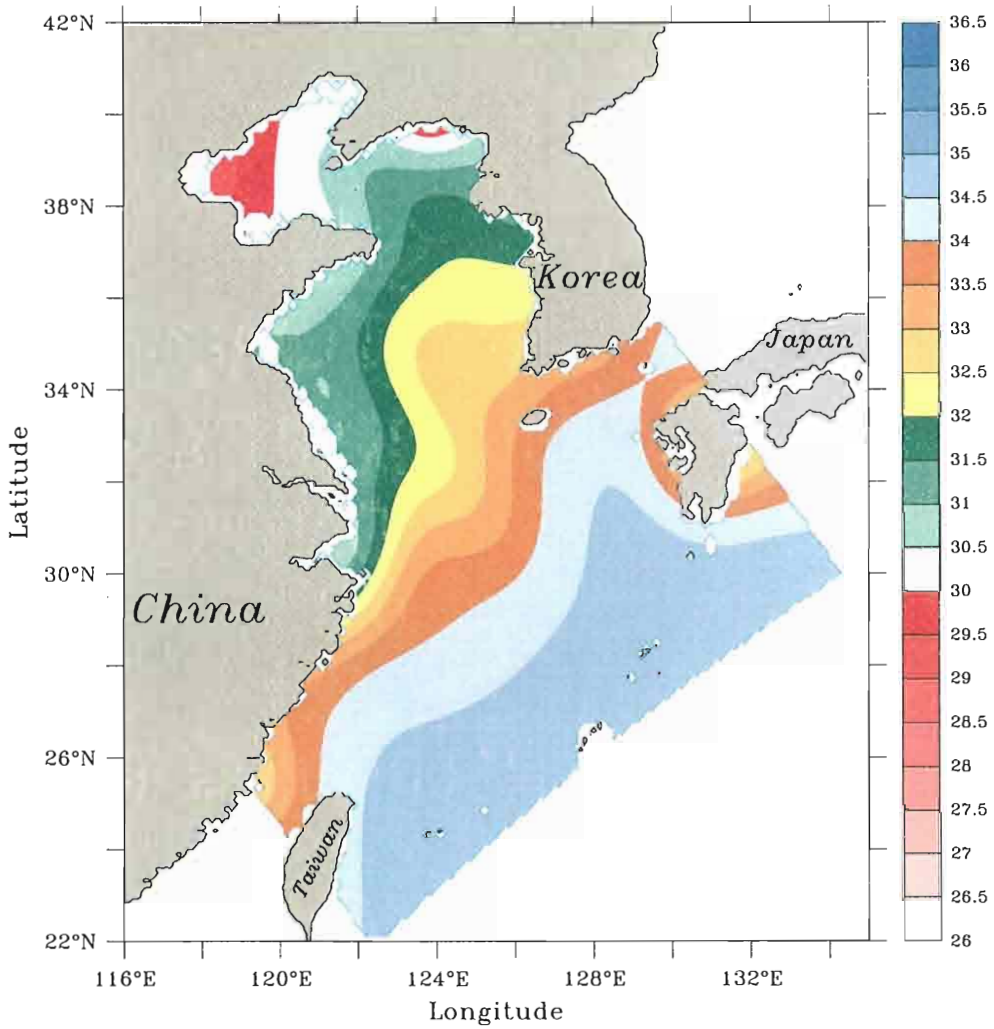


Figure 7: NAVOCEANO's January climatology for salinity at the surface.

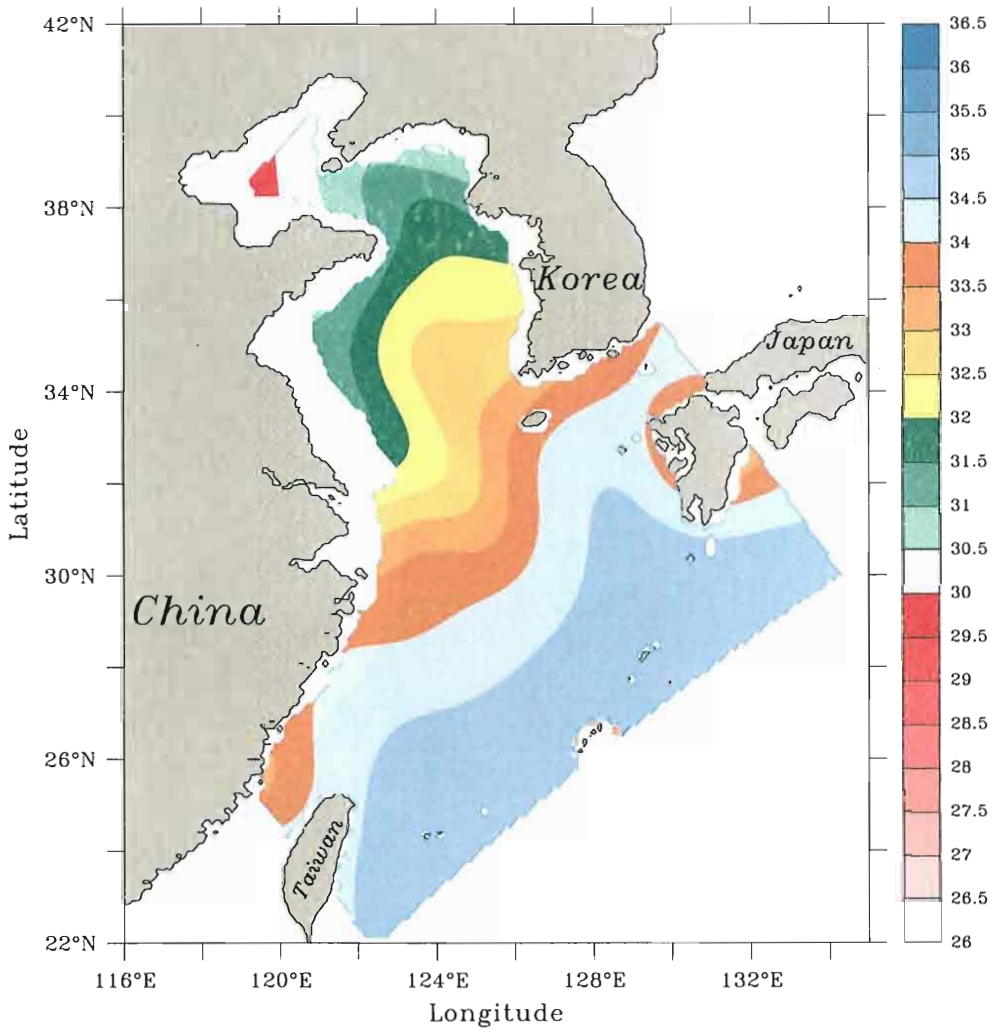


Figure 8: NAVOCEANO's January climatology for salinity at 20 m depth.

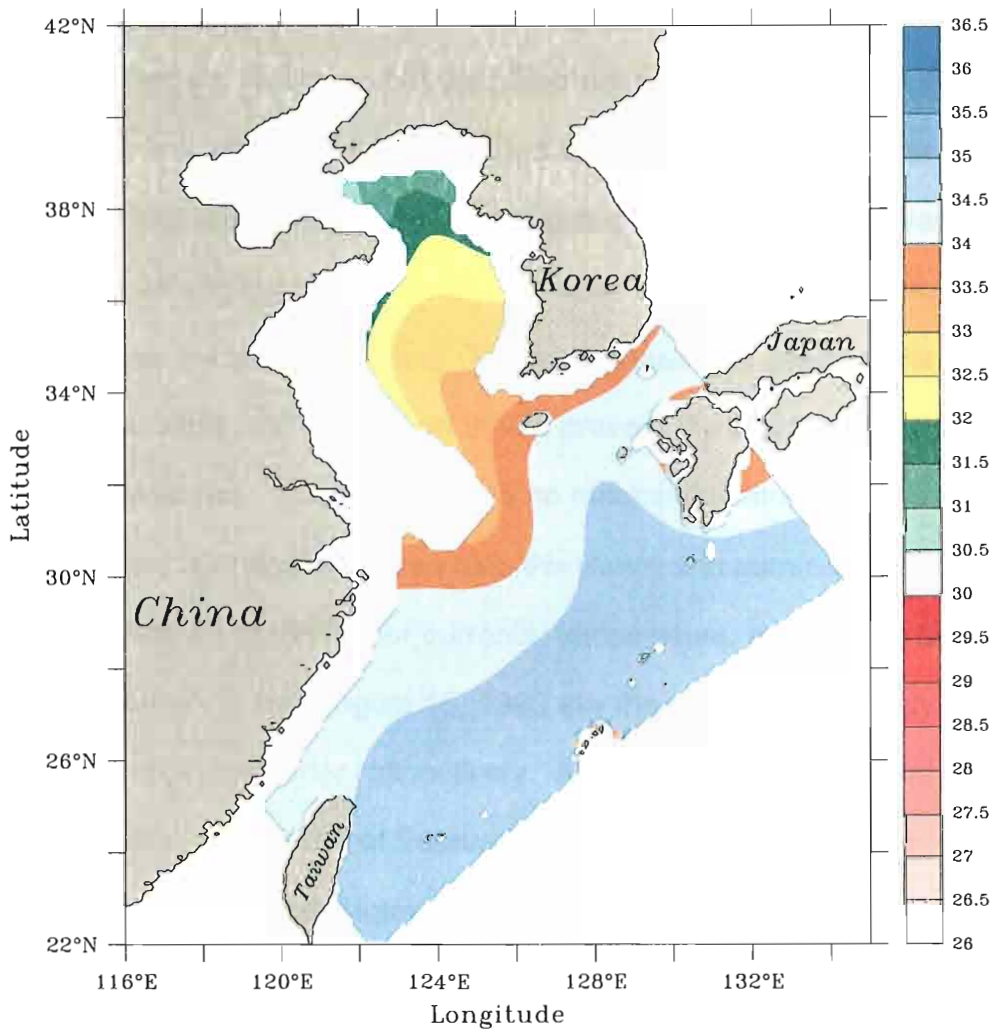


Figure 9: NAVOCEANO's January climatology for salinity at 50 m depth.

# 3. YELLOW SEA MODEL RESULTS

Two runs of the model were performed to study the Yellow Sea Warm Current. The first run, for the rest of the paper will be called the full wind case, was completed with all the forcing described in the model section. The second run, for the rest of the paper will be called the no wind case, was completed with all original forcing except the wind stress was set to zero after the calculation for the latent heat flux. The wind stress was used for the calculation of sensible and latent heat flux to prevent the build-up of heat in this semi-enclosed sea. The wind exerts no mechanical stress on the ocean in this experiment. For each of these runs the winter and summer output at the surface, 20 m, and 50 m depths for currents, temperature, and salinity are presented. February 3 and August 15, 1993 are the representative days chosen for winter and summer respectively. Also presented is the wind stress for these two days. On the 3rd of February (Figure 10), the wind has a magnitude smaller than most winter days, and is from the west to the east over the Yellow Sea and north to south over most of the East China Sea. In August (Figure 11), the stress is again of low magnitude. The wind is from the north over the Yellow Sea and from the west over the East China Sea.

## 3.1 Full Wind Case at the Surface

3.1 Full Wind Case at the Surface

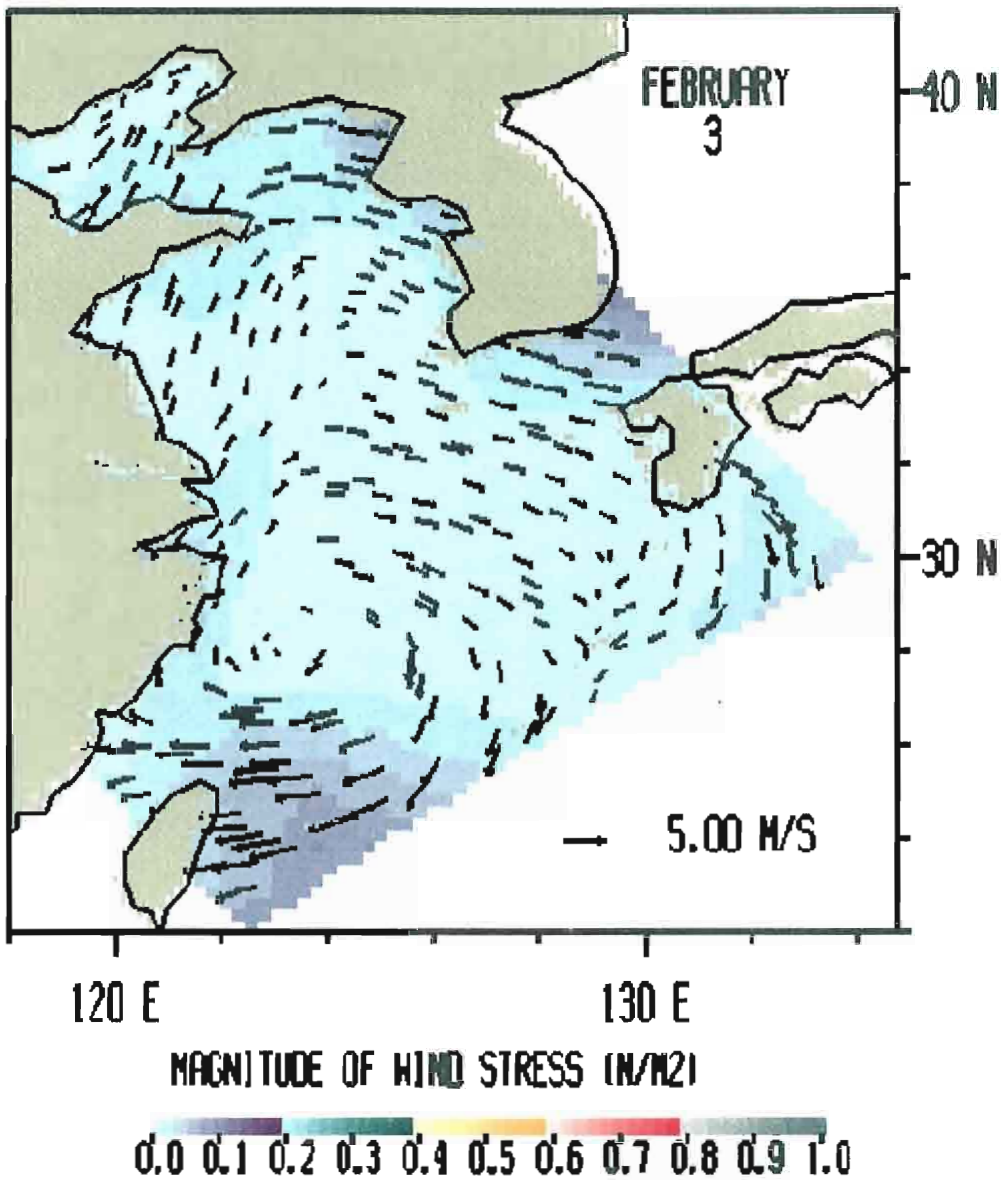


Figure 10: Magnitude of wind stress on February 3, 1993. Colors are in $N/m^2$ and the vectors are in m/s.

Figure 10: Magnitude of wind stress on February 3, 1993. Colors are in $N/m^2$ and the vectors are in m/s.

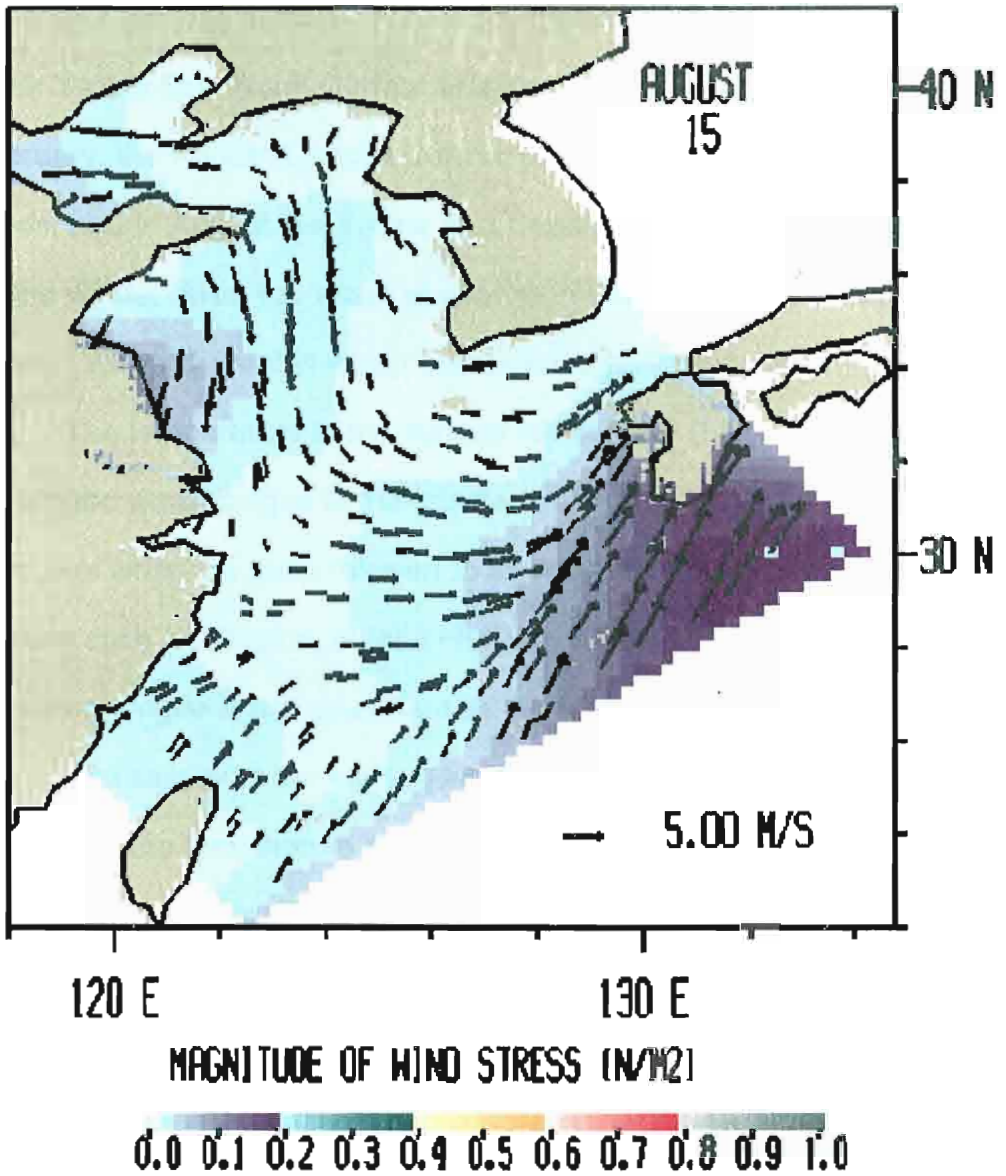


Figure 11: Magnitude of wind stress on August 15, 1993. Colors are in N/m$^2$ and the vectors are in m/s.

Figure 11: Magnitude of wind stress on August 15, 1993. Colors are in N/m$^2$ and the vectors are in m/s.

In February (Figure 12), there is a weak Yellow Sea Warm current moving northwest into the basin. There is a weak Yellow Sea Coastal Current, and a stronger Korean Coastal Current. The Taiwan Warm Current is suppressed and the Tsushima Warm Current is disrupted. The Kuroshio is present in February and August (Figure 13). In August, the Taiwan and Tsushima are well formed. There is a strong Yellow Sea Coastal Current and weak Yellow Sea Warm Current and Korean Coastal Current. Notice in February, the Korean Coastal Current has been strengthened because of the winds, and in August the Yellow Sea Coastal Current has been strengthened by the winds. Also, the winds appear to influence the negligibility of the Taiwan Warm Current in winter and its strength in summer.

The temperature at the surface in February (Figure 12) shows a well developed warm tongue in the middle of the Yellow Sea basin. This warm tongue is what has been referred to as the Yellow Sea Warm Current by authors such as Shuxun, et. al. (1992) and Park (1987). In August (Figure 13), the warm tongue is not as evident as in winter.

The salinity at the surface in February (Figure 14), has features similar to those of the temperature pattern. Notice the low salinity values near the mouths of the Yangtze and the Yellow rivers. In August (Figure 15), the salinity again has similar patterns as the temperature. Notice the lower salinity at the mouth of all four rivers, and especially the low salinity from the Yangtze that reaches almost to the Korean Peninsula. This has been verified by Lie (1986) who found salinity properties of the Yangtze all the way to coastal Korea.

by Lie (1986) who found salinity properties of the Yangtze all the way to coastal Korea.

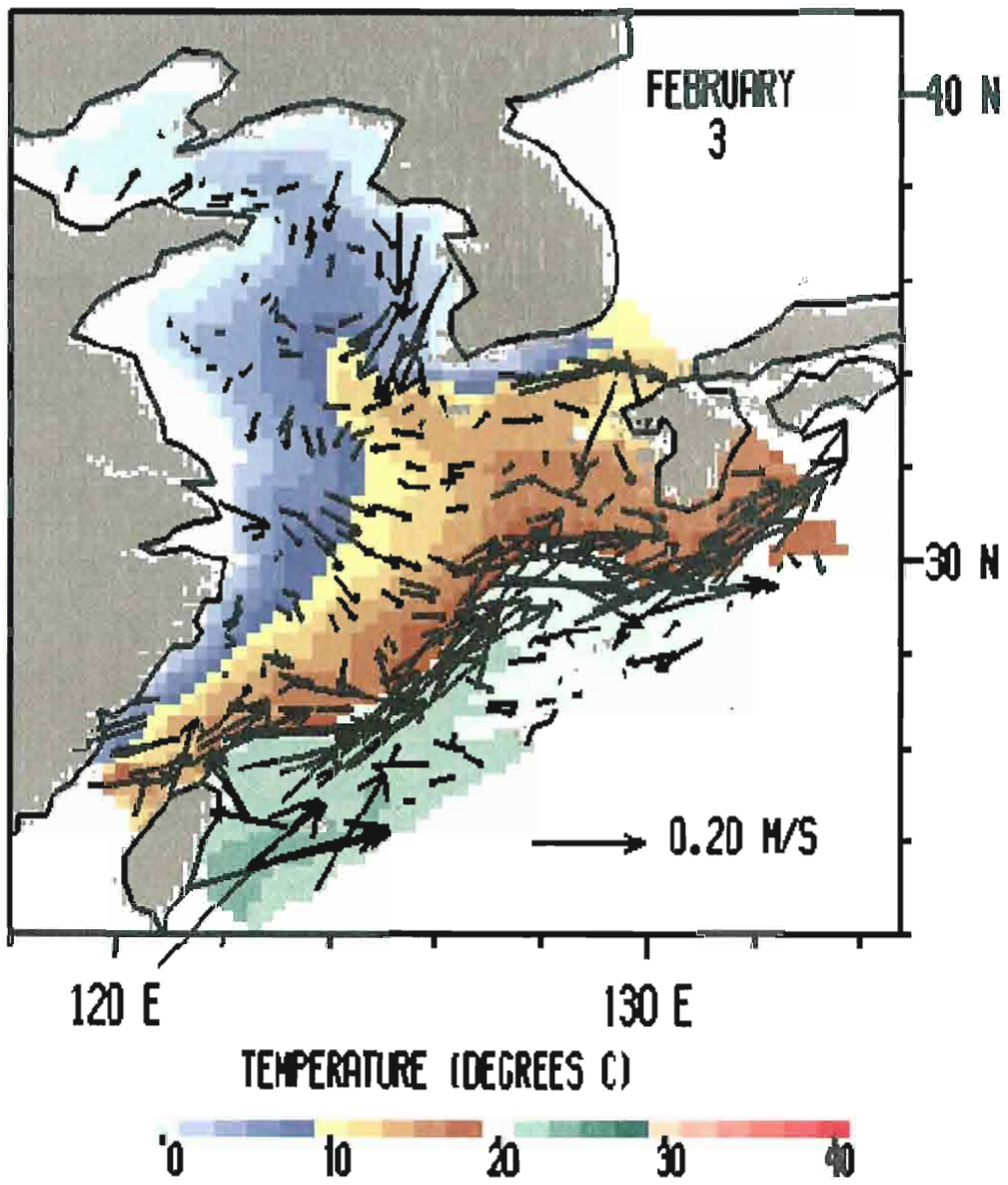


Figure 12: Temperature and currents at the surface for the full wind case on February 3, 1993. The arrows have been truncated for currents greater than

Figure 12: Temperature and currents at the surface for the full wind case on February 3, 1993. The arrows have been truncated for currents greater than 0.5 m/s.

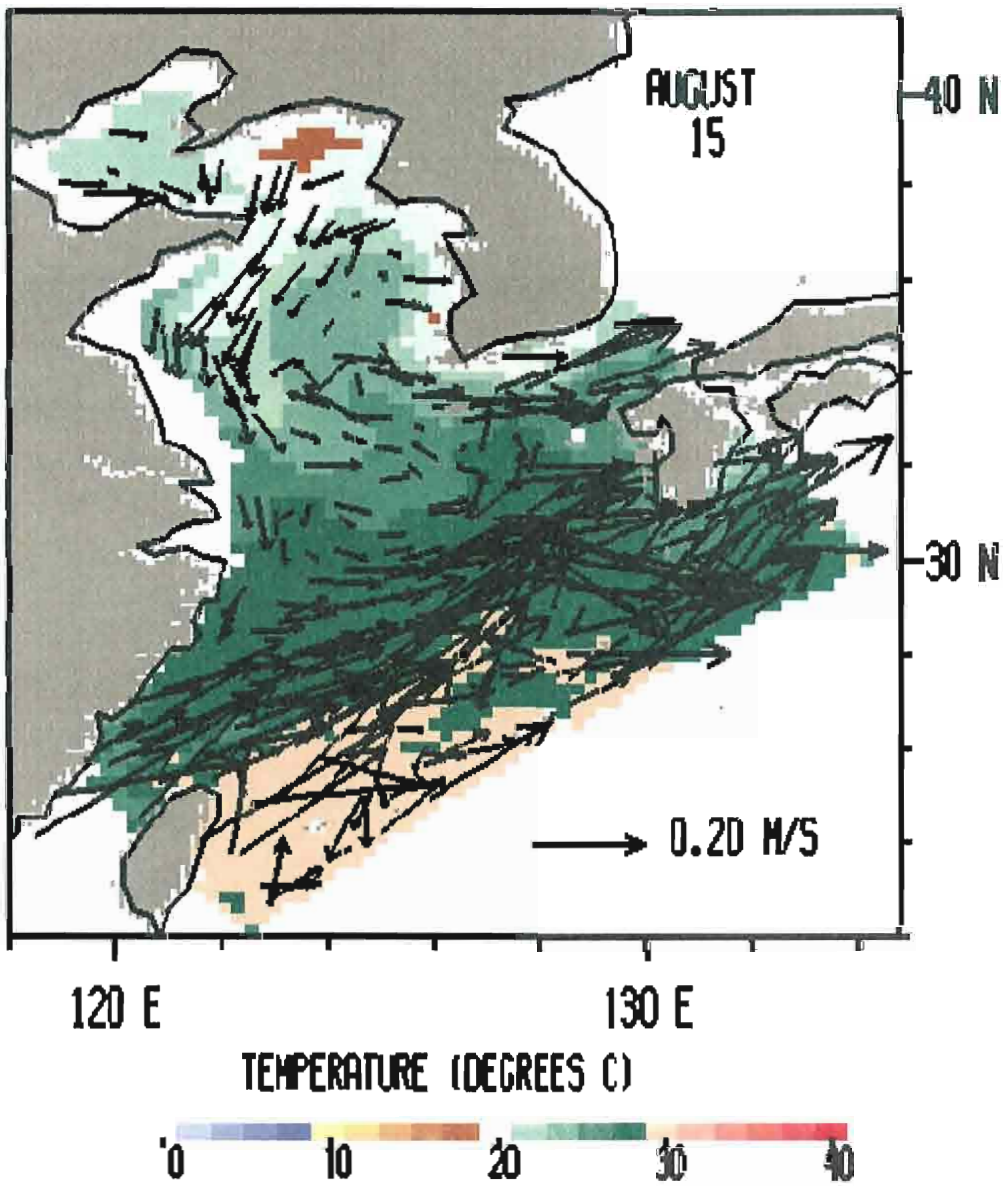


Figure 13: Temperature and currents at the surface for the full wind case on August 15, 1993. The arrows have been truncated for currents greater than

Figure 13: Temperature and currents at the surface for the full wind case on August 15, 1993. The arrows have been truncated for currents greater than 0.5 m/s.

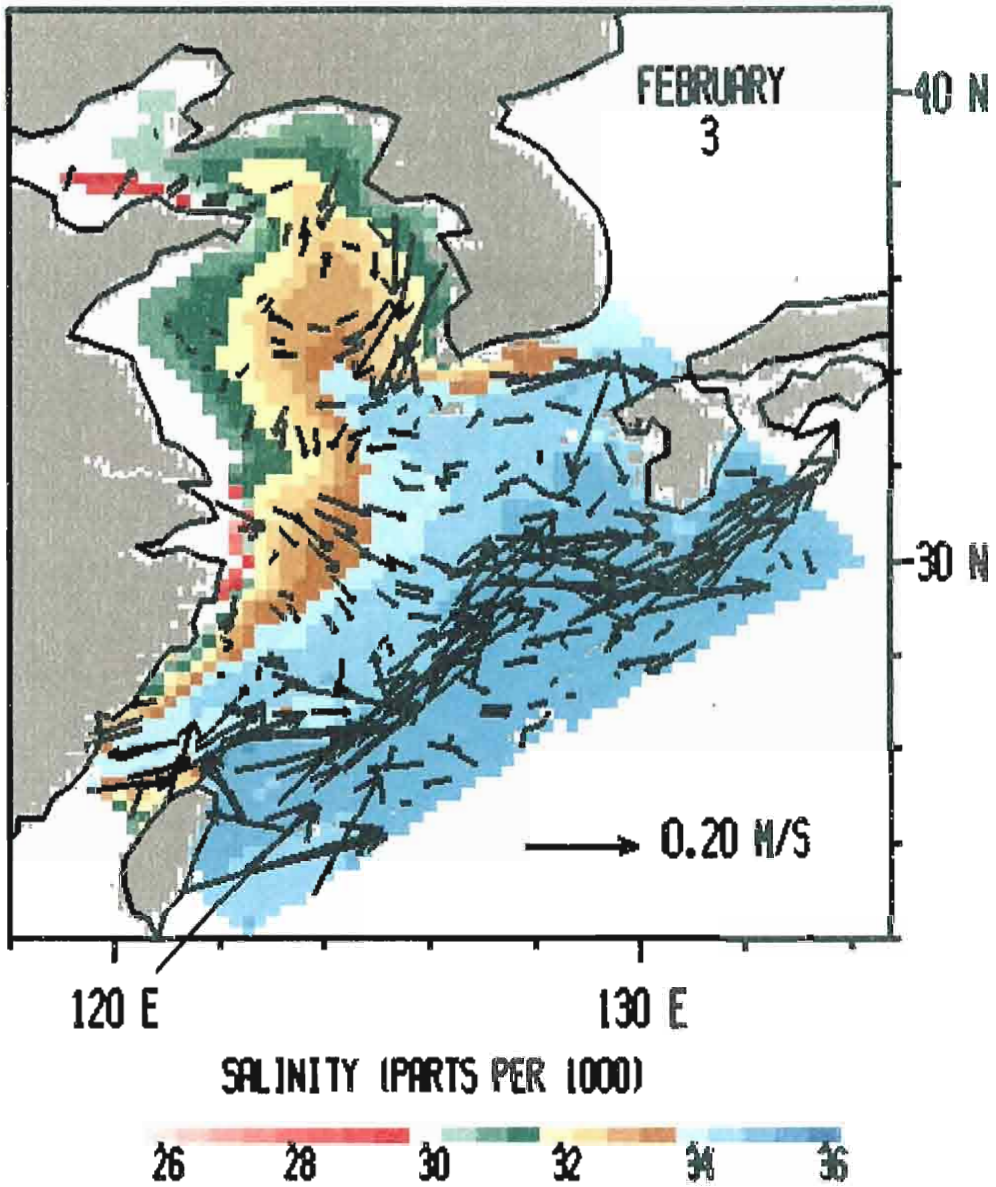


Figure 14: Salinity and currents at the surface for the full wind case on Februarv 3. 1993. The arrows have been truncated for currents greater than

Figure 14: Salinity and currents at the surface for the full wind case on February 3, 1993. The arrows have been truncated for currents greater than 0.5 m/s.

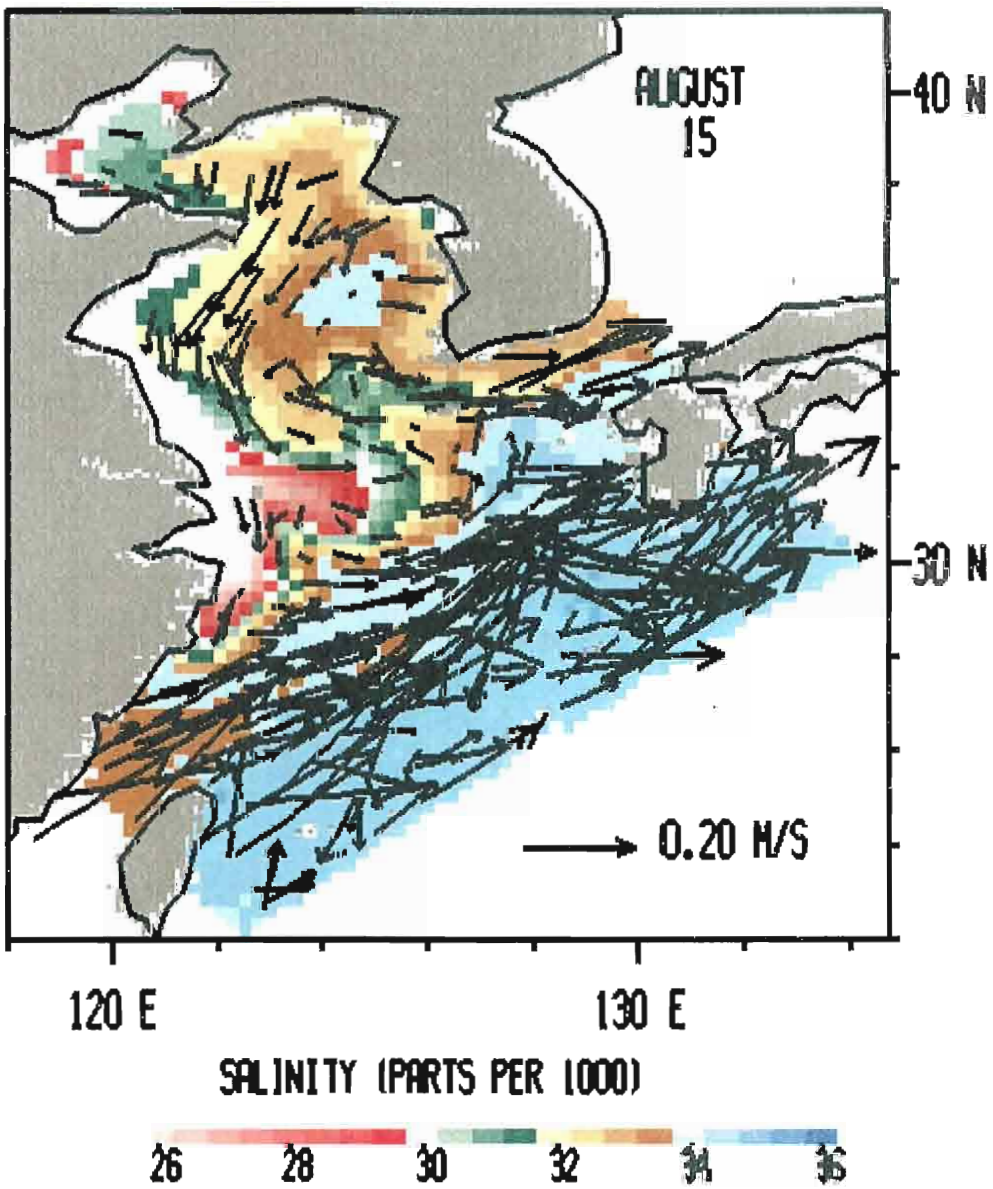


Figure 15: Salinity and currents at the surface for the full wind case on August 15, 1993. The arrows have been truncated for currents greater than 0.5 m/s.

Figure 15: Salinity and currents at the surface for the full wind case on August 15, 1993. The arrows have been truncated for currents greater than 0.5 m/s.

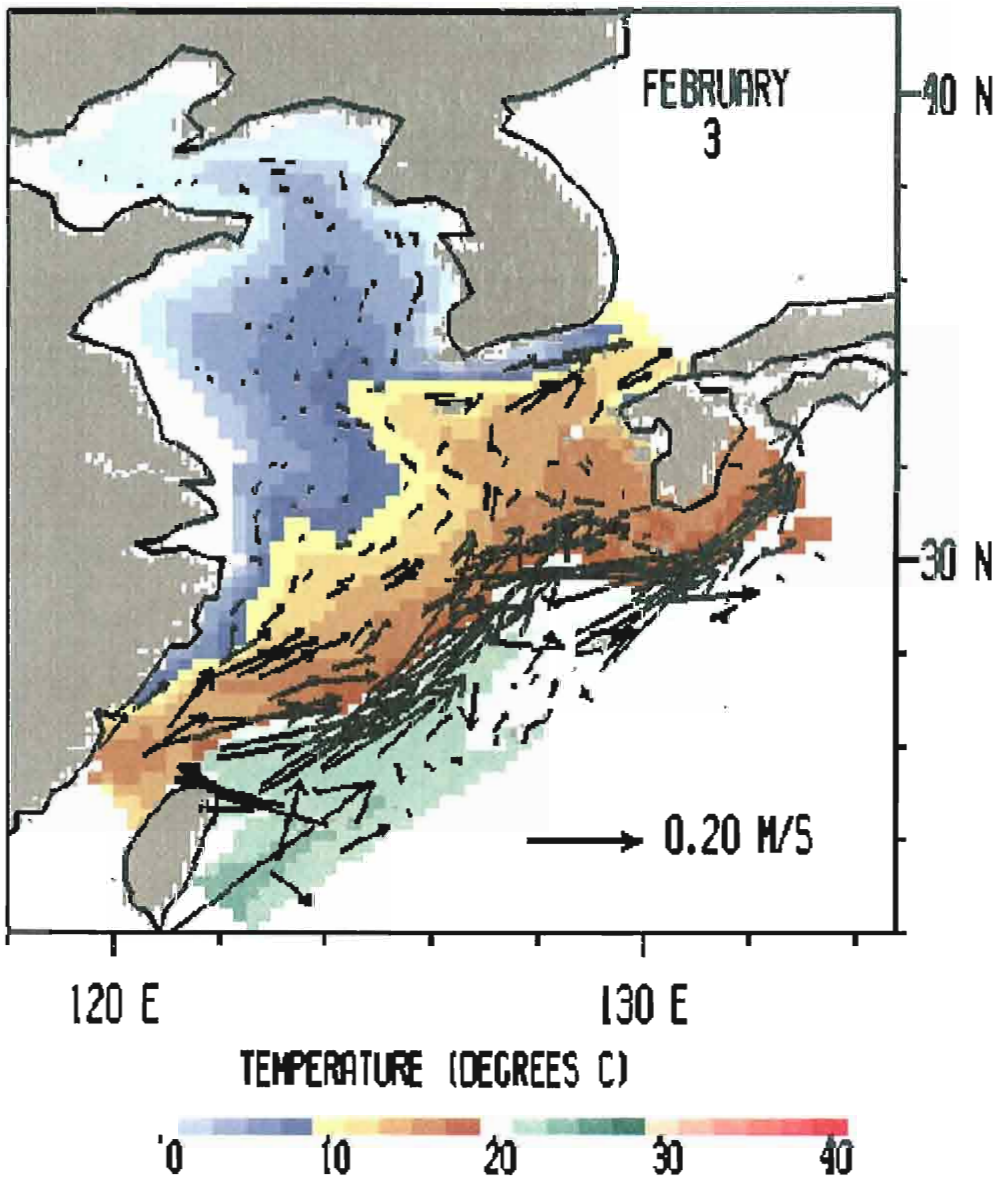


Figure 16: Temperature and currents at the surface for the no wind case on February 3, 1993. The arrows have been truncated for currents greater than

Figure 16: Temperature and currents at the surface for the no wind case on February 3, 1993. The arrows have been truncated for currents greater than 0.5 m/s.

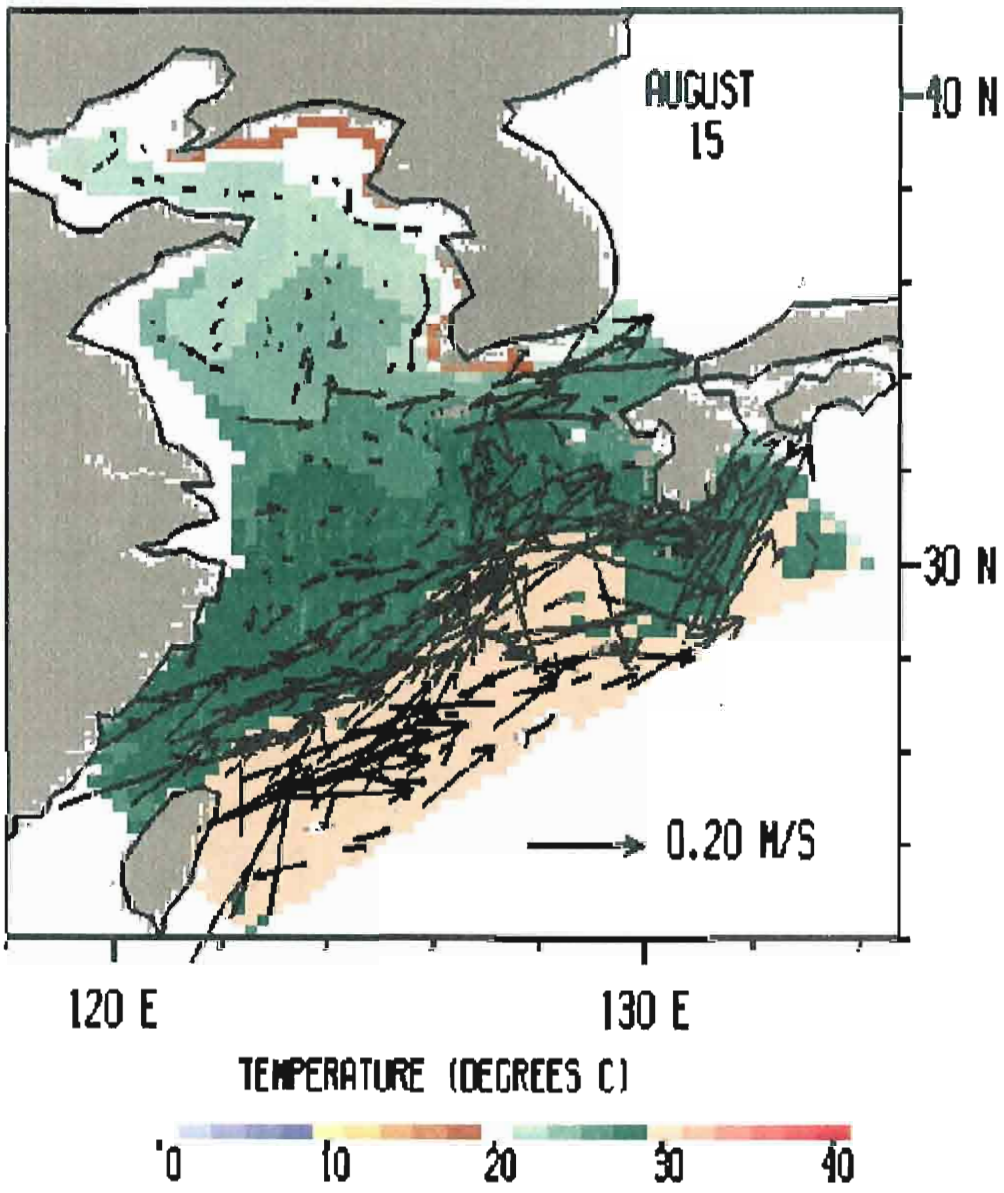


Figure 17: Temperature and currents at the surface for the no wind case on August 15, 1993. The arrows have been truncated for currents greater than

Figure 17: Temperature and currents at the surface for the no wind case on August 15, 1993. The arrows have been truncated for currents greater than 0.5 m/s.

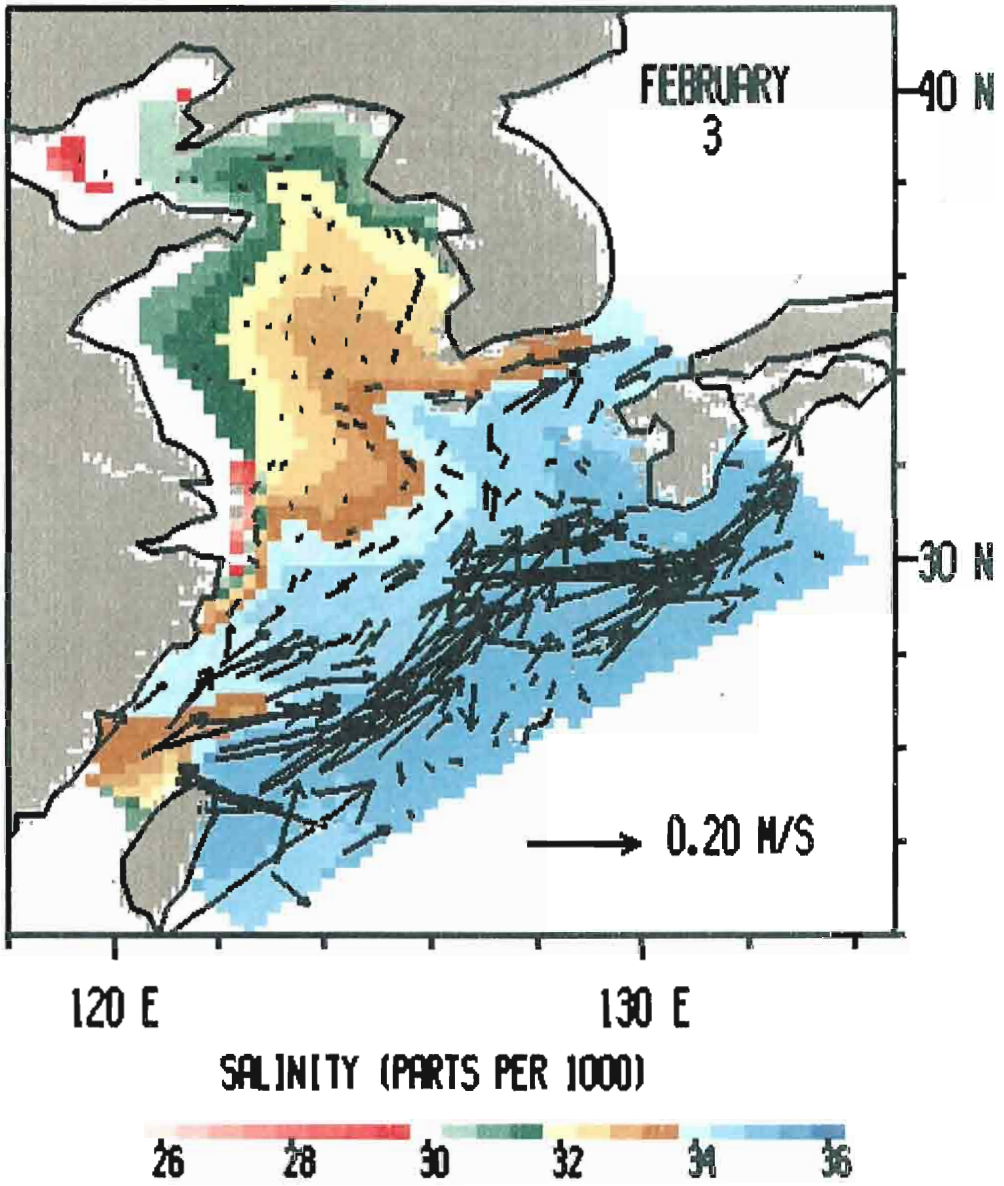


Figure 18: Salinity and currents at the surface for the no wind case on February 3, 1993. The arrows have been truncated for currents greater than 0.5 m/s.

Figure 18: Salinity and currents at the surface for the no wind case on February 3, 1993. The arrows have been truncated for currents greater than 0.5 m/s.

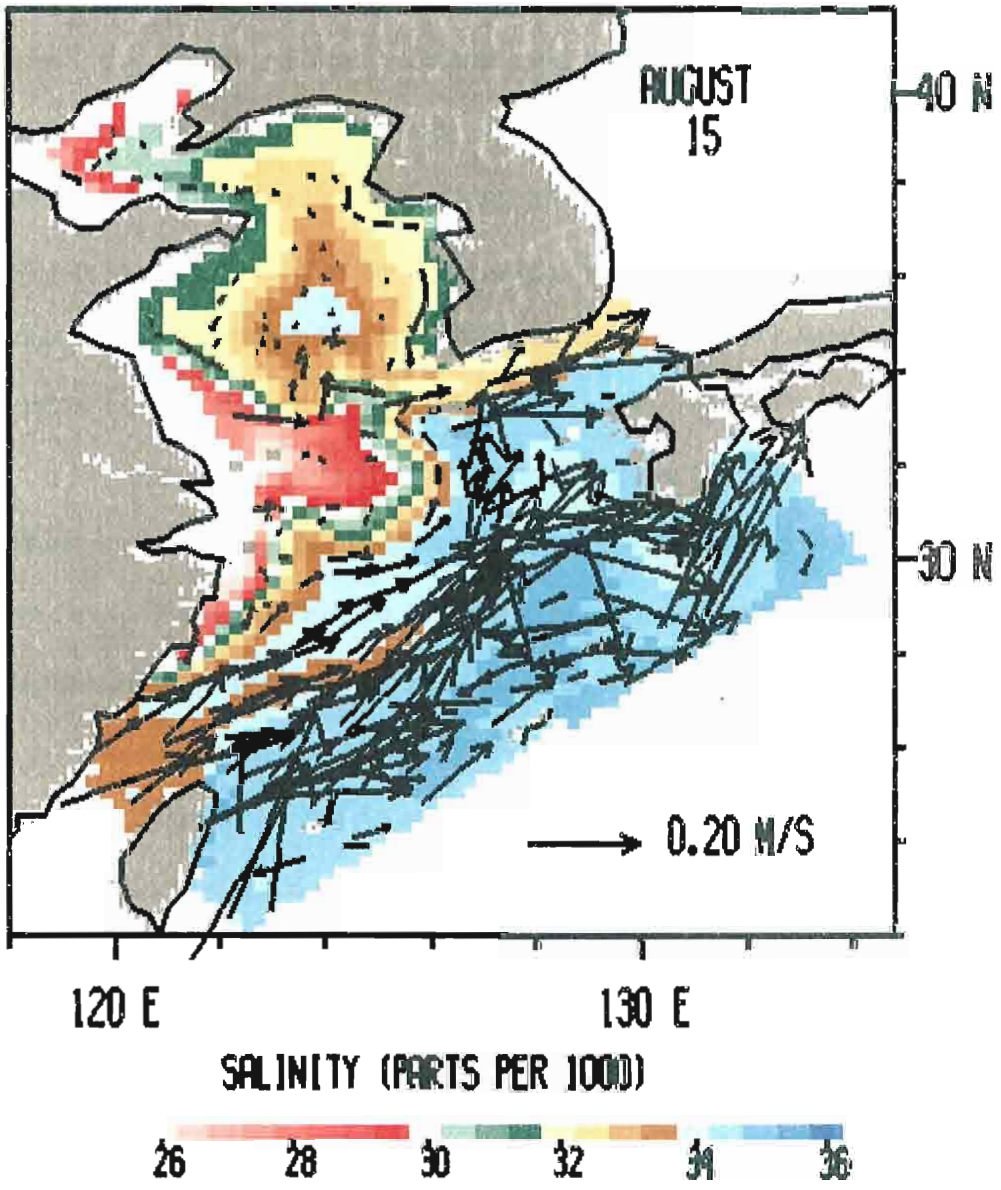


Figure 19: Salinity and currents at the surface for the no wind case on August 15, 1993. The arrows have been truncated for currents greater than 0.5 m/s.

Figure 19: Salinity and currents at the surface for the no wind case on August 15, 1993. The arrows have been truncated for currents greater than 0.5 m/s.

3.2 No Wind Case at the Surface

The currents in February (Figure 16) show, at the surface, a decrease in strength of the currents in the entire Yellow Sea basin. There is a small magnitude, when compared to the full wind case, Yellow Sea Warm Current that enters the Yellow Sea basin along the warm tongue. The Taiwan Warm Current, the Tsushima Warm Current and the Kuroshio are all well developed despite the lack of wind influence. In August (Figure 17), the Taiwan Warm Current, the Tsushima Warm Current, and the Kuroshio have increased strength as they did in the full wind case. The Yellow Sea Warm Current partially penetrates into the, but a flow across the basin caused by the Yangtze outflow disrupts the current.

In February (Figure 16), the temperature at the surface has a well defined warm tongue, but it does not penetrate as far into the basin as the full wind case. In August (Figure 17), there is not a definable warm tongue, most likely because of the Yangtze river outflow.

The salinity at the surface, in February (Figure 18), has a similar pattern as the temperature for the no wind case. Notice the lower salinity at the rivers' outflow regions when compared to the full wind case. In August (Figure 19), the salinity in the Yellow Sea is dominated by the Yangtze river outflow.

3.3 Full Wind Case at 20 m

In February (Figure 20), the Yellow Sea Warm Current is present almost all the way into the Bohai Sea. The southward moving Yellow Sea Coastal Current and the Korean Coastal Current are present. The Taiwan

almost all the way into the Bohai Sea. The southward moving Yellow Sea Coastal Current and the Korean Coastal Current are present. The Taiwan Warm Current, the Kuroshio, and the Tsushima Warm Current are present in

the February and August plots. In August (Figure 21), the Korean Coastal Current is not present, but the Yellow Sea Warm Current is still present, but it does not penetrate as far into the basin and appears less organized. The Yellow Sea Coastal Current is also still present. Also, note the outflow from the Yangtze River at approximately 32°N.

In February (Figure 20), there is a tongue of warm water at 20 m intruding deep into the Yellow Sea basin. In August (Figure 21), this tongue of warm water is not evident in the Yellow Sea basin, even though there is a hint of it at the entrance to the Yellow Sea. In both February and August the warmer water is along the path of a northward moving current.

In February (Figure 22), the salinity structure at 20 m depth is very similar to that of the temperature structure in February. In August (Figure 23), there is a salinity minimum at 20 m depth across the entrance to the Yellow Sea. This minimum is the result of the increased outflow of the Yangtze River in summer.

3.4 No Wind Case at 20 m

In February (Figure 24) and August (Figure 25) a well formed Kuroshio, Taiwan Warm Current, and Tsushima Warm Current are present just as in the full wind case. In February, the Yellow Sea Warm Current seems to barely penetrate the basin, then it turns toward Korea and exits out the Tsushima Strait unlike the full wind case. The Korean Coastal Current is still present, but the Yellow Sea Coastal Current is practically absent. In August, there is not only a northward current up the middle of the basin, but also along the Chinese coast. There is still turning of the Yellow Sea Warm Current toward

not only a northward current up the middle of the basin, but also along the Chinese coast. There is still turning of the Yellow Sea Warm Current toward the Tsushima Strait. The Korean Coastal Current is still present.

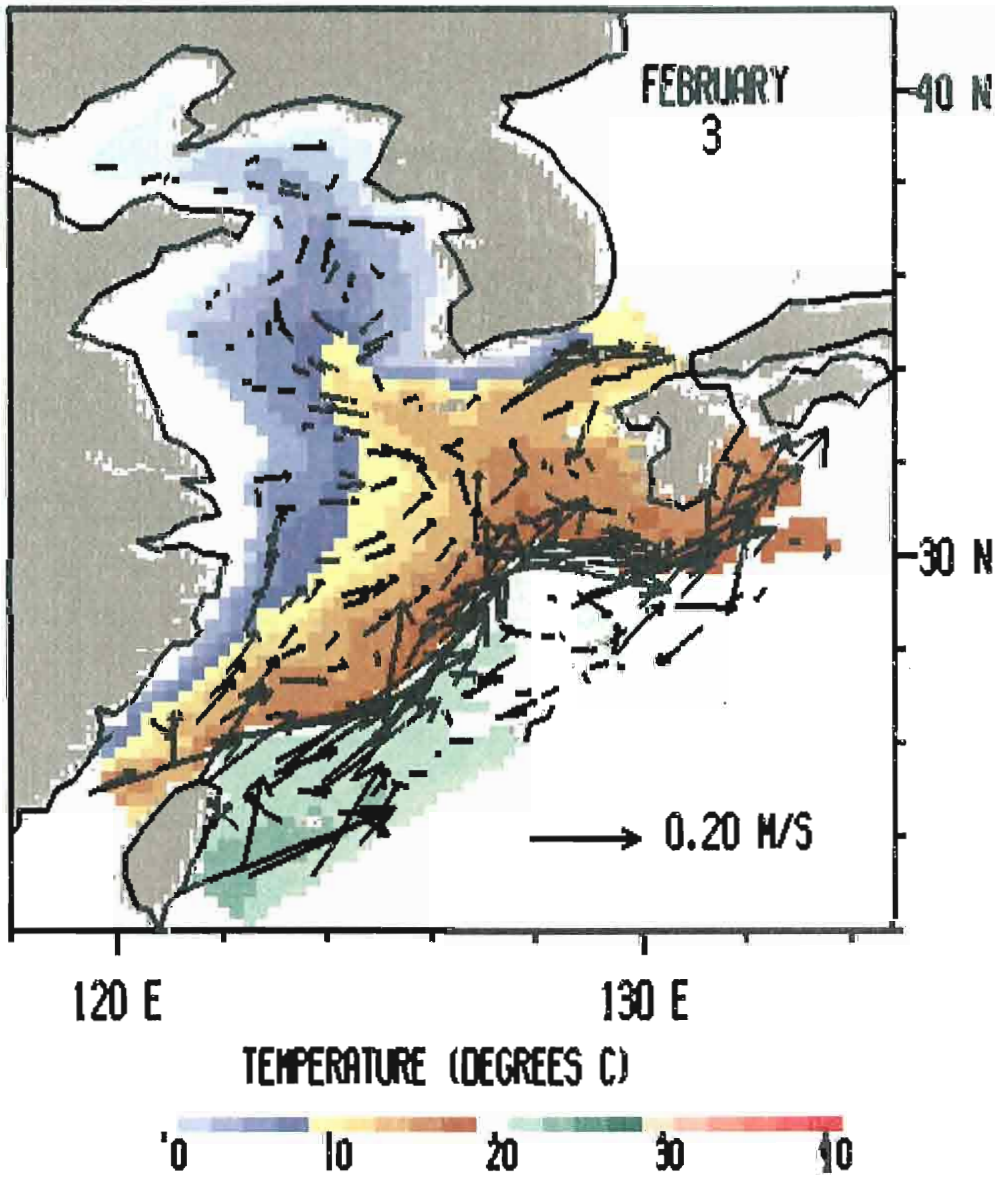


Figure 20: Temperature and currents at 20 m depth for the full wind case on February 3, 1993. The arrows have been truncated for currents greater than

Figure 20: Temperature and currents at 20 m depth for the full wind case on February 3, 1993. The arrows have been truncated for currents greater than 0.5 m/s.

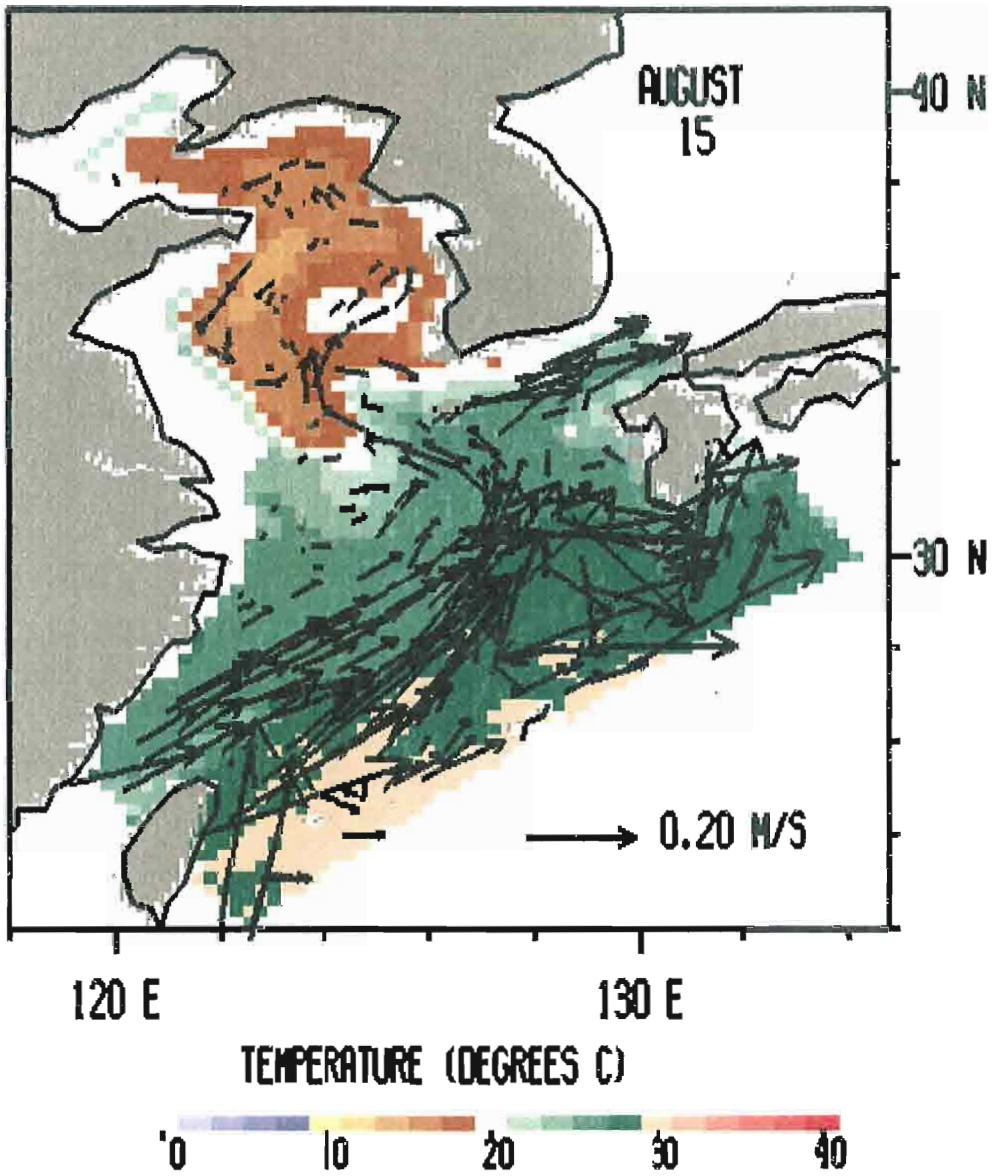


Figure 21: Temperature and currents at 20 m depth for the full wind case on

Figure 21: Temperature and currents at 20 m depth for the full wind case on August 15, 1993. The arrows have been truncated for currents greater than 0.5 m/s.

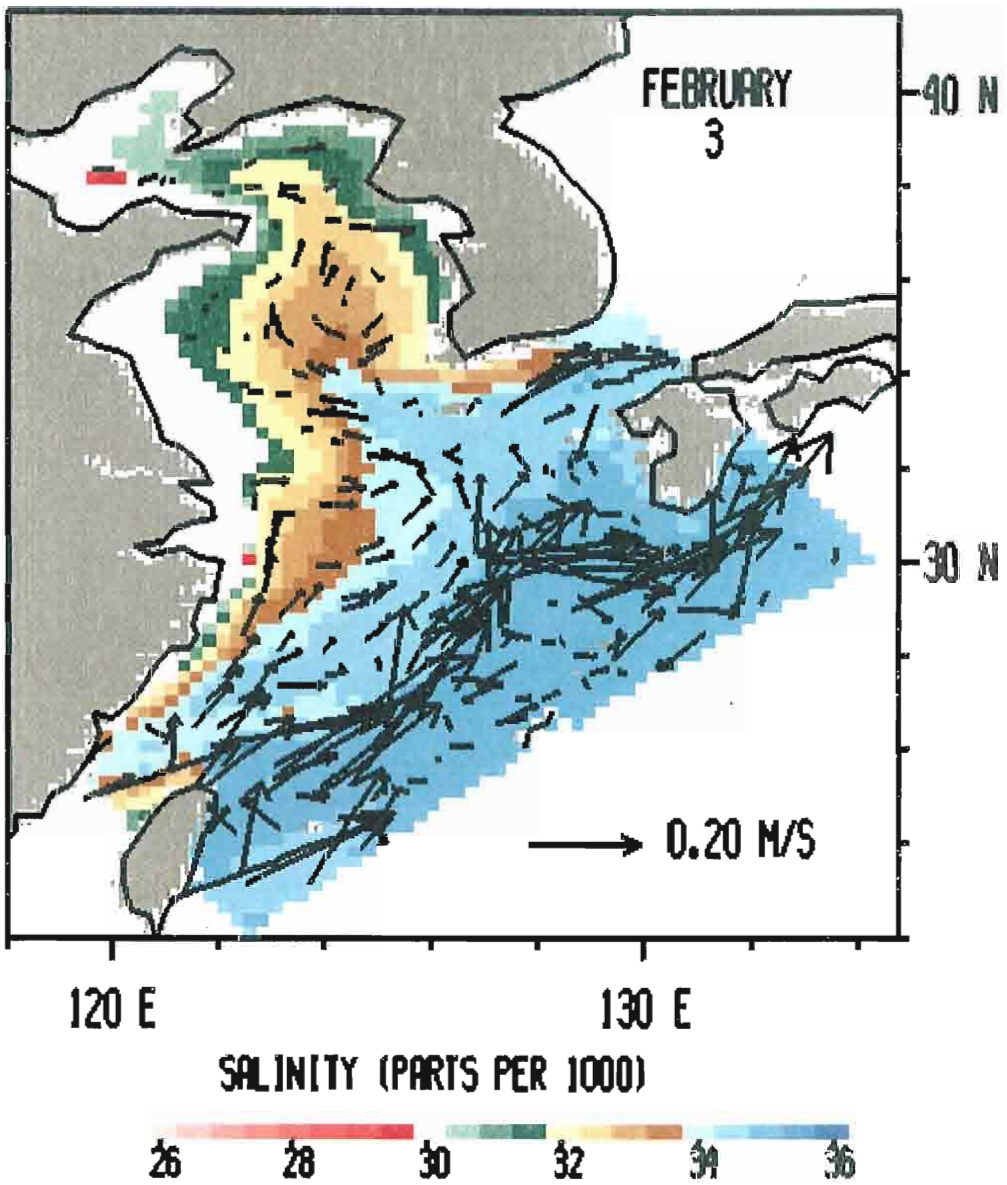


Figure 22: Salinity and currents at 20 m depth for the full wind case on February 3, 1993. The arrows have been truncated for currents greater than 0.5 m/s.

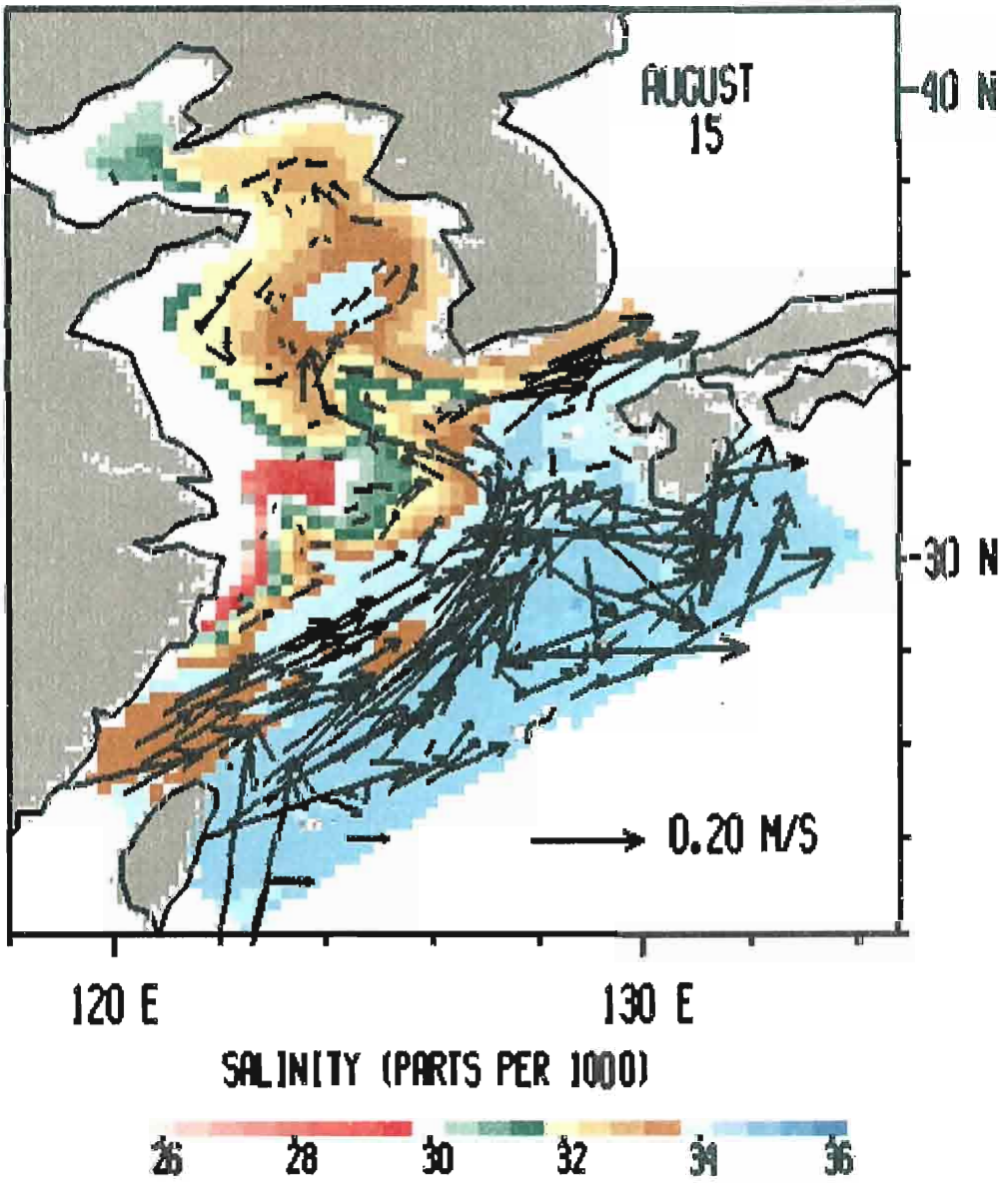


Figure 23: Salinity and currents at 20 m depth for the full wind case on August 15, 1993. The arrows have been truncated for currents greater than

Figure 23: Salinity and currents at 20 m depth for the full wind case on August 15, 1993. The arrows have been truncated for currents greater than 0.5 m/s.

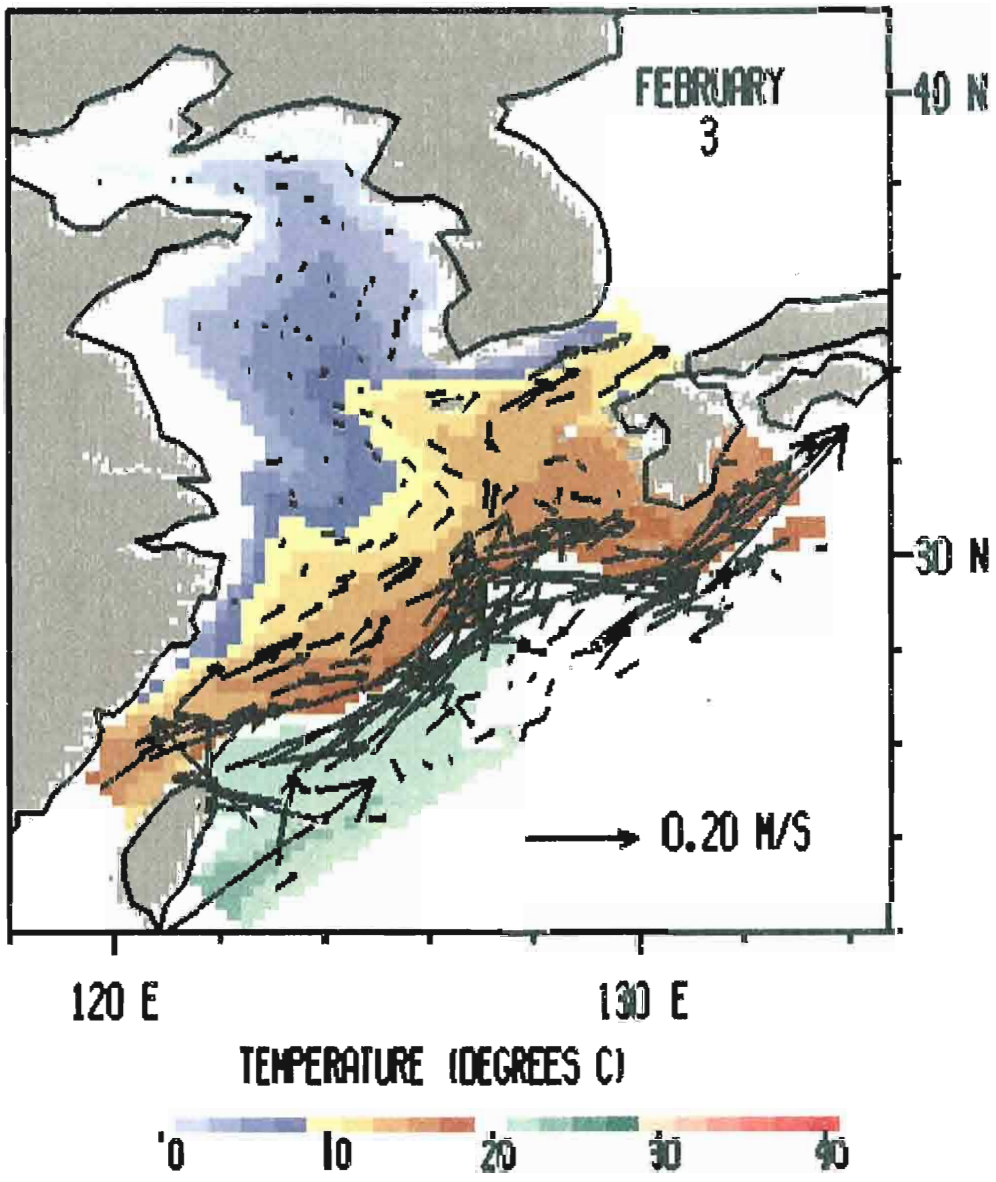


Figure 24: Temperature and currents at 20 m depth for the no wind case on February 3, 1993. The arrows have been truncated for currents greater than

Figure 24: Temperature and currents at 20 m depth for the no wind case on February 3, 1993. The arrows have been truncated for currents greater than 0.5 m/s.

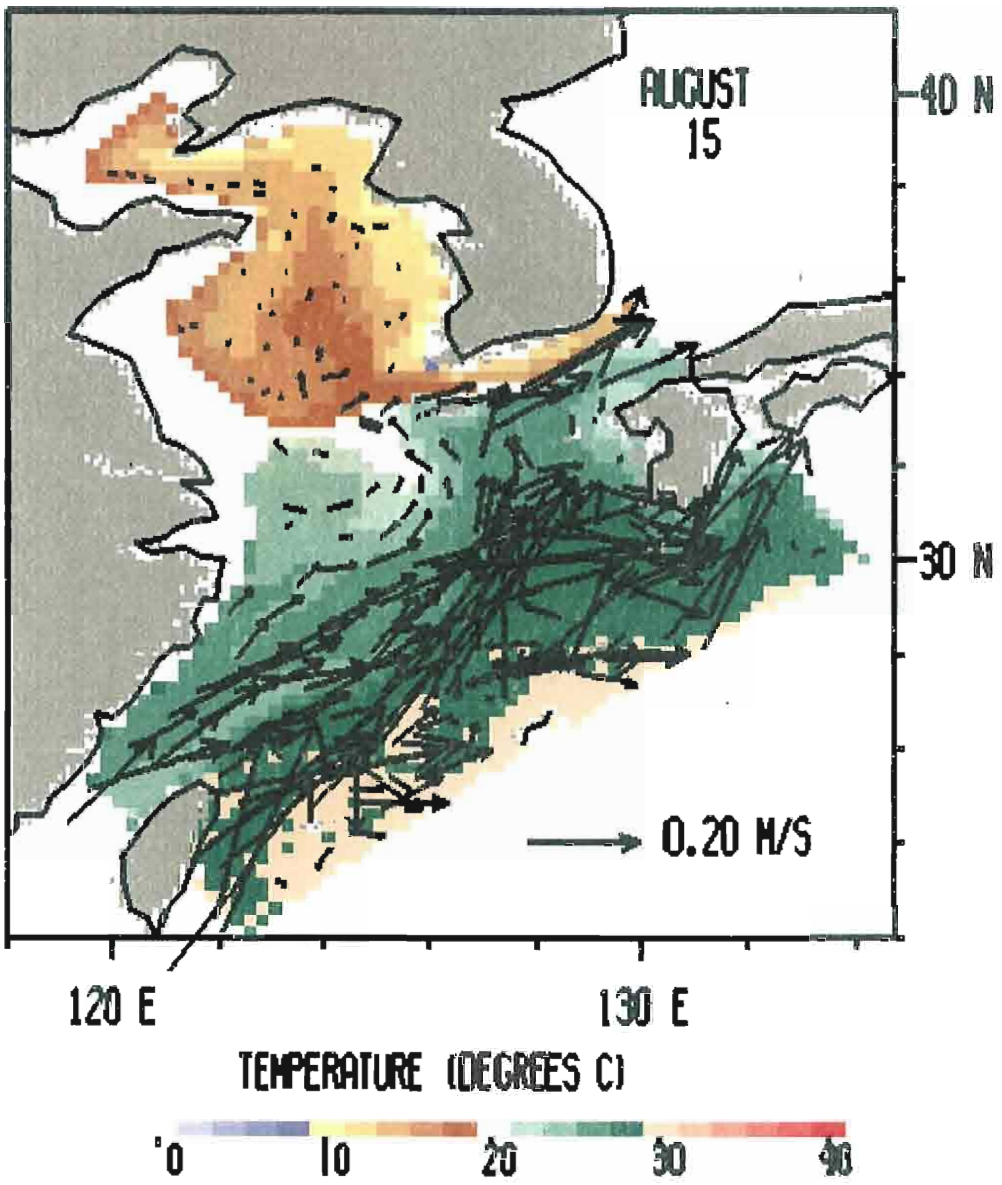


Figure 25: Temperature and currents at 20 m depth for the no wind case on August 15, 1993. The arrows have been truncated for currents greater than

Figure 25: Temperature and currents at 20 m depth for the no wind case on August 15, 1993. The arrows have been truncated for currents greater than 0.5 m/s.

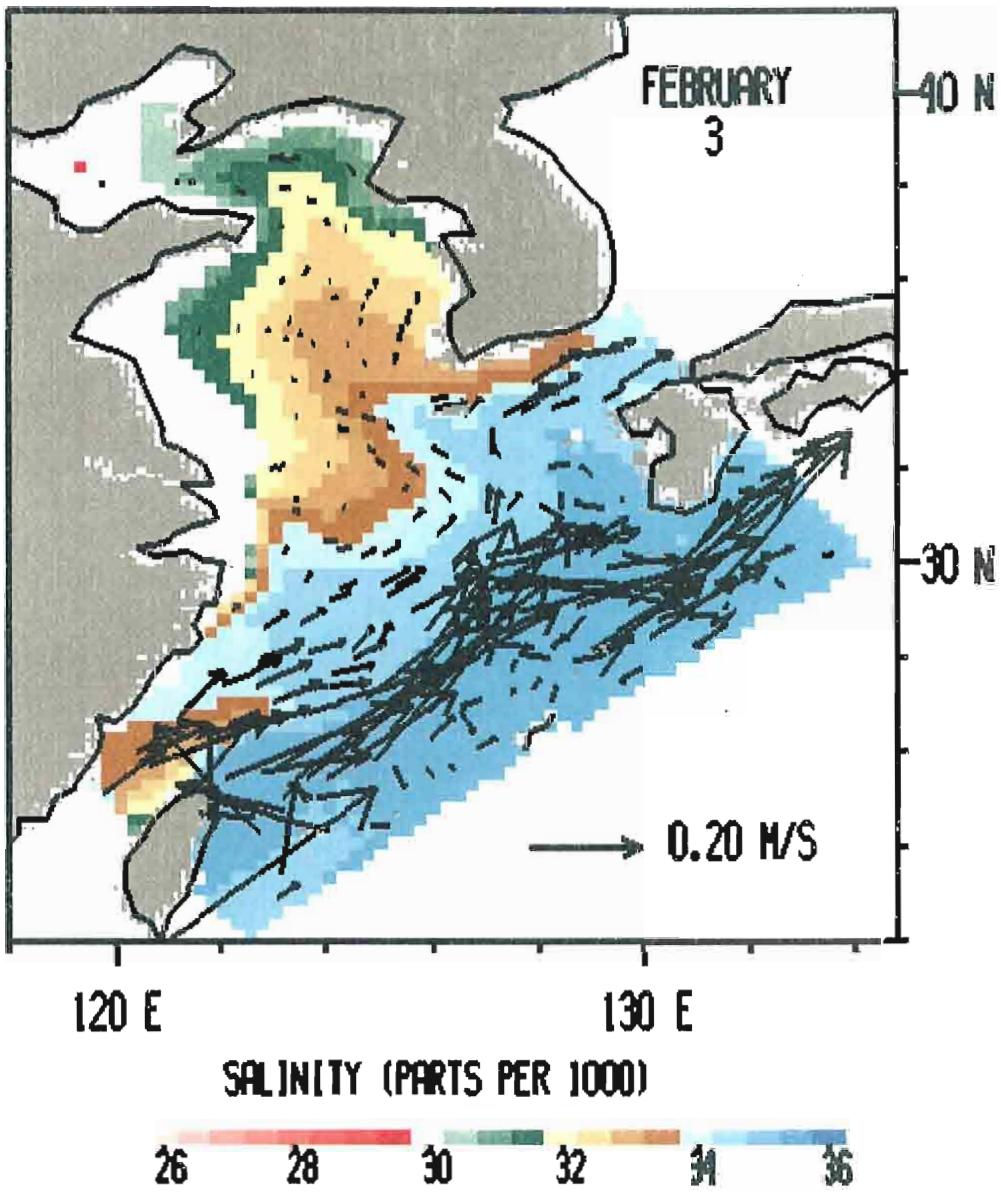


Figure 26: Salinity and currents at 20 m depth for the no wind case on February 3, 1993. The arrows have been truncated for currents greater than 0.5 m/s.

Figure 26: Salinity and currents at 20 m depth for the no wind case on February 3, 1993. The arrows have been truncated for currents greater than 0.5 m/s.

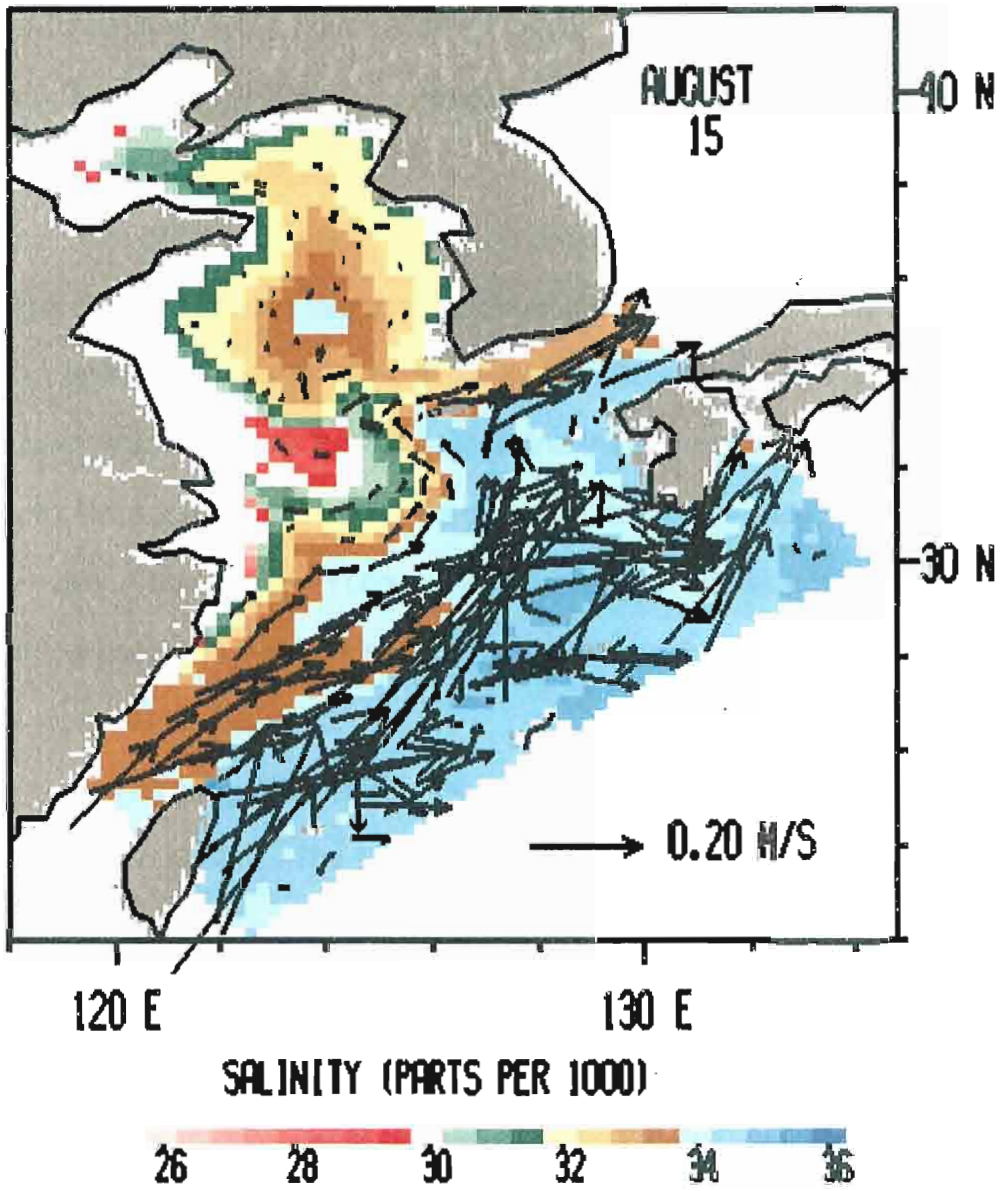


Figure 27: Salinity and currents at 20 m depth for the no wind case on August 15, 1993. The arrows have been truncated for currents greater than

Figure 27: Salinity and currents at 20 m depth for the no wind case on August 15, 1993. The arrows have been truncated for currents greater than 0.5 m/s.

In February (Figure 24), the tongue of warm water at 20 m depth has not intruded into the basin as far as the full wind case. In August (Figure 25), the warm tongue at 20 m depth is more organized than the full wind case.

In February (Figure 26), the salinity features at 20 m depth are similar to the temperature field for the no wind case. In August (Figure 27), the Yangtze River salinity crosses only half of the basin. Also, the salinity from the northern rivers are more evident along the coasts.

3.5 Full Wind Case at 50 m

The 50 m currents in February (Figure 28), shows the Yellow Sea Warm Current flowing into the Yellow sea basin approximately following the 60 m isobath. There is also a weak Korean Coastal Current at this depth. The Taiwan Warm Current, the Tsushima and the Kuroshio are still present at this depth. In August (Figure 29), the current patterns are very similar to those in February; however, the Yellow Sea Warm Current does not penetrate as far into the basin. In both February (Figure 28) and August (Figure 29) the warm tongues are well defined.

In February (Figure 30), the salinity again has the features of the temperature at 50m. The salinity in August (Figure 31), has a high salinity pool in the middle of the Yellow Sea.

3.6 No Wind Case at 50 m

In February (Figure 32) and in August (Figure 33) the currents at 50 m are very similar. The major difference being the increased strength of the Taiwan Warm Current, the Tsushima Warm Current, and the Kuroshio. Also notice that in winter and summer. the Yellow Sea Warm Current does not

Taiwan Warm Current, the Tsushima Warm Current, and the Kuroshio. Also notice that in winter and summer, the Yellow Sea Warm Current does not

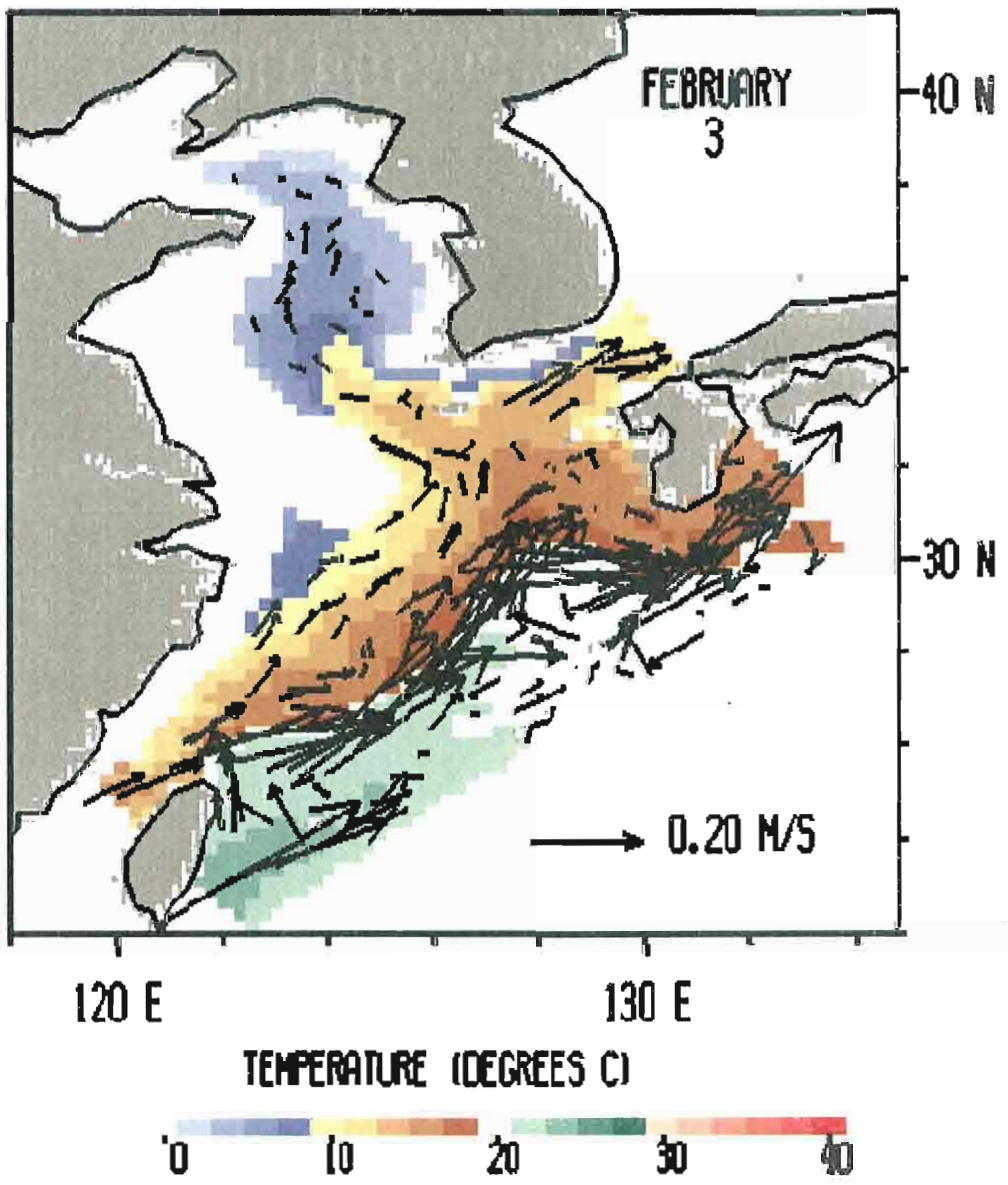


Figure 28: Temperature and currents at 50 m depth for the full wind case on February 3, 1993. The arrows have been truncated for currents greater than

Figure 28: Temperature and currents at 50 m depth for the full wind case on February 3, 1993. The arrows have been truncated for currents greater than 0.5 m/s.

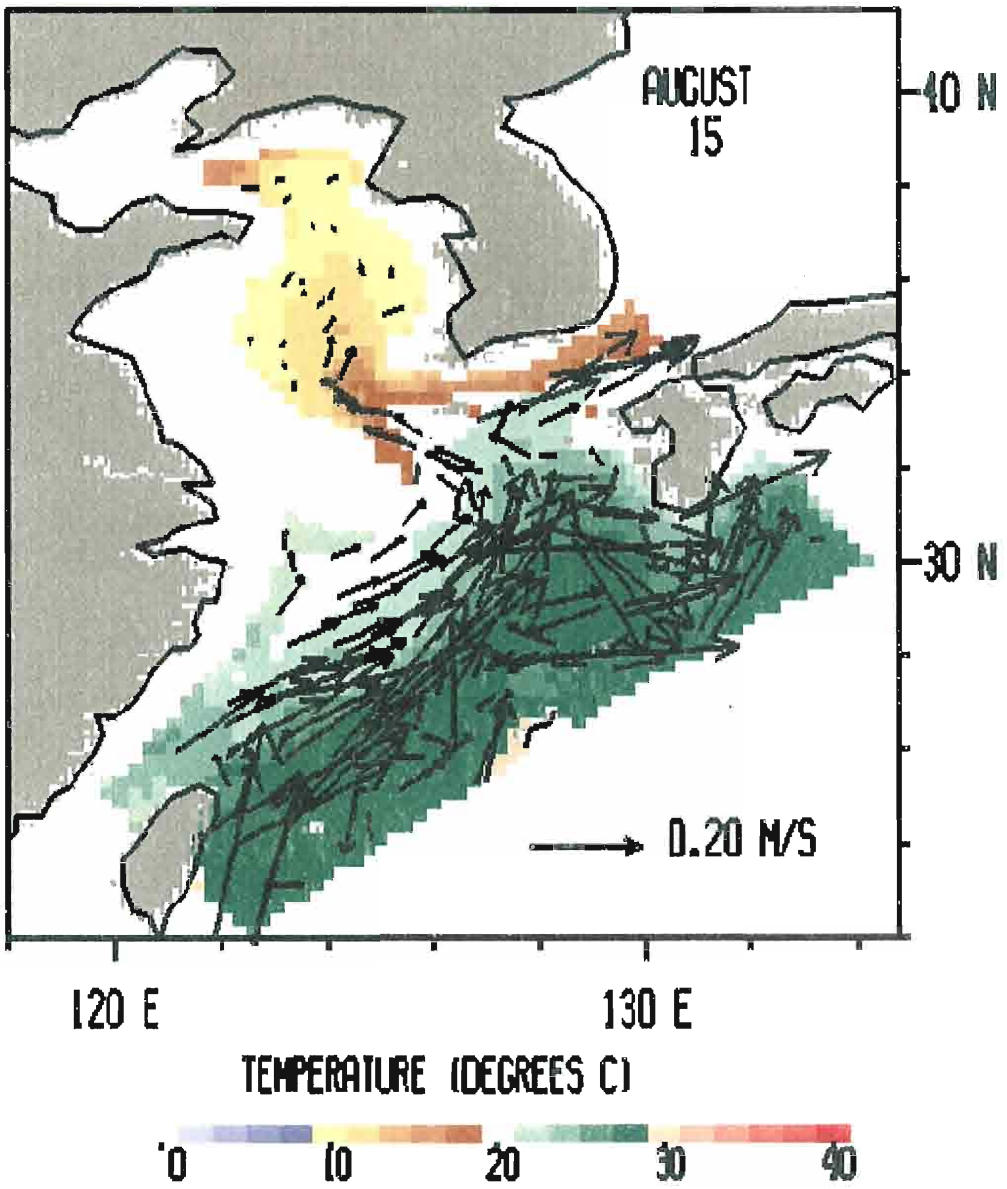


Figure 29: Temperature and currents at 50 m depth for the full wind case on August 15, 1993. The arrows have been truncated for currents greater than 0.5 m/s.

Figure 29: Temperature and currents at 50 m depth for the full wind case on August 15, 1993. The arrows have been truncated for currents greater than 0.5 m/s.

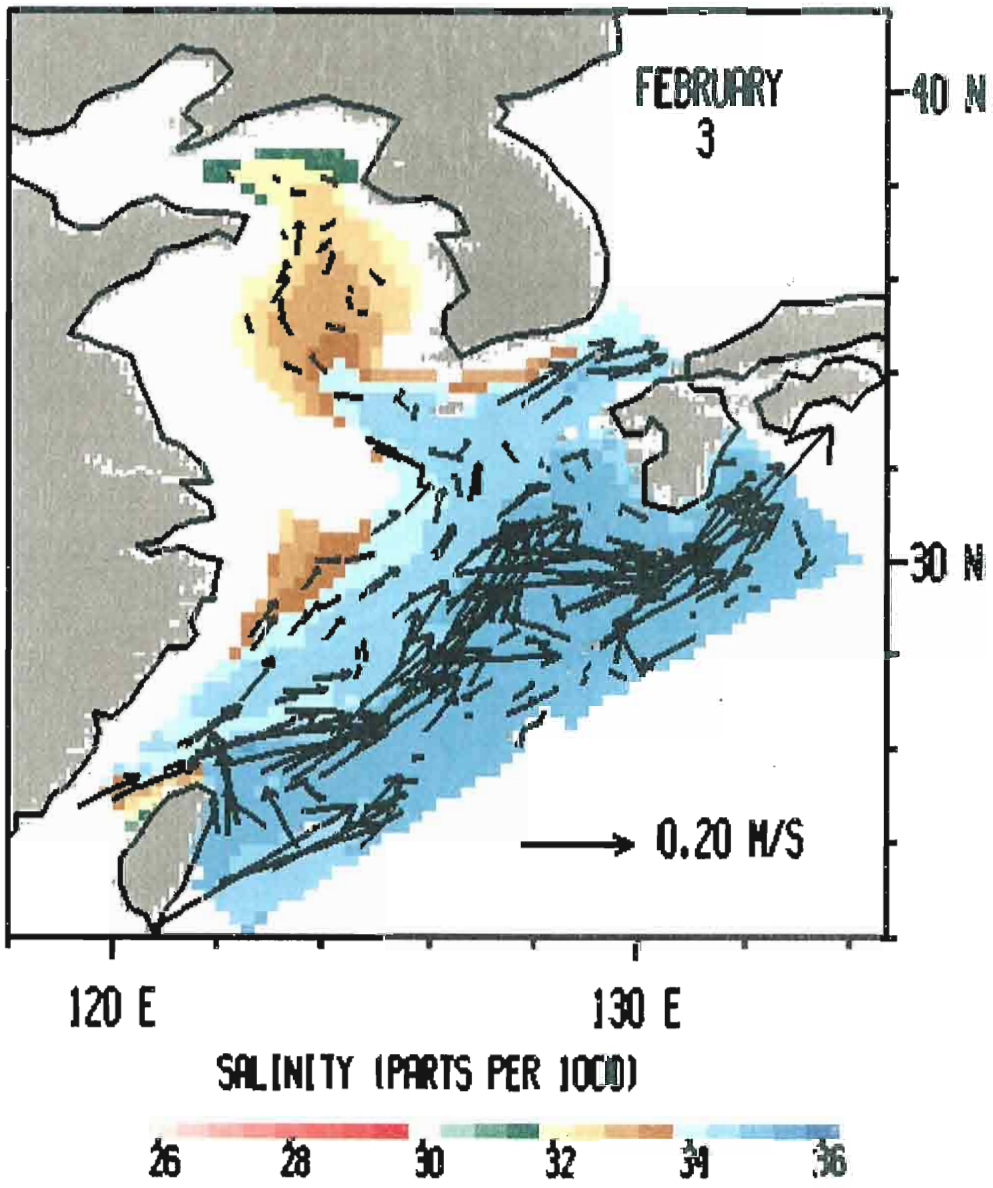


Figure 30: Salinity and currents at 50 m depth for the full wind case on February 3, 1993. The arrows have been truncated for currents greater than

Figure 30: Salinity and currents at 50 m depth for the full wind case on February 3, 1993. The arrows have been truncated for currents greater than 0.5 m/s.

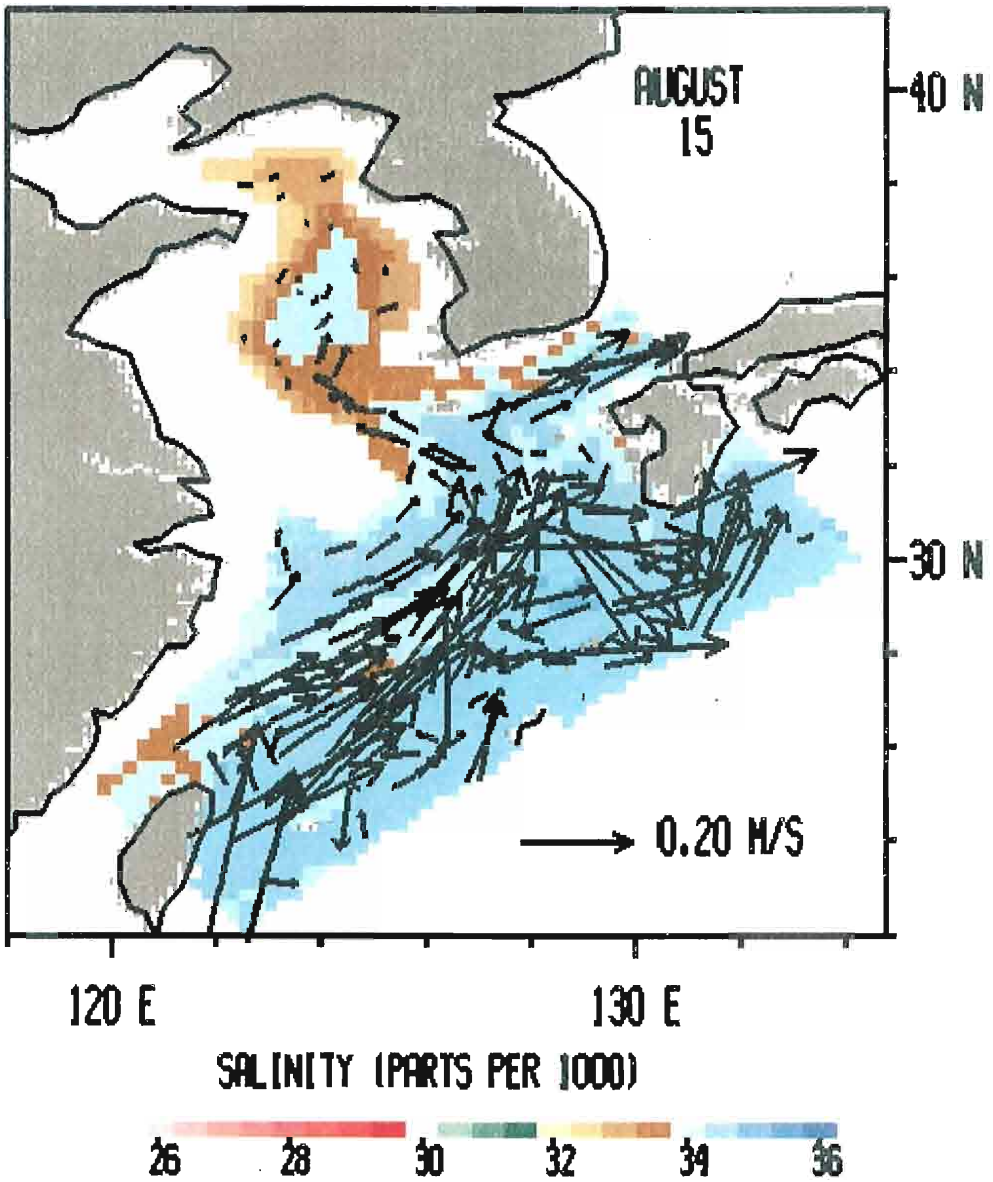


Figure 31: Salinity and currents at 50 m depth for the full wind case on August 15, 1993. The arrows have been truncated for currents greater than 0.5 m/s.

Figure 31: Salinity and currents at 50 m depth for the full wind case on August 15, 1993. The arrows have been truncated for currents greater than 0.5 m/s.

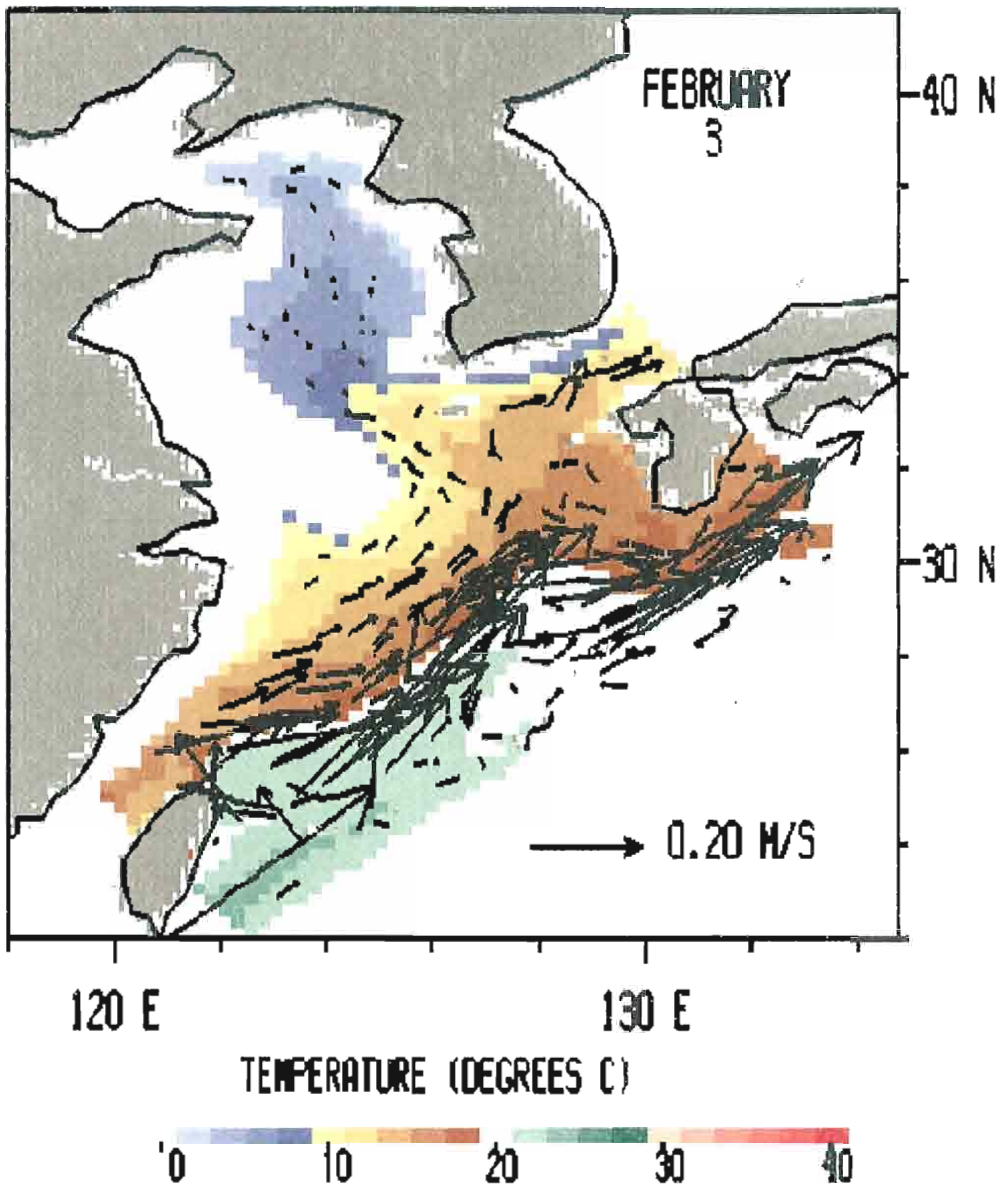


Figure 32: Temperature and currents at 50 m depth for the no wind case on February 3, 1993. The arrows have been truncated for currents greater than

0 10 20 30 40

Figure 32: Temperature and currents at 50 m depth for the no wind case on February 3, 1993. The arrows have been truncated for currents greater than 0.5 m/s.

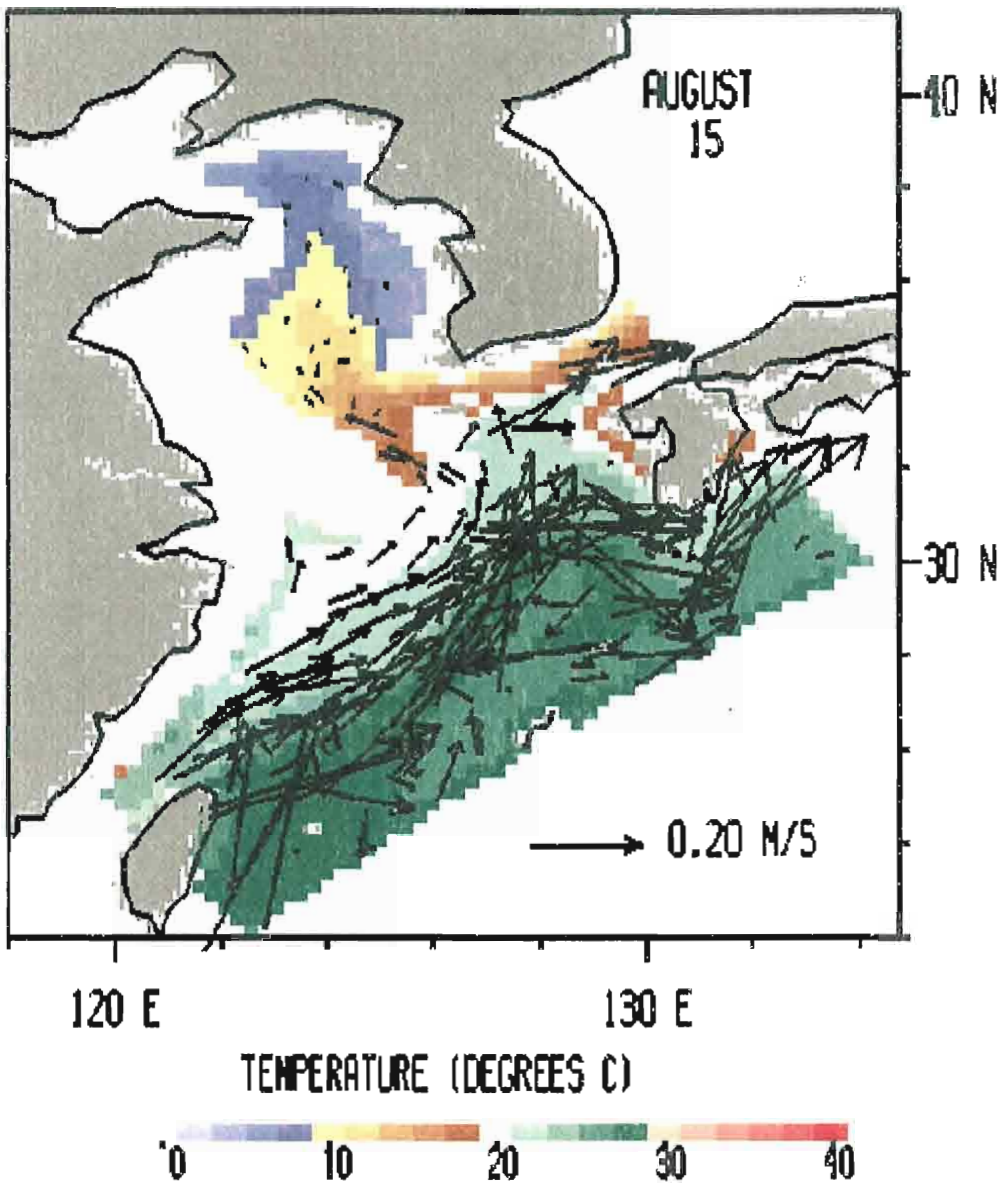


Figure 33: Temperature and currents at 50 m depth for the no wind case on August 15, 1993. The arrows have been truncated for currents greater than

Figure 33: Temperature and currents at 50 m depth for the no wind case on August 15, 1993. The arrows have been truncated for currents greater than 0.5 m/s.

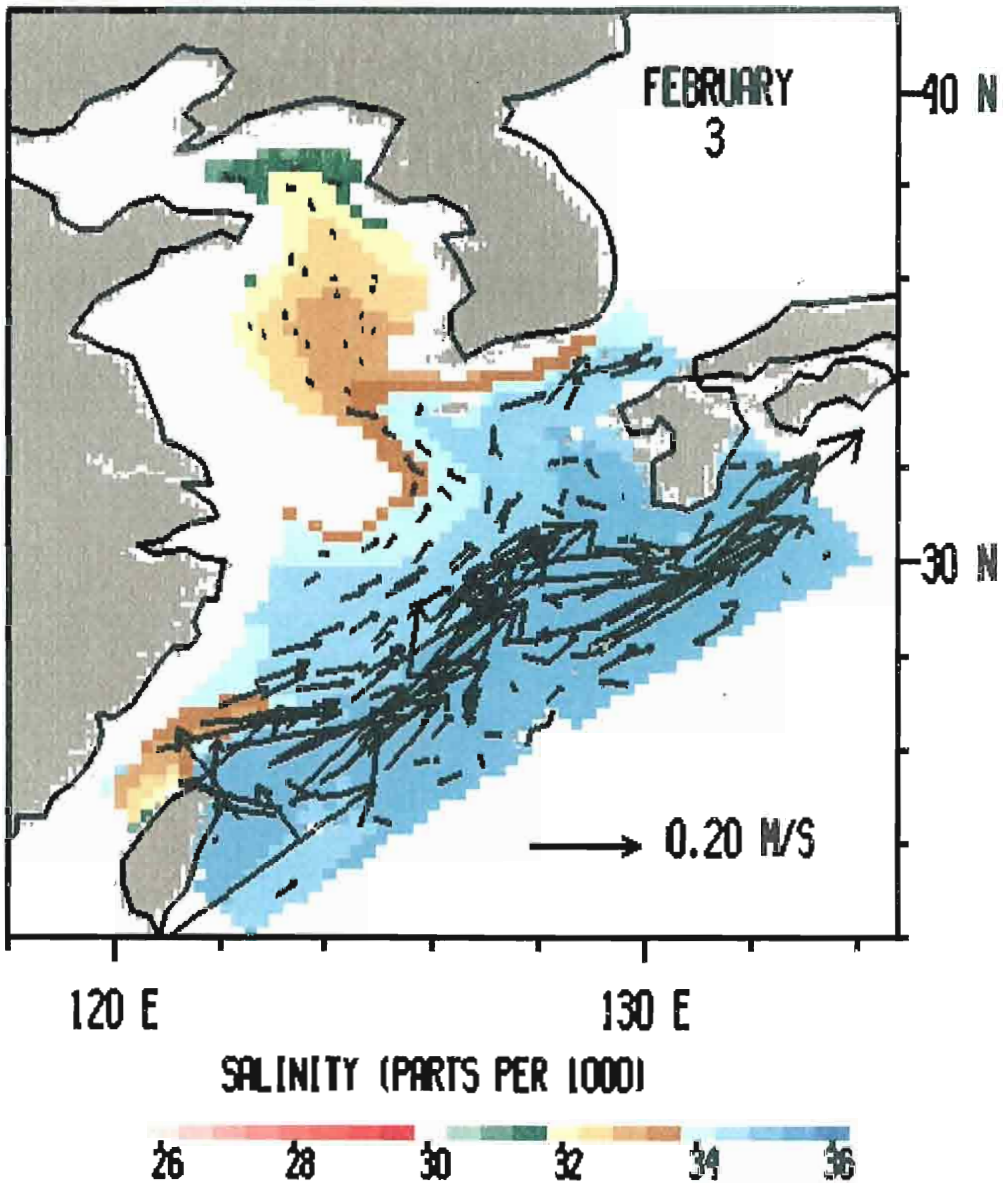


Figure 34: Salinity and currents at 50 m depth for the no wind case on February 3, 1993. The arrows have been truncated for currents greater than 0.5 m/s.

Figure 34: Salinity and currents at 50 m depth for the no wind case on February 3, 1993. The arrows have been truncated for currents greater than 0.5 m/s.

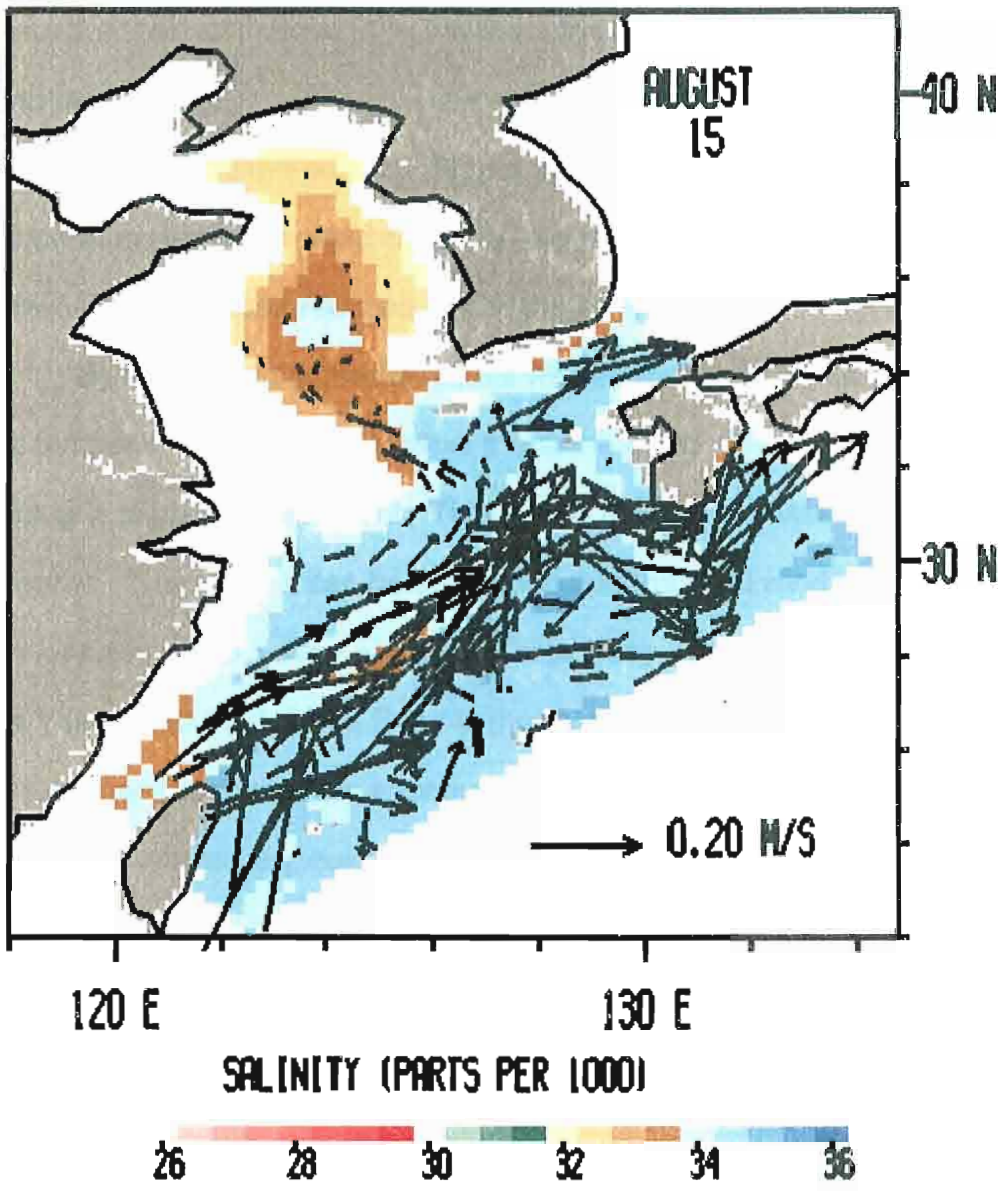


Figure 35: Salinity and currents at 50 m depth for the no wind case on August 15, 1993. The arrows have been truncated for currents greater than 0.5 m/s.

penetrate as far into the basin as with the full wind case.

The temperatures at 50 m in February (Figure 32) are very similar to the full wind case. The main difference being the warm tongue does not penetrate to the Bohai when no wind is applied. In August (Figure 33), the basin does not get above 10° C in the extreme northern region as when the wind is applied.

The salinity in February (Figure 34) follows the same patterns as the temperature for the no wind case. In August (Figure 35), the size of the high salinity pool has been reduced to half the size of that of the full wind case.

By looking at the model results we see that in all levels of the model, the temperature and salinity follow the same basic pattern whether the wind forcing was present or absent. This is also true for the basic positioning of the currents. Therefore, it can be concluded that the local wind is not what defines the features of the Yellow and East China Seas. What defines the features of the Yellow and East China Seas is mostly the boundary conditions. The initial climatology does not show a tongue-like structure of temperature or salinity, but one develops very quickly (within 10 days) in both the full and no wind cases.

## 4. YELLOW SEA WARM CURRENT INTRUSION

The two most common ways of defining the Yellow Sea Warm Current are one, by temperature and salinity and two, by the current's velocity. Depending on the definition, very different intrusions are found. To study the maximum penetration of the Yellow Sea Warm Current, both definitions are examined. First, the water mass characteristics of Su and Wang (1994) were used. Those characteristics are for the surface water and are given as:

| Period | Temperature | Salinity |
|---|---|---|
| June - November | $T > 21^\circ$ C | S > 33.5 ppt |
| December - May | $12^\circ$ C < T < $21^\circ$ C | S > 33.5 ppt |

The monthly average of temperature and salinity were used to make Figures 12 and 13. February (Figure 36) shows that the full wind case penetrates to 34°N, which is also the penetration suggested by Hsueh (1988). The no wind case's penetration is to 33°N. August (Figure 37) shows the full wind case penetrates to 32°N. The no wind case's penetration is to 33°N. The pools of water in the Yellow Sea basin are the result of the temperature being slightly warmer in the model than real measurements (approximately 1° C). If the summer condition had been T > 22°C these pools would not appear. This temperature problem was found during validity tests of the model completed at

summer condition had been T > 22°C these pools would not appear. This temperature problem was found during validity tests of the model completed at NRL.

Second, the Yellow Sea Warm current was defined as velocities at 20 m depth with magnitudes less than 0.5 kts (~ 0.25 m/s) and an arctangent (v/u) between 0° and 180°. The magnitude came from the Encyclopedia of Oceanography and the angle was chosen broadly since most of the flow in the Yellow Sea basin is either northward or southward and very little eastward or westward flow. In February (Figure 38), the flow continues into the Bohai Sea in the full wind case. The no wind case does not penetrate into the Bohai Sea and the path of the flow is to the west of the path of the full wind case. In August (Figure 39), the flow for the full wind case does not continue to the Bohai Sea, but instead gets caught in the Bay of Korea. The no wind case still has a flow path further to the west and continues into the Bohai Sea.

From these results we can see that for the water mass definition, in winter the wind seems to force temperature and salinity into the basin. While in summer the wind keeps the water mass out of the Yellow Sea. For the velocity definition, the wind seems to be a steering force in both winter and summer. In winter, the wind forces the current further to the west. In summer, it is pushed so far to the west that it cannot continue into the Bohai Sea. In the summer this picture can easily be understood by Ekman transport. During this period the wind is predominately from the south, so as the flow turns right under the wind, the current is pushed to the east.

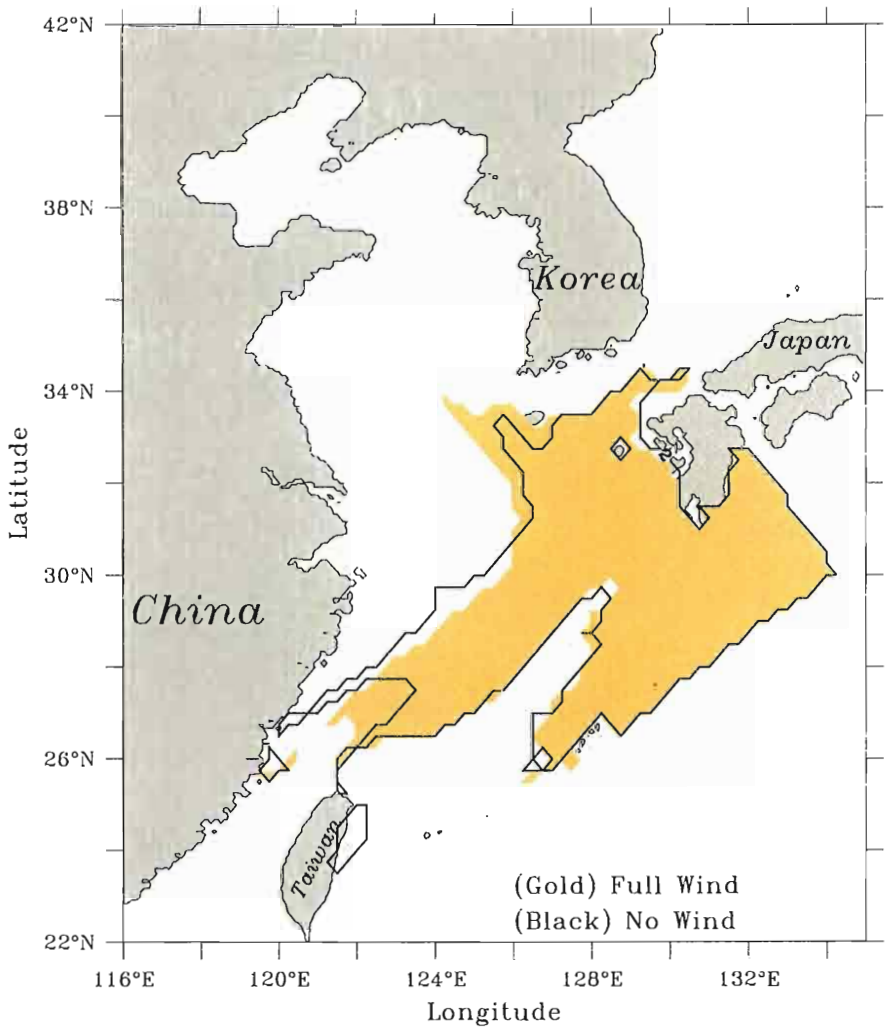


Figure 36: February's monthly averaged Yellow Sea Warm Current water mass properties. The gold shaded area is the area defined by the water mass properties for the full wind case. The black outline is the area defined by the water mass properties for the no wind case.

properties for the full wind case. The black outline is the area defined by the water mass properties for the no wind case.

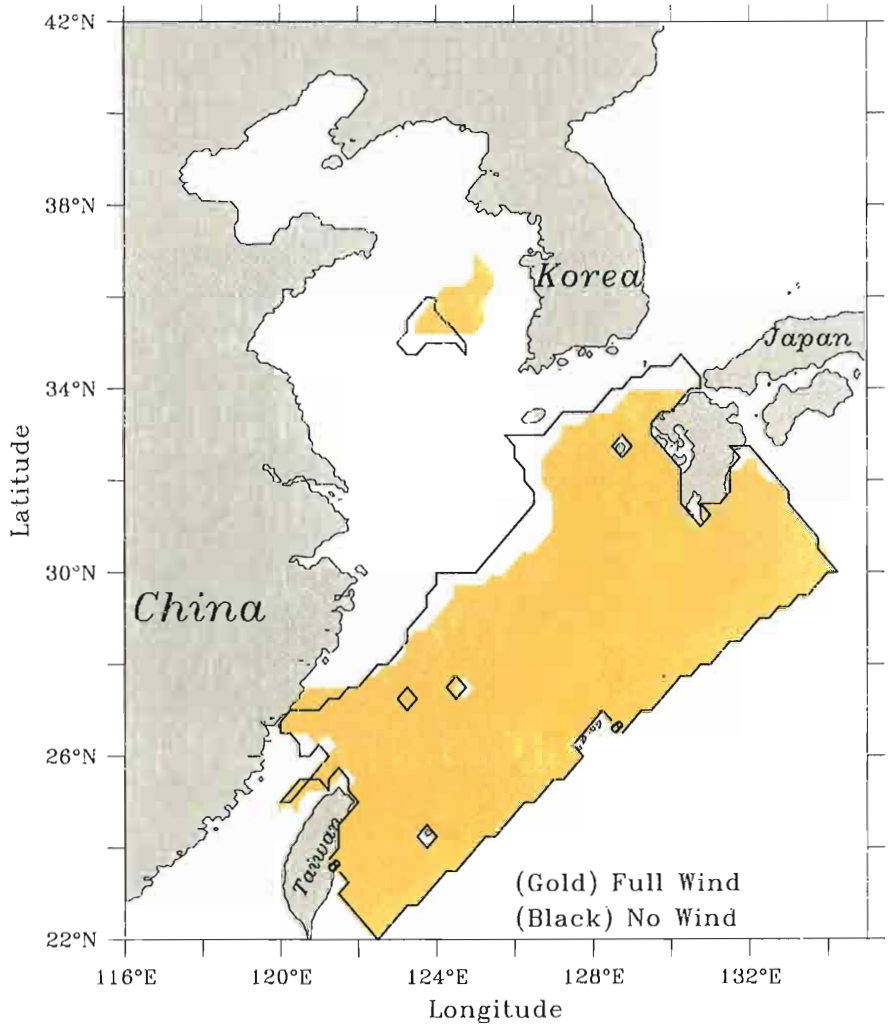


Figure 37: August's monthly averaged Yellow Sea Warm Current water mass properties. The gold shaded area is the area defined by the water mass properties for the full wind case. The black outline is the area defined by the water mass properties of the no wind case.

properties for the full wind case. The black outline is the area defined by the water mass properties of the no wind case.

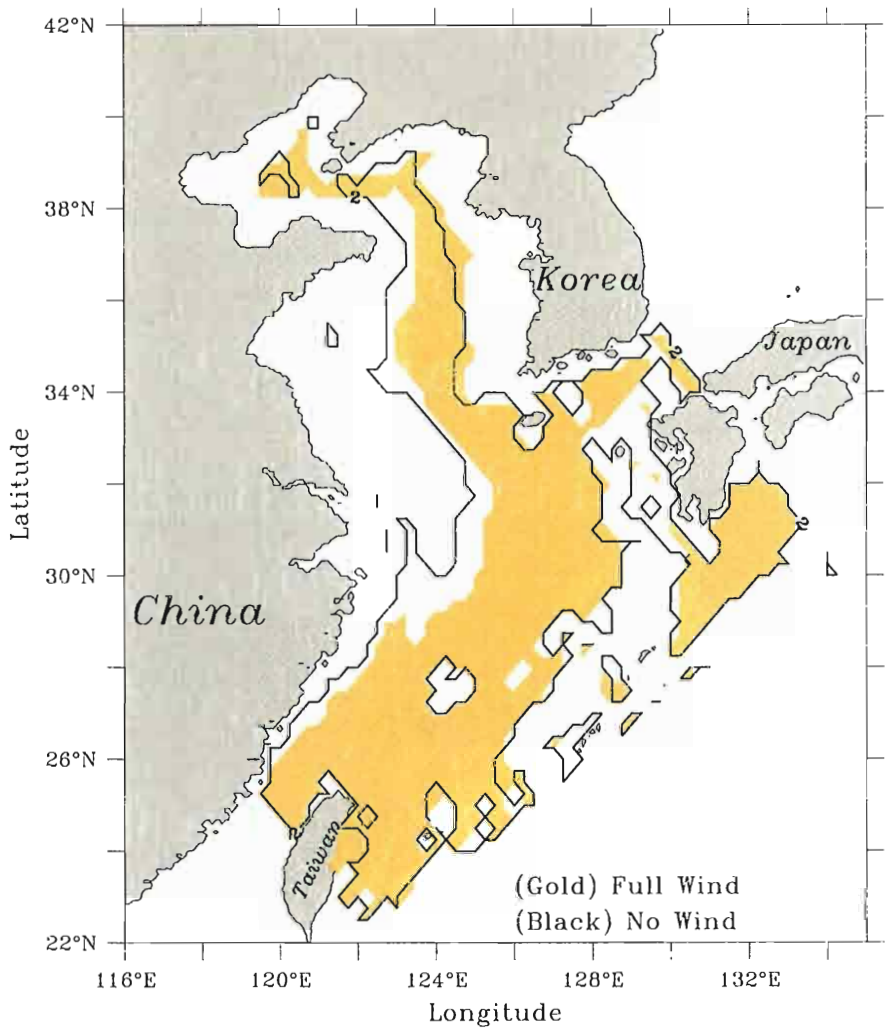


Figure 38: February's monthly averaged northward velocities. The gold shaded area is the area of northward moving water for the full wind case. The black outline is the area of northward moving water for the no wind case.

black outline is the area of northward moving water for the no wind case.

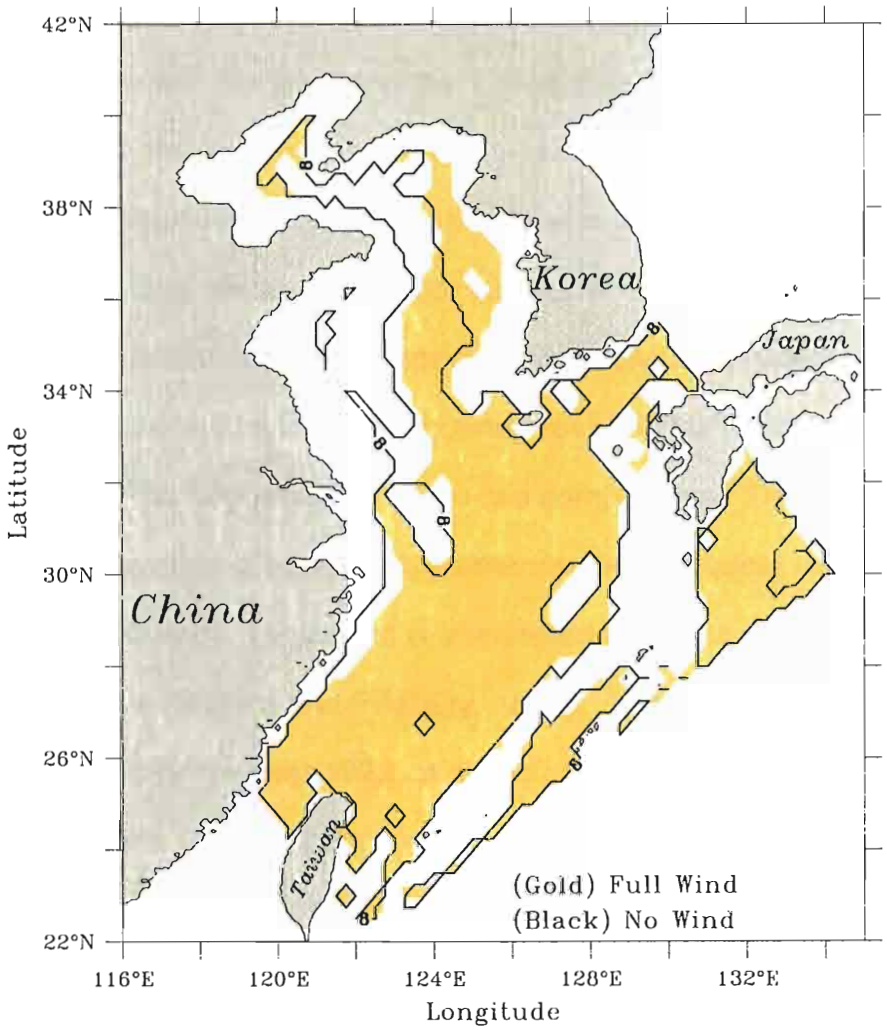


Figure 39: August's monthly averaged northward velocities. The gold shaded area is the area of northward moving water for the full wind case. The black outline is the area of northward moving water for the no wind case.

outline is the area of northward moving water for the no wind case.

# 5. WIND AND THE YELLOW SEA WARM CURRENT RELATIONSHIP

Rotary spectra and coherences were employed to investigate the relationship between the wind and the Yellow Sea Warm Current. This investigation on the Yellow Sea Warm Current was performed at 20 m depth so as to be in a relatively steady current. This is desired because spikes and quick jumps or drop offs are difficult for fast fourier transforms (FFT's) to analyze. Also, recall that a rotary spectrum is a way to represent a vector time series as a variance spectrum in frequency space. This is done by dividing the variance of the frequency band into two components. The negative frequency component is interpreted as the clockwise rotating variance, and the positive frequency component is interpreted as the counter-clockwise rotating variance (O'Brien and Pillsbury, 1974). This investigation was done with daily output for the year 1993, at six points that represent not only the Yellow Sea Warm Current, but other major currents in the model region that maybe influencing the Yellow Sea Warm Current (Figure 40). Of the points chosen, points 1 and 2 represent the Yellow Sea Warm Current. Point 1 is in the Yellow Sea Warm Current in winter when the water mass definition is used, and point 2 is approximately in the center of the area defined by the northward velocity. Points 3 and 5 are representative of the Taiwan Warm Current. Point 4 is representative of the Tsushima Warm Current in an area

northward velocity. Points 3 and 5 are representative of the Taiwan Warm Current. Point 4 is representative of the Tsushima Warm Current in an area

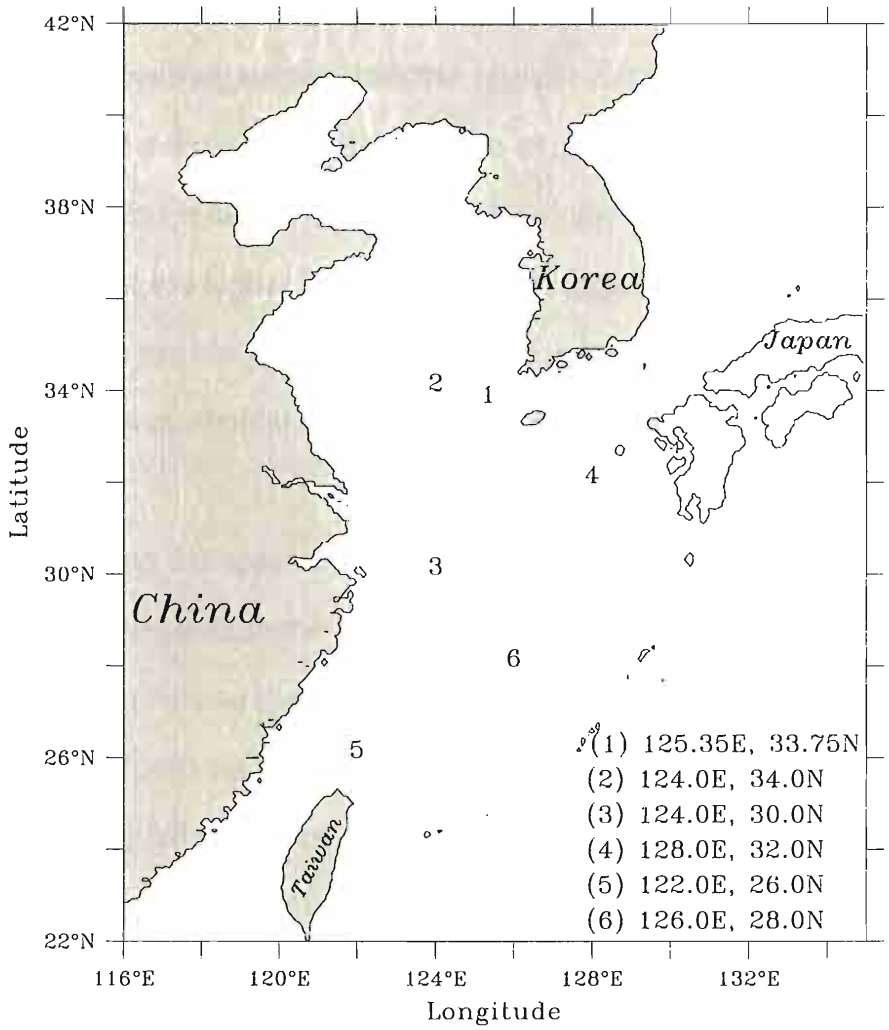


Figure 40: Points chosen to study relationship between the wind and the Yellow Sea Warm Current.

considered the water mass "source" for the Yellow Sea Warm Current. Point 6 is representative of the Kuroshio.

5.1 Rotary Spectra

Looking at the rotary spectra of the wind we find that there are two general patterns, one over the Yellow Sea and another over the East China Sea. Over the Yellow Sea (Figure 41a), the clockwise rotation has more energy at the low frequencies than the counter-clockwise rotation. This is not the case over the East China Sea (Figure 41b). Over the East China Sea, the counter-clockwise rotation has the majority of the energy at the low frequencies. At the higher frequencies, both regions appear to have slightly more energy in the clockwise rotation. Also, notice over the Yellow Sea that there are peaks at approximately 11 and 6 days in the higher frequency region.

Examining the spectra of the currents we find at point 1 (Figure 42a) the clockwise rotation in both the full and no wind cases have the greatest amount of energy at low frequencies. At point 2 ( Figure 42b) the full wind case has more energy in both rotations than the no wind case at low frequencies. Point 3's (Figure 42c) full wind case has much more energy than the no wind case, which is practically zero, at low frequencies. The low frequencies at point 4 (Figure 42d) show higher energy in the counter-clockwise rotations of both the full and no wind cases. For point 5 (Figure 42e) the counter-clockwise rotation of the full wind case has more energy at low frequencies, but the no wind case has more energy in the clockwise rotation. At point 6 (Figure 42f) only the full wind case's counter-clockwise rotation does not have a high energy

has more energy in the clockwise rotation. At point 6 (Figure 42f) only the full wind case's counter-clockwise rotation does not have a high energy

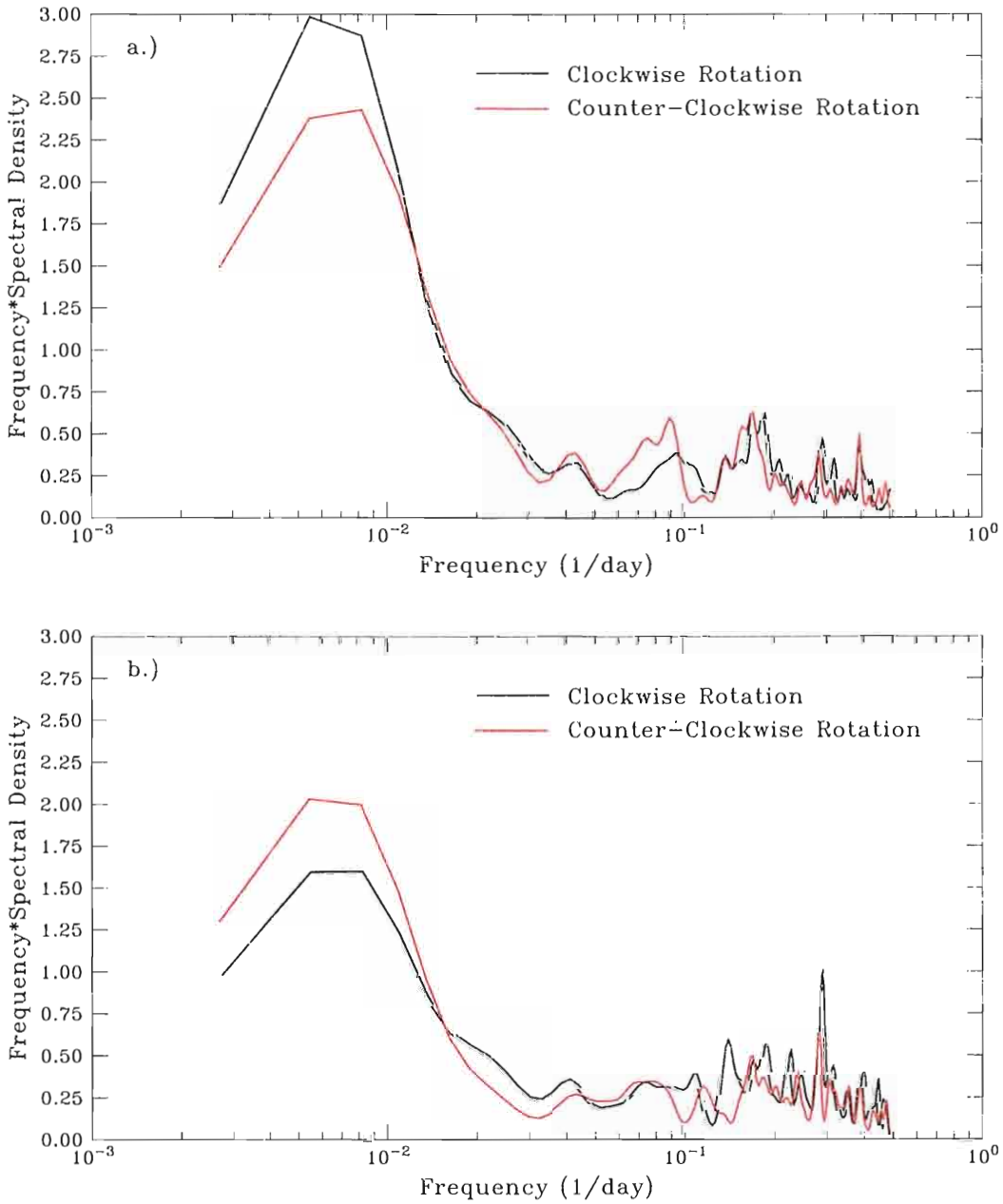


Figure 41: Rotary Spectra of the wind at a.) point 2 (124.0E, 34.0N) and b.) at

Frequency (1/day)

Figure 41: Rotary Spectra of the wind at a.) point 2 (124.0E, 34.0N) and b.) at point 6 (126.0E, 28.0N) with prewhitening and six hanning windows.

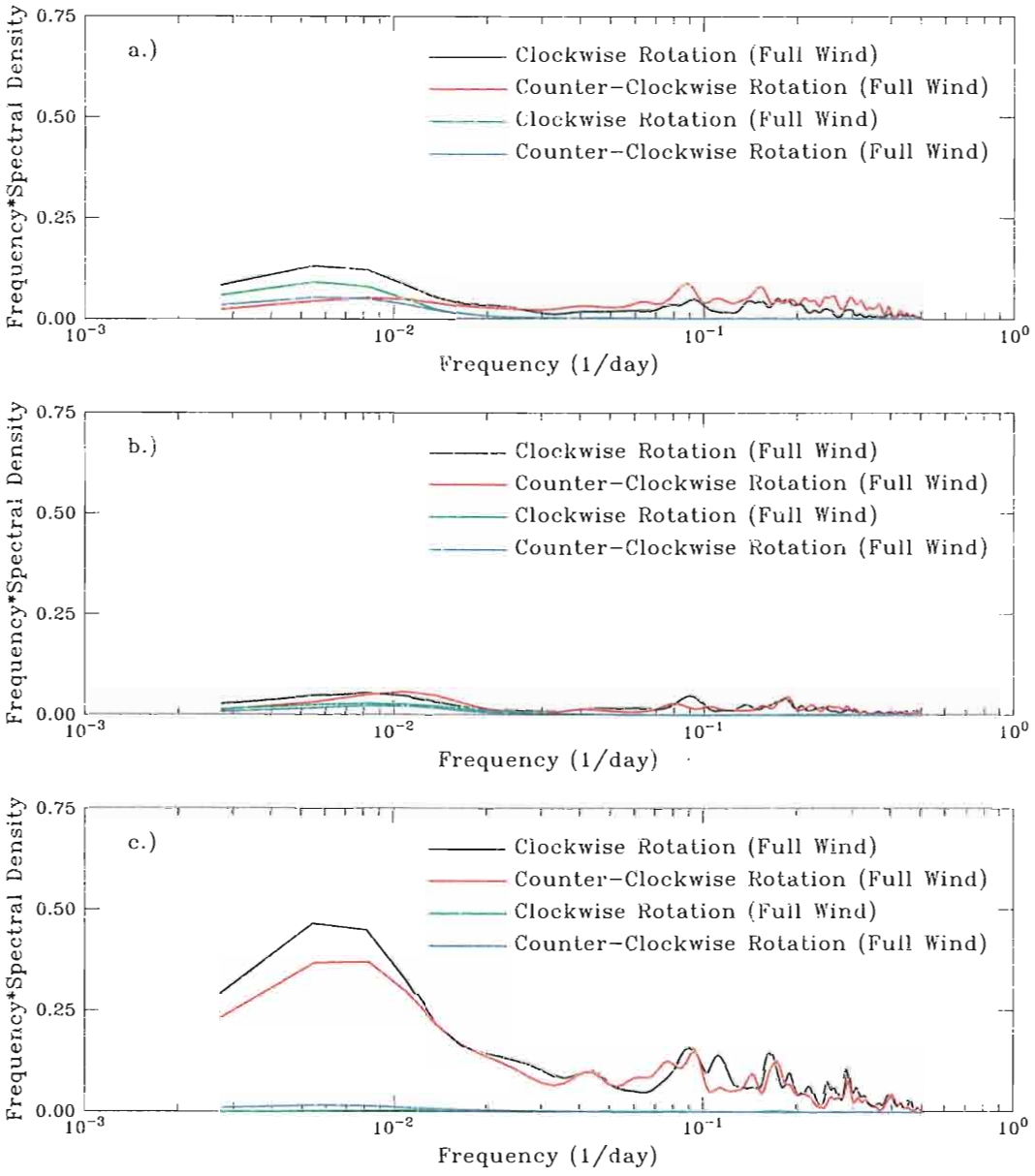


Figure 42: Rotary Spectra with prewhitening and 6 hanning windows of the full

Figure 42: Rotary Spectra with prewhitening and 6 hanning windows of the full wind case and the no wind case at a.) point 1 (125.35E, 33.75N), b.) point 2 (124.0E, 34.0N), c.) point 3 (124.0E, 30.0N)

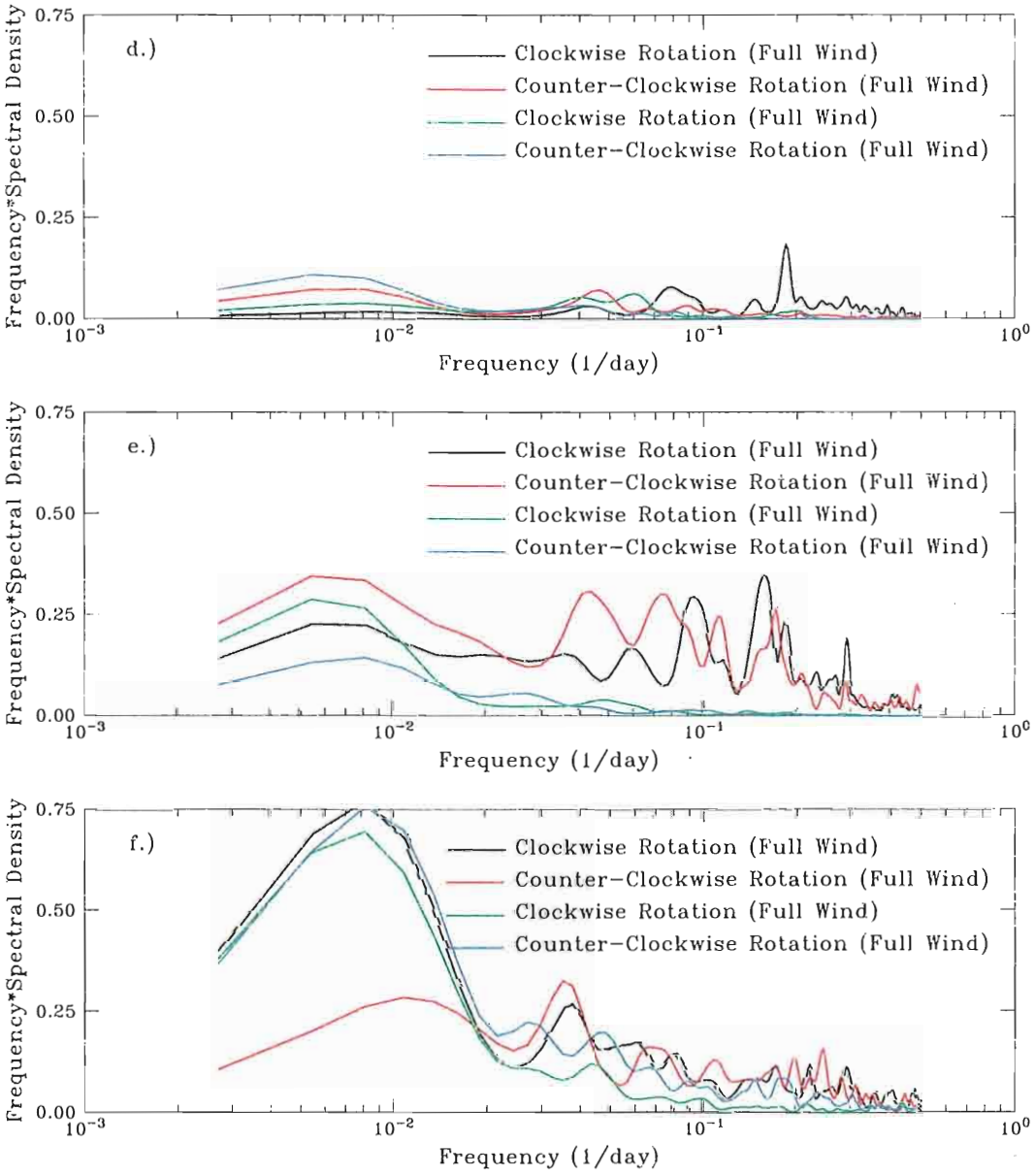


Figure 42 cont. : d.) point 4 (128.0E, 32.0N), e.) point 5 (122.0E, 26.0N) and f.) point 6 (126.0E, 28.0N).

level at low frequencies. Notice at high frequencies that the no wind case drops off to zero at all points. In the full wind case, at all points but 6, there are peaks at 11 and 6 days in either the clockwise or counter-clockwise rotation.

5.2 Coherency

The rotary spectra of the wind shows two patterns, one for the Yellow Sea and another for the East China Sea. The coherence (Mooers, 1973) shows how these two patterns are interconnected. These comparisons are at the 99% significance level of 0.319 (Thompson, 1979) First, note that when comparing the wind at point 1 with that of point 2 (Figure 43a) that there is full coherence, as one would expect. The coherence between points 1 and 2 and the points in the East China yield very similar results, thus the discussion will only include the interconnection of the winds with point 2. The coherence between points 2 and 3 (Figure 43b), shows that there is full coherence on periods longer than 50 days. Also, at higher frequencies there is more coherence in the clockwise direction. Between points 2 and 4 (Figure 43c) the coherence is significant for periods greater than 5 days, and like 2 and 3, at high frequencies, more coherence is present in the clockwise rotation. The coherence between 2 and 5 and 2 and 6 are almost indentical. For points 2 and 6 (Figure 43d) the coherence is significant for periods longer than 50 days, and again the coherence at higher frequencies is larger in the clockwise direction. For all the coherencies presented, notice that the coherence has peaks around 11 and 6 days.

By comparing the full wind case and no wind case coherence between the currents, the effect of the wind becomes evident at low frequencies, i.e.

By comparing the full wind case and no wind case coherence between the currents, the effect of the wind becomes evident at low frequencies, i.e.

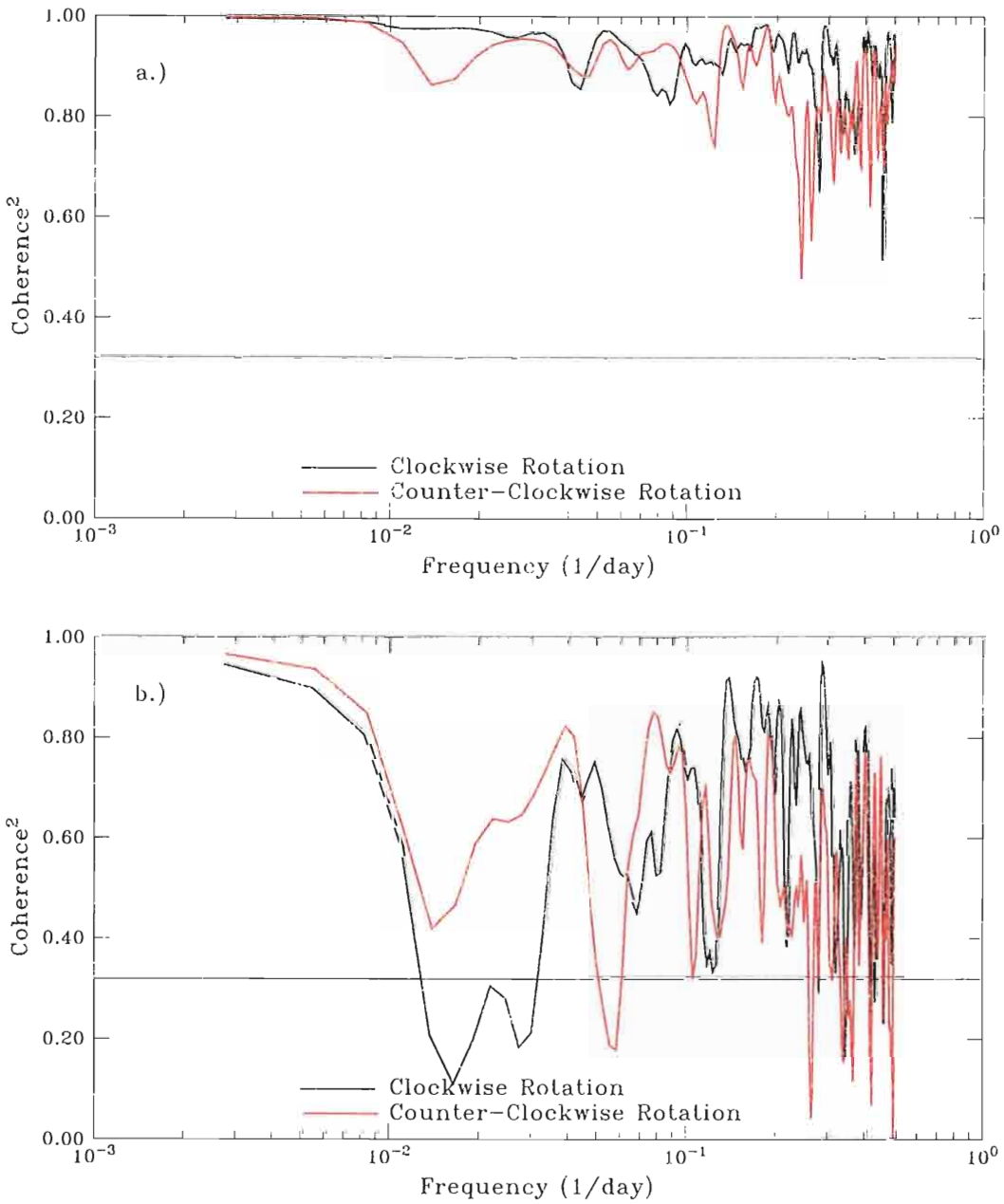


Figure 43 : Coherence of the wind between a.) point 1(125.35E, 33.75N) and point 2 (124.0E, 34.0N) , b.) point 2 (124.0E, 34.0N) and point 3 (124.0E, 30.0N)

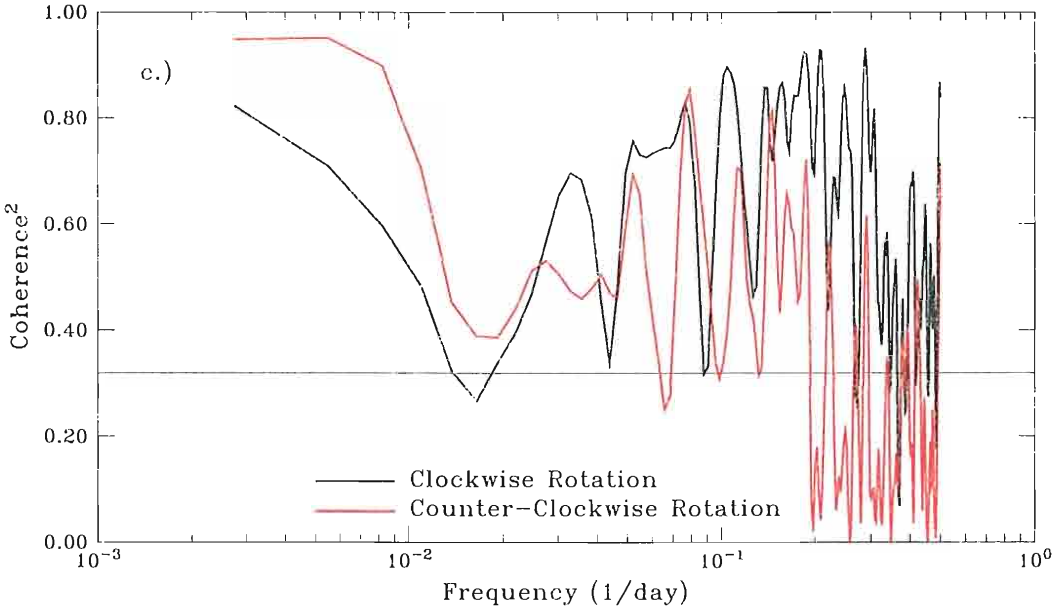


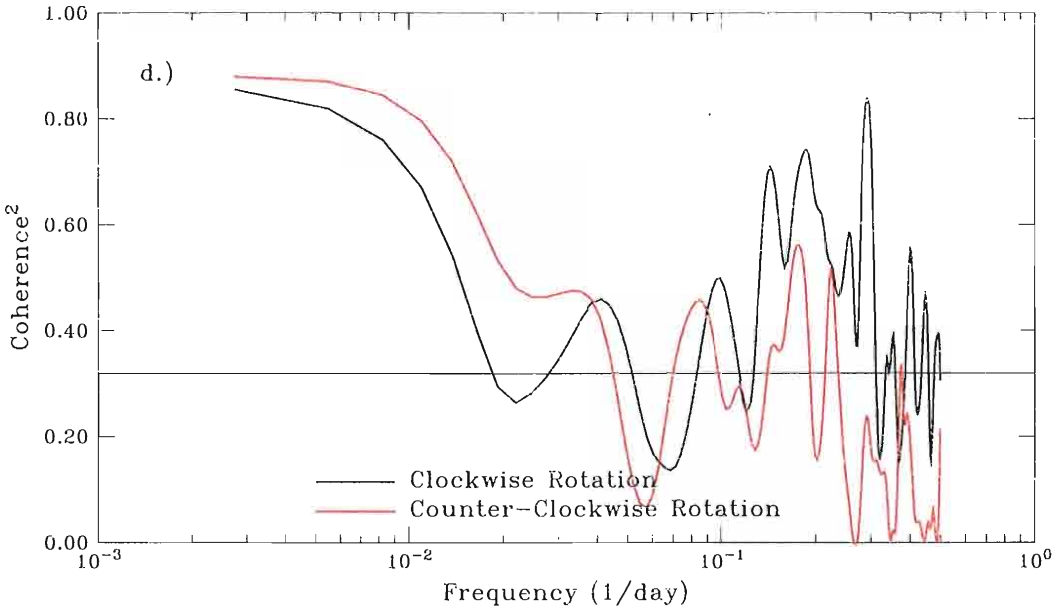


Figure 43 cont. : c.) point 2 (124.0E, 34.0N) and point 4 (128.0E, 32.0N) and
Frequency (1/day)

Figure 43 cont. : c.) point 2 (124.0E, 34.0N) and point 4 (128.0E, 32.0N) and d.) point 2 (124.0E, 34.0N) and point 6 (126.0E, 28.0N).

periods longer than 50 days. The comparison must be done at low frequencies because, as seen in the rotary spectra in the no wind case, the energy drops off toward zero around the 50 day period. First, looking at the coherence between 1 and 2 (Figure 44a), the no wind case has higher coherence than the full wind case. Therefore, the wind is influencing the flow. This influence by the wind is also seen by studying the coherences between points 1 and 3 (Figure 44b), points 1 and 4 (Figure 44c), points 2 and 4 (Figure 44f) and to a smaller extent points 2 and 3 (Figure 44e) counter-clockwise rotation. Since the coherence between points 1 and 5 (Figure 44d) does not change between the full and no wind cases, something besides the wind is dominating the flow at low frequencies. The comparisons between 2 and 5 and between points 1 and 6 and 2 and 6 are non-significant coherences, so the comparisons cannot be made.

If the coherence between the full wind currents at point 1 or point 2 and the wind at the other points are plotted, two patterns are found. For point 1 (Figure 45a), there is a high coherence at low frequencies, a bulge of coherence at mid-frequencies (periods 15 to 50 days) and a dominating clockwise rotation at high frequencies. For point 2 (Figure 45b), there is low coherence at high frequencies, with no significant clockwise rotation. There is a small bulge of coherence between 30 and 50 days, and overall dominating clockwise coherence at high frequencies. The summer and winter winds are quite different, so do these yearly coherences really show the relationship between the monsoonal winds and the currents?

between the monsoonal winds and the currents?

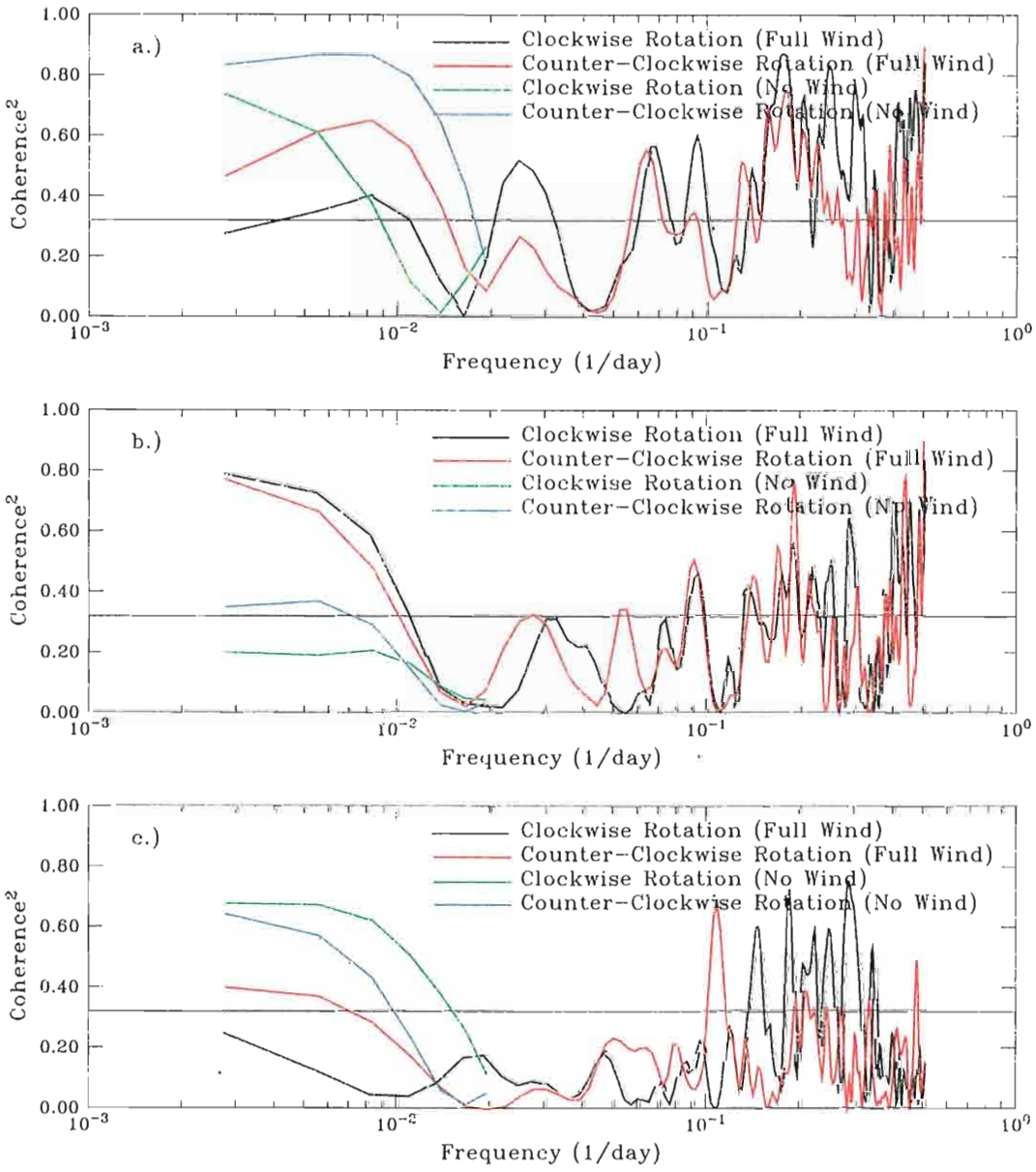


Figure 44 : Coherence of the Yellow Sea Warm Current for the full and no wind cases between a.) point 1 (125.35E, 33.75N) and point 2 (124.0E,

Figure 44 : Coherence of the Yellow Sea Warm Current for the full and no wind cases between a.) point 1 (125.35E, 33.75N) and point 2 (124.0E, 34.0N), b.) point 1 (125.35E, 33.75N) and point 3 (124.0E, 30.0N), c.) point 1 (125.35E, 33.75N) and point 4 (128.0E, 32.0N),

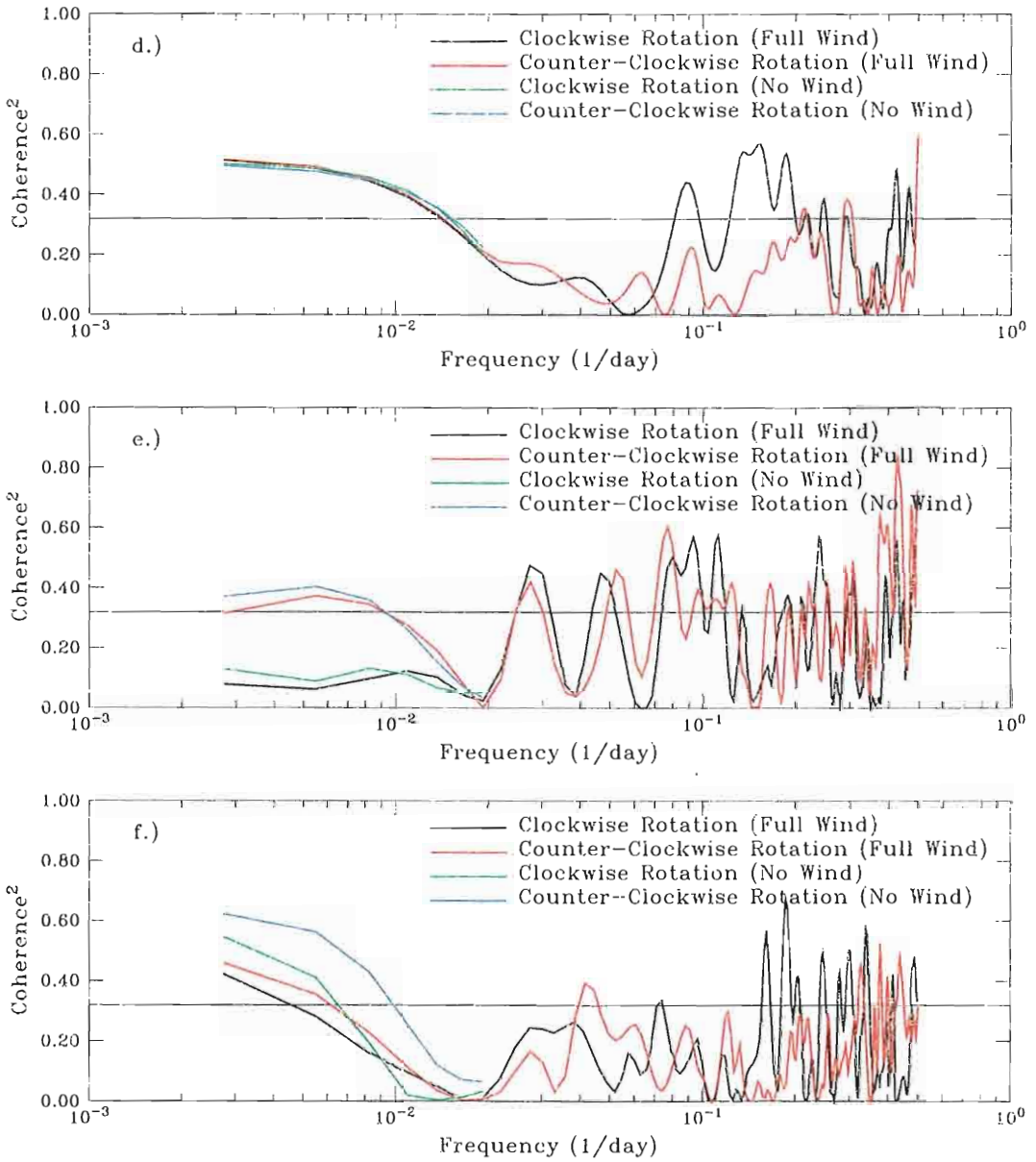


Figure 44 cont. : d.) point 1 (125.35E, 33.75N) and point 5 (122.0E, 26.0N), e.) point 2 (124.0E, 34.0N) and point 3 (124.0E, 30.0N) and f.) point 2 (124.0E,

Figure 44 cont. : d.) point 1 (125.35E, 33.75N) and point 5 (122.0E, 26.0N), e.) point 2 (124.0E, 34.0N) and point 3 (124.0E, 30.0N) and f.) point 2 (124.0E, 34.0N) and point 4 (128.0E, 32.0N)

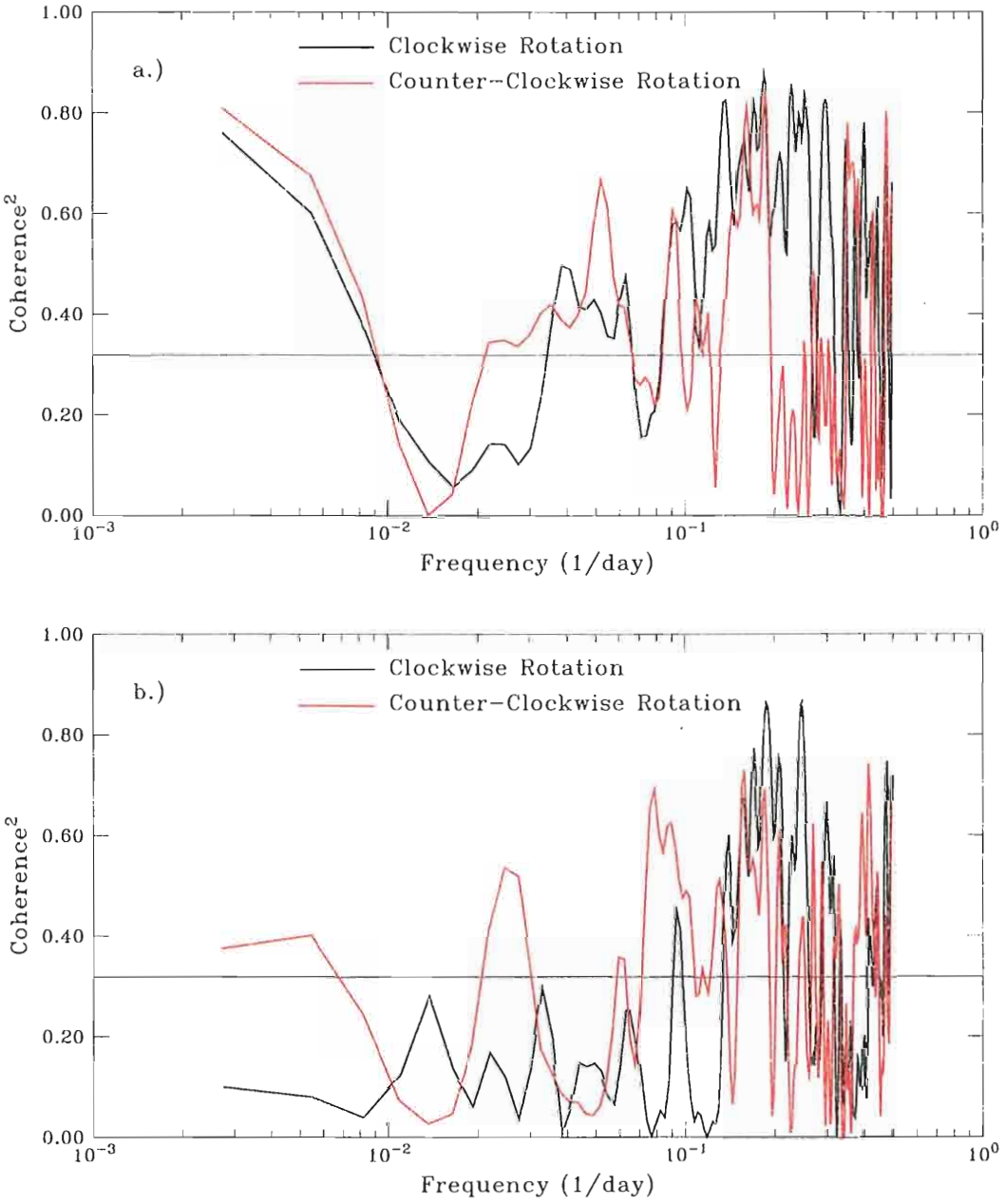


Figure 45 : Coherence between the full wind current and the wind at a.) point
Frequency (1/day)

Figure 45 : Coherence between the full wind current and the wind at a.) point 1 (125.35E, 33.75N) and b.) point 2 (124.0E, 34.0N) for a years worth of daily data.

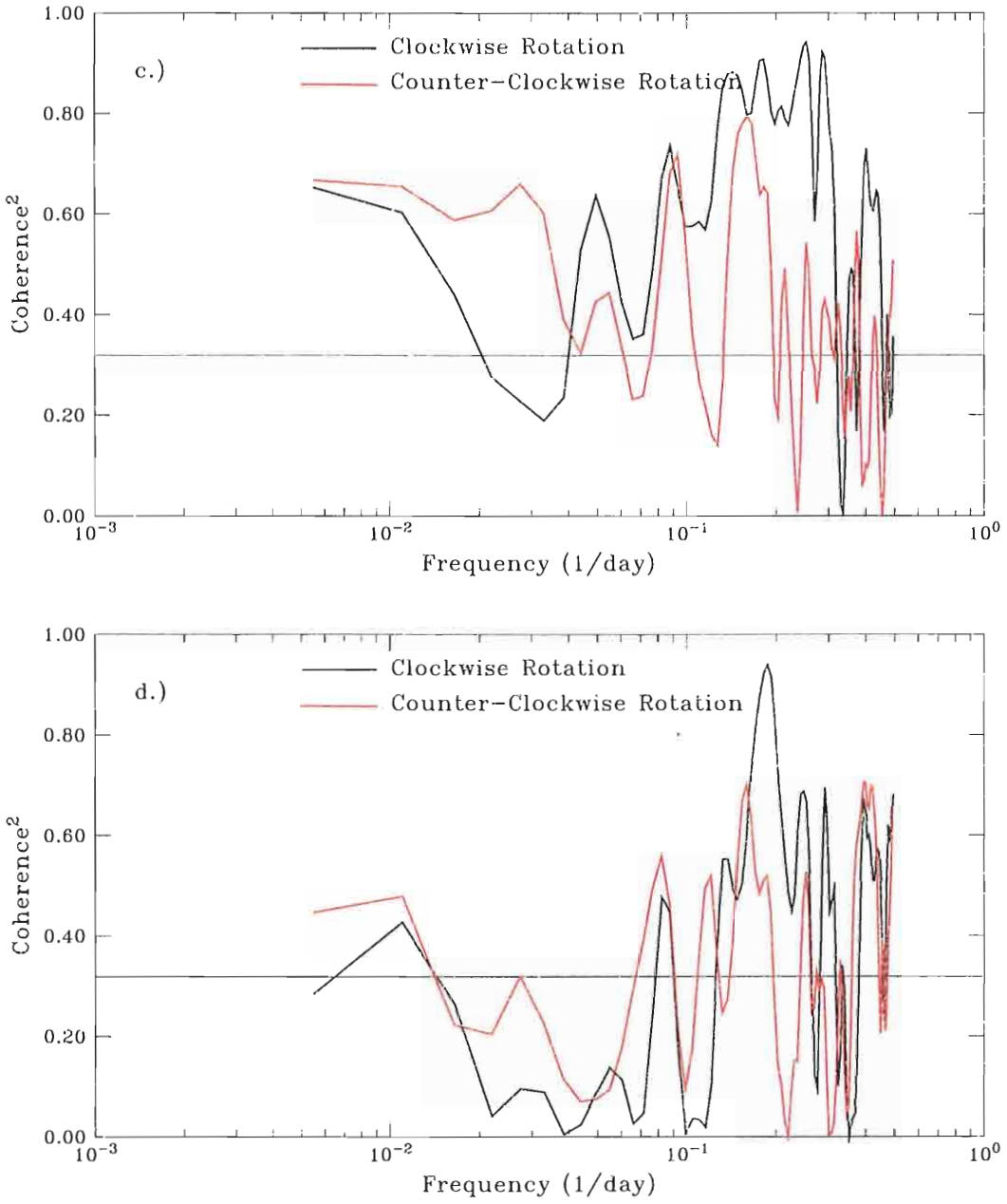


Figure 45 cont. : Coherence between the full wind current and the wind at c.)
Frequency (1/day)

Figure 45 cont. : Coherence between the full wind current and the wind at c.) point 1 (125.35E, 33.75N) and d.) point 2 (124.0E, 34.0N) for winter.

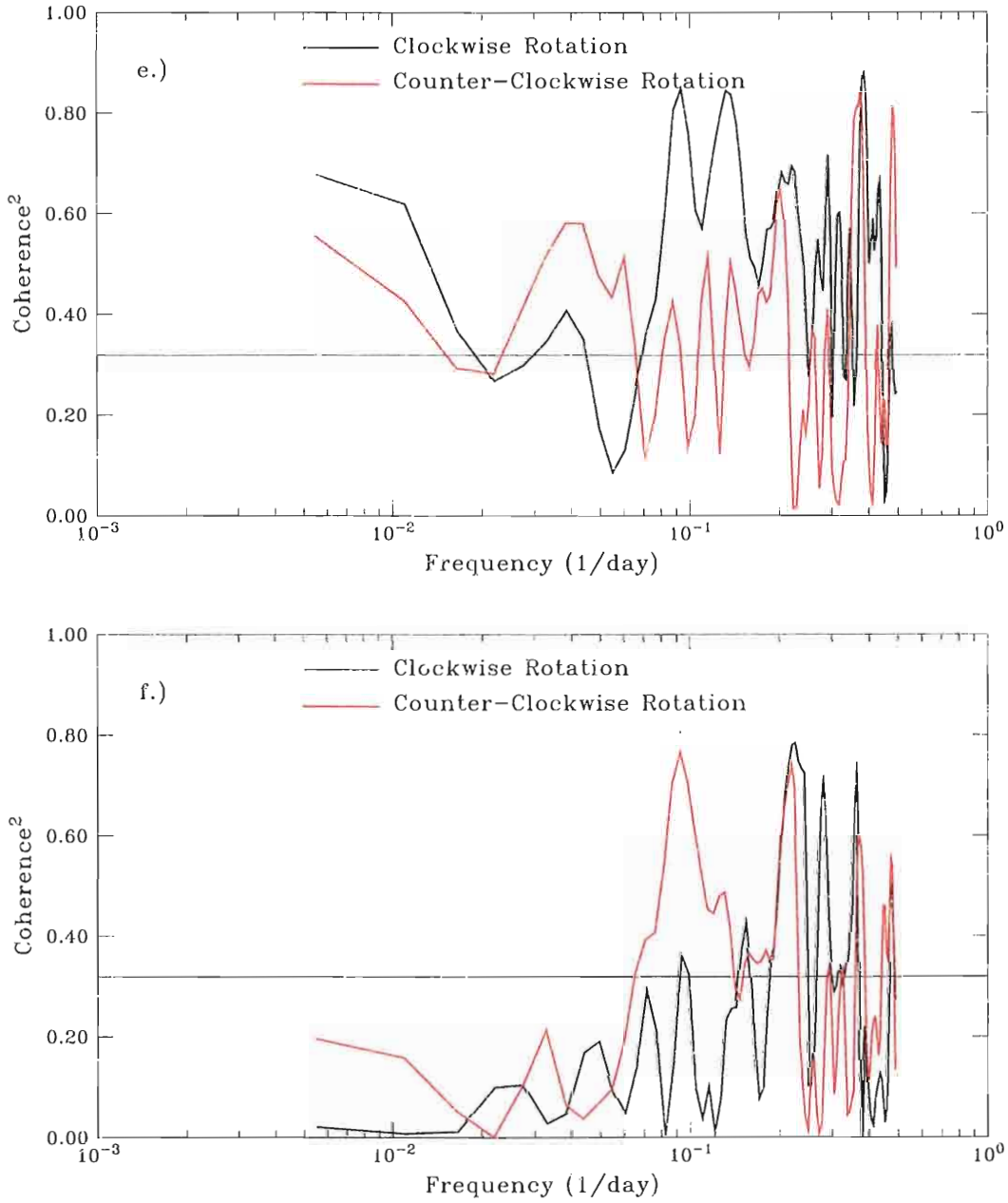


Figure 45 cont. : Coherence between the full wind current and the wind at e.) point 1 (125.35E, 33.75N) and f.) point 2 (124.0E, 34.0N) for the summer.

The yearly coherences actually are quite good at representing the seasonal coherencies between the winds and the Yellow Sea Warm Current. We define winter as December to May and summer as June to November. At point 1 in winter (Figure 45c) and summer (Figure 45e) the biggest difference to the yearly case is that the coherence does not dip towards zero around 0.15 $day^{-1}$. Also, between winter and summer, the dominate coherence at low frequencies switches from counter-clockwise to clockwise rotation. At point 2, winter (Figure 45d) and summer (Figure 45f) are also quite similar to the yearly coherence. In winter, there is more low frequency clockwise rotation than in the yearly coherence, and in summer all significant low frequency coherence is lost. Other patterns remain similar.

Another way of showing the relationship between the wind and the Yellow Sea Warm Current is to look at the coherencies between the full wind and no wind currents at points 1 and 2. On a yearly scale, the coherence at point 1 (Figure 46a) and the coherence at point 2 (Figure 46b) are different, but both show a high coherence at low frequencies. At higher frequencies it is harder to find a distinguishing pattern. In winter at point 1 (Figure 46c) and point 2 (Figure 46d) the clockwise coherence is still quite high at low frequencies, but the counter-clockwise coherence has almost fallen off to non-significant levels. In summer at point 1 (Figure 46e) and point 2 (Figure 46f), at low frequencies, the coherence is relatively high, with the counter-clockwise rotation dominating like in the yearly case. Therefore, even though the yearly coherence is high, it is actually the summer flow that is producing this significance.

coherence is high, it is actually the summer flow that is producing this significance.

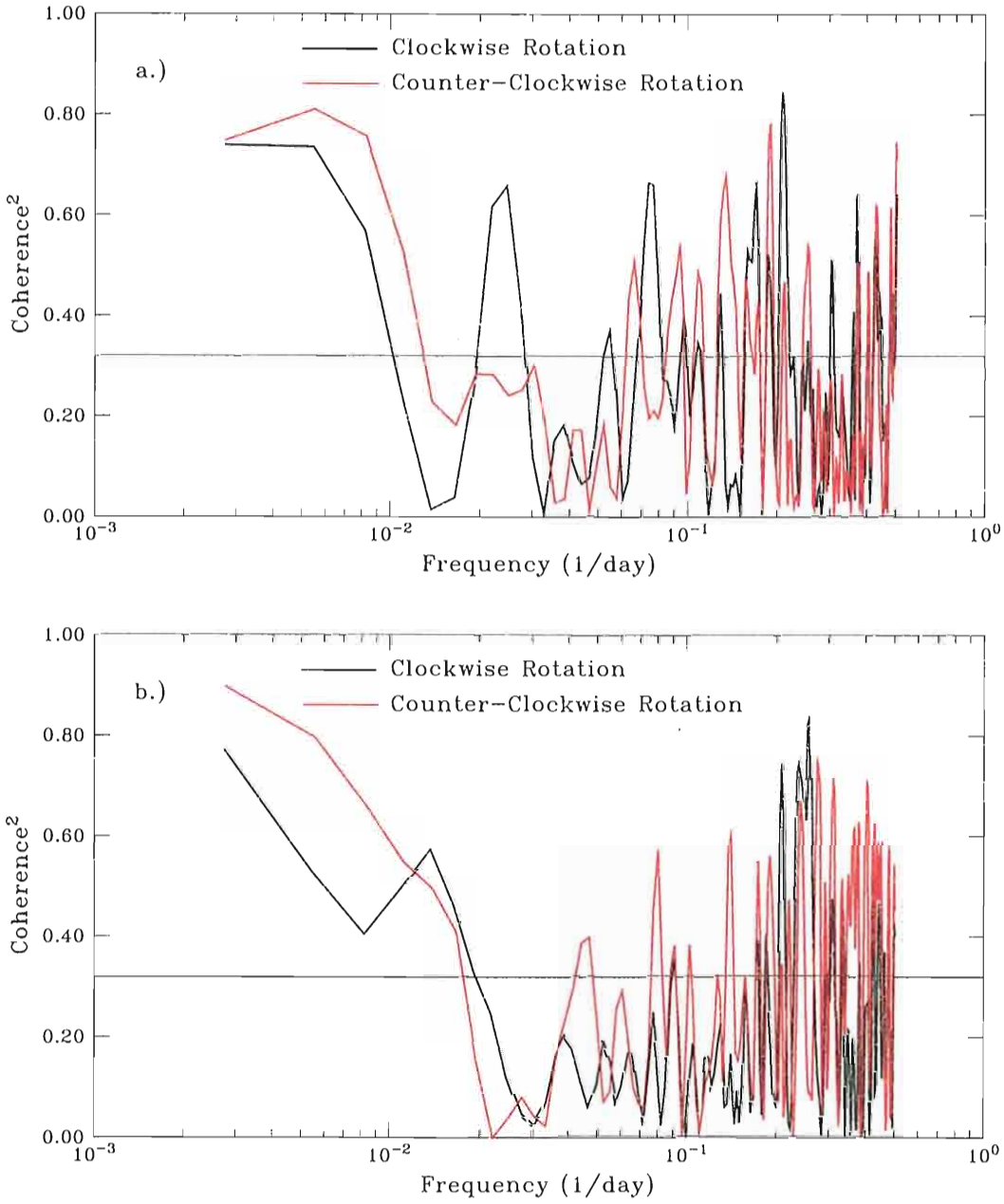


Figure 46: Coherences for the full wind case to the no wind case of the Yellow
Frequency (1/day)

Figure 46: Coherences for the full wind case to the no wind case of the Yellow Sea Warm Current at a.) point 1 (125.35E, 33.75N) and b.) point 2 (124.0E, 34.0N) for a year of daily output.

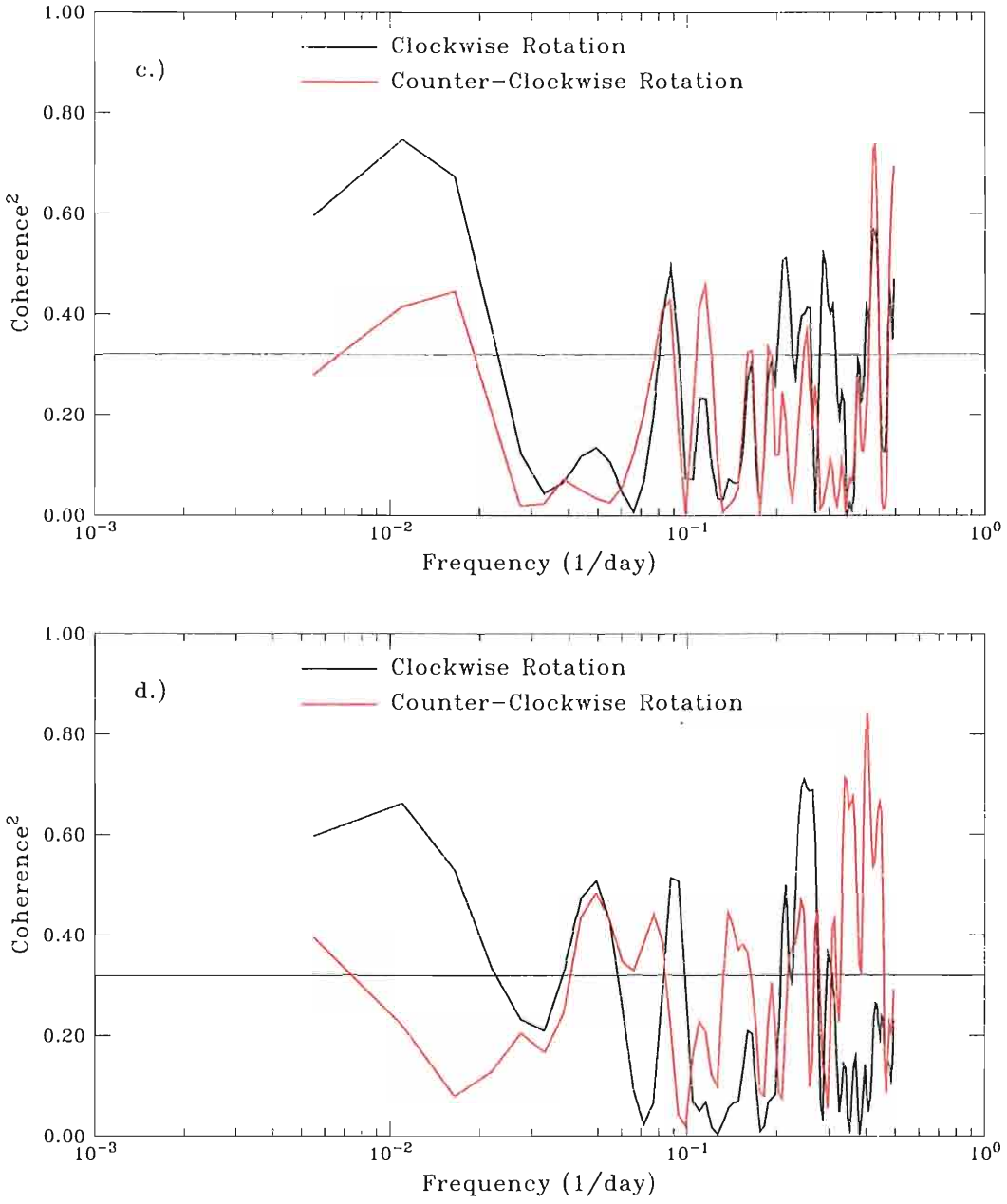


Figure 46 cont. : Coherences for the full wind case to the no wind case of the
Frequency (1/day)

Figure 46 cont. : Coherences for the full wind case to the no wind case of the Yellow Sea Warm Current at c.) point 1 (125.35E, 33.75N) and d.) point 2 (124.0E, 34.0N) for winter.

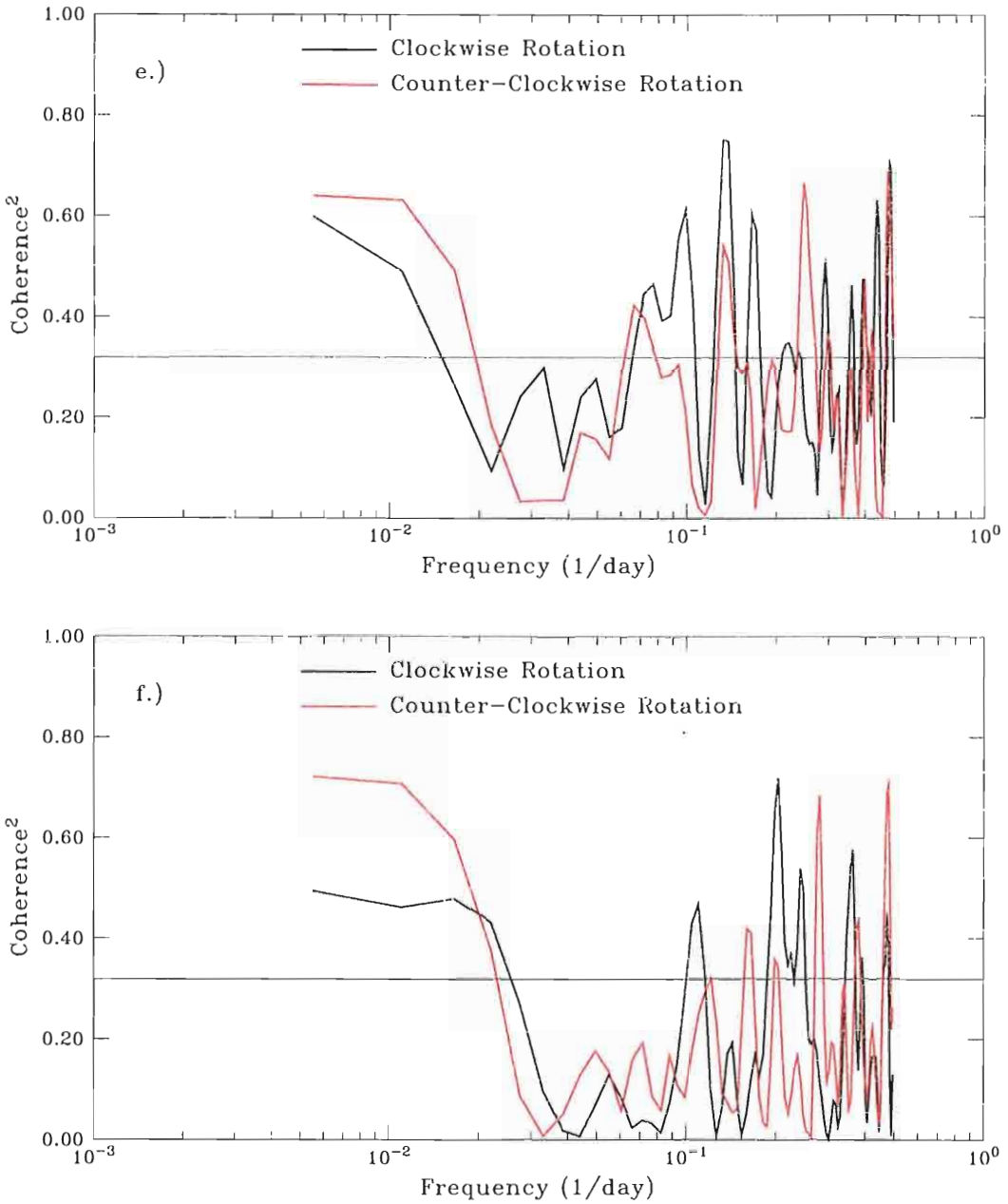


Figure 46 cont. : Coherences for the full wind case to the no wind case of the Yellow Sea Warm Current at e.) point 1 (125.35E, 33.75N) and f.) point 2 (124.0E, 34.0N) for summer.

# 6. CONCLUSION

The POM version of the Yellow Sea Model developed at NRL has been shown to properly represent the major currents circulation in the Yellow Sea and the surrounding regions. The results of the model have shown that the circulation in the Yellow Sea is caused by the conditions set-up at the open boundaries of the model, i.e. the inflowing Taiwan Warm Current and the Kuroshio as well as the boundary conditions set-up at the Korean Strait. This leaves the wind to act on the Yellow Sea Warm Current as a steering force and also cause a pulse like flow of the current. From the rotary spectra and the coherences, it has been shown that the wind is coherent to the Yellow Sea Warm Current year round, but it has also been shown that the wind is not what causes the Yellow Sea Warm Current to form. Also, the NOGAPS wind stress used to force the model follows the observational wind patterns, i.e. from the north in winter and from the south in summer, and is better than the seasonal climatological winds that have been used previously to study the region.

Part of the difficulty with studying the Yellow Sea region is terminology. One terminology problem arises when discussing the Yellow Sea Warm Current, does an author mean the actual northward moving current or is he referring to the water mass definition. As shown in this study the northward moving current appears even when there is no wind forcing, but the water mass does not. Therefore, I propose that the current that has a northward velocity component and travels along the central part of the Yellow Sea basin be called the Yellow Sea Warm Current, and the water mass associated with

mass does not. Therefore, I propose that the current that has a northward velocity component and travels along the central part of the Yellow Sea basin be called the Yellow Sea Warm Current, and the water mass associated with

this current and following the previous water mass definition be called the Yellow Sea Warm Intrusion. However, some may argue that since this study was completed at 20 m depth, that the surface current behaves differently and should not follow the names I have suggested. However, looking at Hoffmuller diagrams for the full wind case across 33.875°E at the surface (Figures 47 a and b) shows that there is a current year round, but it is disrupted by the wind pulses from the north that occur approximately once a week during the winter. So the name Yellow Sea Warm Current is valid at the surface also.

This study has found relationships for the Yellow Sea Warm Current and the winds of the Yellow Sea region on periods longer than 50 days, for the year 1993. The next step in this study would be to find interannual relationships for this region, but before that is done longer time series of the wind need to be produced.

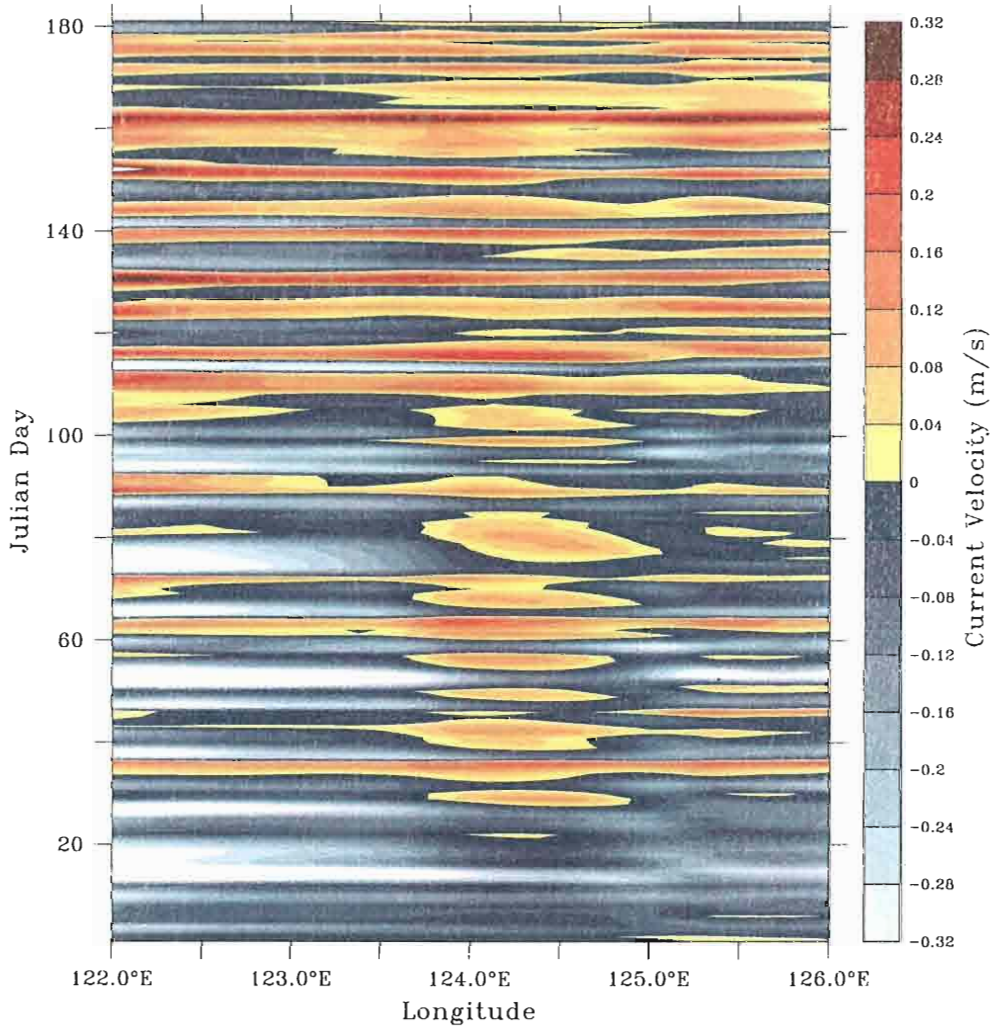


Figure 47 a.) Hoffmuller diagram across 33.875E of the v-velocities for Julian days 1 to 181.

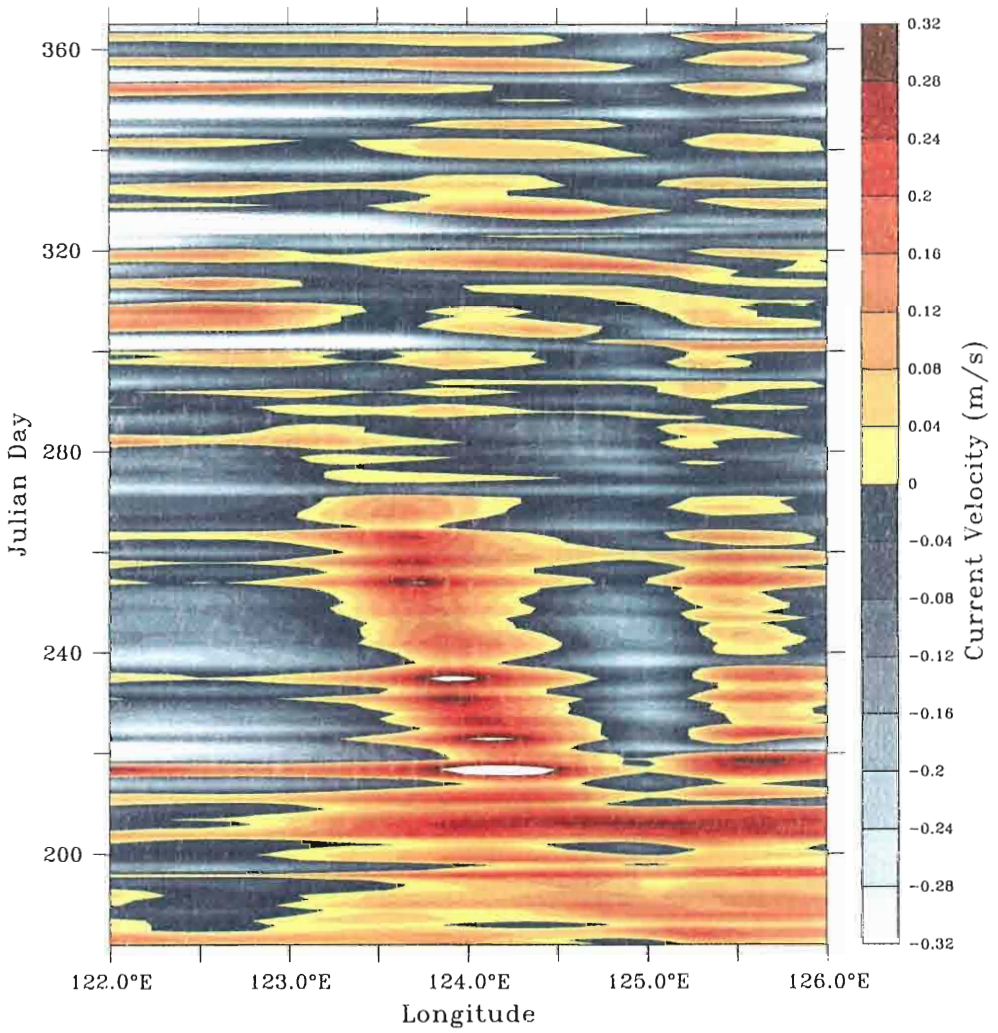


Figure 47 b.) Hoffmuller diagram across 33.875E of the v-velocities for Julian days 182 to 365.

# APPENDIX A

## Governing Equations and Differencing Schemes of POM

The Princeton Ocean Model (POM) (Mellor, 1996) uses a split mode calculation. There is an internal mode that has three-dimensional calculations on a long time step which updates velocities, temperature, salinity, and turbulence quantities. Also, there is an external mode the has two-dimensional calculations on a short time step which updates surface elevation and vertically averaged velocities.

### Internal Mode

Starting from the primitive equations, the governing equations for the vertical structure, the internal mode, of the POM have been transformed into a sigma coordinate system, such that,

$$x^* = x, \quad y^* = y, \quad \sigma = \frac{z-\eta}{H+\eta}, \quad t^* = t$$

where x, y, and z are the Cartesian coordinates. Also, $\eta$ is the surface elevation, and H is the bottom topography. Therefore, $\sigma$=0 at z=$\eta$ and $\sigma$=1 at z=-H. Deleting the asterisks, the governing equations become:

$$\frac{\partial DU}{\partial x} + \frac{\partial DV}{\partial y} + \frac{\partial \omega}{\partial \sigma} + \frac{\partial \eta}{\partial t} = 0 \qquad (1)$$

$$\frac{\partial}{\partial x} \quad \frac{\partial}{\partial y} \quad \frac{\partial}{\partial \sigma} \quad \frac{\partial}{\partial t} \qquad (1)$$

$$\frac{\partial UD}{\partial t}+\frac{\partial U^2D}{\partial x}+\frac{\partial UVD}{\partial y}+\frac{\partial U\omega}{\partial \sigma}-fVD+gH\frac{\partial \eta}{\partial x}=$$
$$\frac{\partial}{\partial \sigma}\left[\frac{K_M}{D}\frac{\partial U}{\partial \sigma}\right]-\frac{gD^2}{\rho_o}\int_\sigma^0\left[\frac{\partial \rho'}{\partial x}-\frac{\sigma'}{D}\frac{\partial D}{\partial x}\frac{\partial \rho'}{\partial \sigma'}\right]d\sigma'+F_x \tag{2}$$

$$\frac{\partial VD}{\partial t}+\frac{\partial UVD}{\partial x}+\frac{\partial V^2D}{\partial y}+\frac{\partial V\omega}{\partial \sigma}+fUD+gD\frac{\partial \eta}{\partial y}=$$
$$\frac{\partial}{\partial \sigma}\left[\frac{K_M}{D}\frac{\partial V}{\partial \sigma}\right]-\frac{gD^2}{\rho_o}\int_\sigma^0\left[\frac{\partial \rho'}{\partial y}-\frac{\sigma'}{D}\frac{\partial D}{\partial y}\frac{\partial \rho'}{\partial \sigma'}\right]d\sigma'+F_y \tag{3}$$

$$\frac{\partial \Theta D}{\partial t}+\frac{\partial \Theta UD}{\partial x}+\frac{\partial \Theta VD}{\partial y}+\frac{\partial \Theta \omega}{\partial \sigma}=\frac{\partial}{\partial \sigma}\left[\frac{K_H}{D}\frac{\partial \Theta}{\partial \sigma}\right]+F_\Theta-\frac{\partial R}{\partial z} \tag{4}$$

$$\frac{\partial SD}{\partial t}+\frac{\partial SUD}{\partial x}+\frac{\partial SVD}{\partial y}+\frac{\partial S\omega}{\partial \sigma}=\frac{\partial}{\partial \sigma}\left[\frac{K_H}{D}\frac{\partial S}{\partial \sigma}\right]+F_S \tag{5}$$

$$\frac{\partial q^2D}{\partial t}+\frac{\partial Uq^2D}{\partial x}+\frac{\partial Vq^2D}{\partial y}+\frac{\partial \omega q^2}{\partial \sigma}=\frac{\partial}{\partial \sigma}\left(\frac{K_q}{D}\frac{\partial q^2}{\partial \sigma}\right)$$
$$+\frac{2K_M}{D}\left[\left(\frac{\partial U}{\partial \sigma}\right)^2+\left(\frac{\partial V}{\partial \sigma}\right)^2\right]+\frac{2g}{\rho_o}K_H\frac{\partial \rho}{\partial \sigma}-\frac{2Dq^3}{B_1\ell}+F_q \tag{6}$$

$$\frac{\partial q^2\ell D}{\partial t}+\frac{\partial Uq^2\ell D}{\partial x}+\frac{\partial Vq^2\ell D}{\partial y}+\frac{\partial \omega q^2\ell}{\partial \sigma}=\frac{\partial}{\partial \eta}\left[\frac{K_q}{D}\frac{\partial q^2\ell}{\partial \sigma}\right]$$
$$+E_1\ell\left\{\frac{K_M}{D}\left[\left(\frac{\partial U}{\partial \sigma}\right)^2+\left(\frac{\partial V}{\partial \sigma}\right)^2\right]+E_3\frac{g}{\rho_o}K_H\frac{\partial \rho}{\partial \sigma}\right\}\tilde{W}+F_\ell \tag{7}$$

where,

U,V are the eastward and northward velocity components, respectively,

ω is the vertical velocity component normal to the sigma surfaces,

U,V are the eastward and northward velocity components, respectively,

ω is the vertical velocity component normal to the sigma surfaces,

D is equal to H+η,

f is the Coriolis parameter,

g is gravity,

$\tilde{W}$ is the so-called wall proximity function
$\tilde{W} = 1 + E_2(\ell / k)\left((\eta - z)^{-1} + (H - z)^{-1}\right)$,

$q^2$ is twice the turbulence kinetic energy,

$\ell$ is the turbulence length scale,

$\rho/\rho_O$ is the density,

$\Theta$ is the potential temperature,

S is the salinity,

$K_M$ is the vertical kinematic viscosity,

$K_H$ is the vertical diffusivity,

R is the short-wave radiation flux,

$B_1$ is one of the turbulence closure constants,

$E_i$ are empirical constants of turbulence closure (i=1,2,3).

The horizontal diffusion terms are defined by:

$$F_x \equiv \frac{\partial}{\partial x}\left(D\tau_{xx}\right) + \frac{\partial}{\partial y}\left(D\tau_{xy}\right) \tag{8}$$

$$F_y \equiv \frac{\partial}{\partial x}\left(D\tau_{xy}\right) + \frac{\partial}{\partial y}\left(D\tau_{yy}\right) \tag{9}$$

$$F_\phi \equiv \frac{\partial}{\partial x}\left(Dq_x\right) + \frac{\partial}{\partial y}\left(Dq_y\right) \tag{10}$$

where $\phi$ can be $\Theta$, S, $q^2$, or $q^2\ell$, and

$$\tau_{xx} = 2A_M \frac{\partial U}{\partial x} \tag{11}$$

$$\tau_{xy} = A_M\left(\frac{\partial U}{\partial y} + \frac{\partial V}{\partial x}\right) \tag{12}$$

$$\tau_{yy} = 2A_M \frac{\partial V}{\partial y} \tag{13}$$

$$\tau_{yy} = 2A_M \frac{\partial \phi}{\partial y} \tag{13}$$

$$q_x \equiv A_H \frac{\partial \phi}{\partial x} \tag{14}$$

$$q_y \equiv A_H \frac{\partial \phi}{\partial y} \tag{15}$$

where,

$A_M$ is the horizontal kinematic viscosity calculated by the Smagorinsky Diffusivity,

$A_H$ is the horizontal heat diffusivity.

External Mode

The external mode contains the vertically integrated internal mode equations. These equations are:

$$\frac{\partial \eta}{\partial t} + \frac{\partial \overline{U} D}{\partial x} + \frac{\partial \overline{V} D}{\partial y} = 0 \tag{16}$$

$$\frac{\partial \overline{U} D}{\partial t} + \frac{\partial \overline{U}^2 D}{\partial x} + \frac{\partial \overline{U}\overline{V} D}{\partial y} - \tilde{F}_x - f\overline{V} D + gD\frac{\partial \eta}{\partial x} = - < \omega u(0) > + < \omega u(-1) > + G_x - \frac{gD}{\rho_o}\int_{-1}^{0}\int_{\sigma}^{0}\left[ D\frac{\partial \rho}{\partial x} - \frac{\partial D}{\partial x}\sigma' \frac{\partial \rho}{\partial \sigma}\right] d\sigma' \, d\sigma \tag{17}$$

$$\frac{\partial \overline{V} D}{\partial t} + \frac{\partial \overline{U}\overline{V} D}{\partial x} + \frac{\partial \overline{V}^2 D}{\partial y} - \tilde{F}_y + f\overline{U} D + gD\frac{\partial \eta}{\partial y} = - < \omega v(0) > + < \omega v(-1) > + G_y - \frac{gD}{\rho_o}\int_{-1}^{0}\int_{\sigma}^{0}\left[ D\frac{\partial \rho}{\partial y} - \frac{\partial D}{\partial y}\sigma' \frac{\partial \rho}{\partial \sigma}\right] d\sigma' \, d\sigma \tag{18}$$

where, $\overline{U}$ is defined as $\int_{-1}^{0} U d\sigma$, and $\overline{V}$ similarly. $- < \omega u(0) >$ and $- < \omega v(0) >$ are the wind stress components. $< \omega u(-1) >$ and $< \omega v(-1) >$ are the bottom stress components. Also, the diffusion terms become:

$$\tilde{F}_x = \frac{\partial}{\partial x}\left[ H 2 \overline{A}_M \frac{\partial \overline{U}}{\partial x}\right] + \frac{\partial}{\partial y}\left[ H \overline{A}_M \left( \frac{\partial \overline{U}}{\partial y} + \frac{\partial \overline{V}}{\partial x}\right)\right] \tag{19}$$

$$\tilde{F}_x = \frac{\partial}{\partial x}\left[ H 2 \overline{A}_M \frac{\partial U}{\partial x}\right] + \frac{\partial}{\partial y}\left[ H \overline{A}_M \left( \frac{\partial U}{\partial y} + \frac{\partial V}{\partial x}\right)\right] \tag{19}$$

$$\tilde{F}_y = \frac{\partial}{\partial y}\left[H2\bar{A}_M \frac{\partial \bar{V}}{\partial y}\right] + \frac{\partial}{\partial y}\left[H\bar{A}_M\left(\frac{\partial \bar{U}}{\partial y} + \frac{\partial \bar{V}}{\partial x}\right)\right] \tag{20}$$

And the so-called dispersion terms are:

$$G_x = \frac{\partial \bar{U}^2 D}{\partial x} + \frac{\partial \bar{U}\bar{V}D}{\partial y} - \tilde{F}_x - \frac{\partial \overline{U^2} D}{\partial x} - \frac{\partial \overline{UV}D}{\partial y} + \bar{F}_x \tag{21}$$

$$G_y = \frac{\partial \bar{U}\bar{V}D}{\partial x} + \frac{\partial \bar{V}^2 D}{\partial y} - \tilde{F}_y - \frac{\partial \overline{UV}D}{\partial x} - \frac{\partial \overline{V^2} D}{\partial y} + \bar{F}_y \tag{22}$$

The right hand sides of (17) and (18) are calculated only at the internal mode time steps. While the external mode time steps are run, they are held constant.

Differencing Schemes

The rectilinear horizontal grid uses a staggered finite differencing scheme, often called an Arakawa-C grid. See Figures 48 and 49 for depictions of the external and internal mode grids respectively.

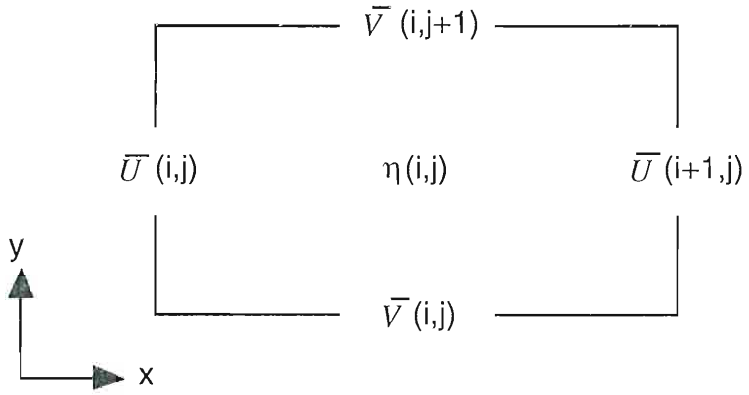


Figure 48 : Two-dimensional external mode grid.

x

Figure 48 : Two-dimensional external mode grid.

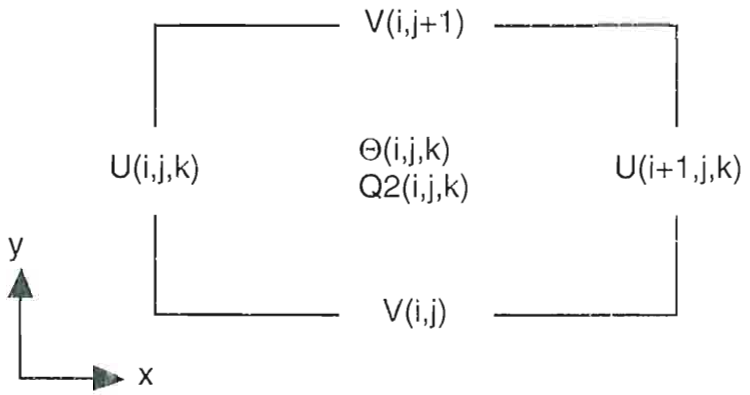


plane view

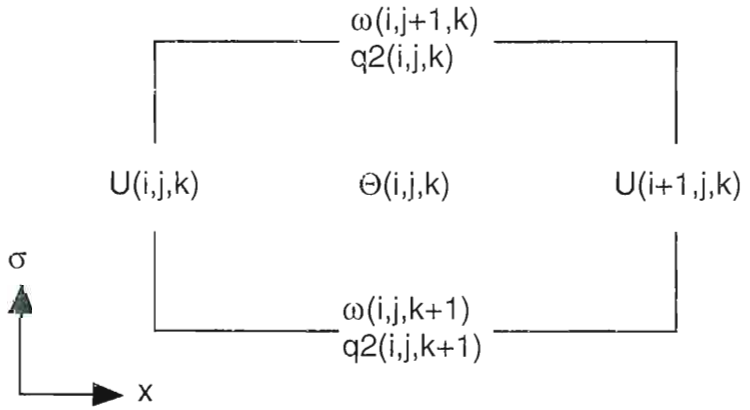


elevation view

Figure 49 : Three-dimensional internal mode grid.

q2 represents : $K_M$, $K_H$, $q^2$, or $q^2\ell$.

Θ represents : Θ, S, or ρ.

The time integration scheme is the leap frog method. This is used for both the internal and external modes. This particular model uses a time step of 720 seconds for the internal mode, and a time step of 24 seconds for the external mode.

external mode.

# REFERENCES

Fairbridge, Rhodes W., ed., 1966: *The Encyclopedia of Oceanography*. Vol. I, Reinhold Pub. Co., New York, 994-998.

Hsueh, Y., 1988: Recent current observations in the Eastern Yellow Sea, *Journal of Geophysical Research*, **93** (C6), 6875-6884.

Kantha, Lakshmi H., and Carol Anne Clayton, 1994: An improved mixed layer model for geophysical applications, *Journal of Geophysical Research*, **99** (C12), 25,235-25,266.

Lie, Heung-Jae,1986: Summertime hydrographic features in the southeatern Hwanghae, *Progressive Oceanography*, **17**, 229-242.

Mellor, George L., 1996: Users guide for a three-dimensional, primitive equation, numerical ocean model.

Mooers, Christopher N. K., 1973: A technique for the cross spectrum analysis of pairs of complex-valued time series, with emphasis on properties of polarized components and rotational invariants, *Deep-Sea* Research, 20, 1129-1141.

polarized components and rotational invariants, *Deep-Sea* Research, 20, 1129-1141.

Park, Young-Hyang,1986: Water Characteristics and movements of the Yellow Sea Warm Current in summer, *Progressive Oceanography*, **17**, 243-254.

Shuxun, Liu, et. al., 1992: Preliminary analysis of distribution and variation of preennial monthly mean water masses in the Bohai Sea, the Huanghai Sea and the East China Sea, *Acta Oceanologica Sinica*, **11** (4), 483-498.

Song, Wanxian,1994: Characteristices of summer and winter circulations and their variability is the source are of the Tsushima Warm Current, *Acta Oceanologica Sinica,* **13**(2), 189-201.

Thompson, Rory O. R. Y., 1979: Coherence Significance Levels, *Journal of Atmospheric Research*, 36, 2020-2021.

World Meterological Organization (WMO) version of the United Nations Educational, Scientific and Cultural Organization river discarge data.

Yuan, Y. and J. Su,1984: Numerical modelling of the circulation in the East China Sea, In:*Ocean Hydrodynamics of the Japan and East China Seas, Elsevier Oceanography Series, 39.* Ichiye, T., ed., Elsevier, New York,167-186.

Zheng, Q.A. and V. Klemas,1982: Determination of Winter Temperature Patterns, Fronts, and Surface Currents in the Yellow Sea and East China Sea from Satellite Imagery. *Remote Sensing of Environment*, **12**, 201-218.

from Satellite Imagery. *Remote Sensing of Environment*, **12**, 201-218.

## BIOGRAPHICAL SKETCH

**Andrea C. Mask**

Place of Birth: Jackson, Mississippi

Date of Birth: March 9, 1972

**Education:**

Bachelor of Science in Physics and Mathematics. University of Southern Mississippi, 1994.

**Experience:**

University of Southern Mississippi, Physics Department. Laboratory Assistant. Conducted introductory laboratory classes. 1992-1993.

Naval Research Laboratory, Stennis Space Center, Mississippi. Physical Scientist Aid. Worked with acoustians on fish migration research. Summer 1992 and 1993.

Sverdrup Inc., Stennis Space Center, Mississippi. Physical Scientist I. Worked with Oceanographers studying ice movement in the Arctic Ocean and investigating the Mediterranean using satellite images. Summer 1994.

Arctic Ocean and investigating the Mediterranean using satellite images. Summer 1994.

Florida State University. Graduate Research Assistant. Conducted research on the circulation of the Yellow Sea region using a numerical model developed at NRL Stennis Space Center, MS. 1994-1996.

**Honors:**

Naval Research Laboratory Fellowship, 1994 - present.

**Memberships:**

American Geophysical Union

**Publications:**

Electric Field and Size Induced Configuration Transitions. Bachelor's Thesis. University of Southern Mississippi.